Model Predictive Control for Linear Systems with Random Packet Dropouts with Application to Quadrotors

by

Yue Song
B.Eng., Northwestern Polytechnical Unversity, 2020

A Thesis Submitted in Partial Fulfillment of the
Requirements for the Degree of

MASTER OF APPLIED SCIENCE

in the Department of Mechanical Engineering

Model Predictive Control for Linear Systems with Random Packet Dropouts with Application to Quadrotors

by

Yue Song

B.Eng., Northwestern Polytechnical Unversity, 2020

Supervisory Committee

Dr. Yang Shi, Supervisor

(Department of Mechanical Engineering)

Dr. Homayoun Najjaran, Departmental Member

(Department of Mechanical Engineering)

ABSTRACT

In recent years, quadrotors have garnered significant attention in both industry and academia due to their excellent maneuverability and hovering ability. This results from onboard sensors with high accuracy, remote controllers with high performance, and network communication among sensors, controllers, and plants with high efficiency. A quadrotor control system of this type can be regarded as a networked control system (NCS) enjoying remarkable scalability, resource efficiency, and ease of maintenance. However, new challenges in controller design arise from network-induced issues. Model predictive control (MPC), as an optimization-based control method, is able to provide not only the optimal control input for the current time instant but also the predicted state and input sequences, which provide a promising solution to handle network-induced issues. Moreover, the state and input constraints that exist in many applications can be effectively dealt with by MPC. These appealing features have motivated the development of many MPC schemes for quadrotors and NCSs. However, how to effectively solve network-related problems by MPC, and how different factors in MPC implementation affect the control performance are still open problems.

We propose a robust output feedback MPC framework for constrained networked quadrotor control systems subject to packet dropouts and external disturbances. The packet dropouts randomly happen in both sensor-controller (S-C) and controller-actuator (C-A) channels. The proposed output feedback MPC scheme consists of a state observer that accommodates the random measurement loss and a state feedback MPC that stabilizes the perturbed system. The proposed observer enables the estimation error dynamics to be represented by a switched system. By developing a generalized robust positive invariant (GRPI) set under the switched system formulation, the estimation error can be confined to this invariant set, which serves as

the explicit error bound of state estimation. Similarly, an extended robust positive invariant (ERPI) set is developed to describe all possible realizations of the deviation between the predicted and actual state. Then, the GRPI and ERPI sets are utilized to tighten the state and input constraints to alleviate the effects of random packet dropouts and disturbances. By imposing tightened constraints on the predicted states and inputs in the optimal control problem, the system can be stabilized by the proposed output feedback MPC scheme with guaranteed constraint satisfaction. Simulation results are provided to validate the effectiveness of the proposed method.

Three MPC schemes are adopted and compared for quadrotor control, including conventional MPC, tube-based MPC, and Lyapunov MPC. Moreover, different factors that may affect the control performance are considered in a dual-loop control framework. Firstly, since the disturbances usually appear in practical implementations, the robustness of three MPC schemes against different levels of disturbances is evaluated and compared. Then, to simulate the real control processes and validate the effectiveness of three MPC frameworks, the control inputs generated by three controllers with different prediction models are applied to the same nonlinear quadrotor system. Moreover, since the sampling rates of inner and outer control loops in the dual-loop control framework are usually assumed to be the same, we explore how different dual-loop sampling ratios affect the control performance, which facilitates the controller design for quadrotors and provides a direction for theoretical studies.

Finally, after concluding the obtained results, future study directions in quadrotor control are provided at the end of this thesis.

Contents

List of Tables

List of Figures

ACKNOWLEDGEMENTS

I am deeply grateful to all those who have contributed to the completion of this thesis and supported me throughout this journey.

Firstly, I would like to express my sincere appreciation to my supervisor, Dr. Yang Shi. His exceptional guidance and expert knowledge have always been invaluable, and his unwavering support carried me through my low moments. In group and individual meetings, his insightful feedback and constructive comments not only shaped the direction of this research but also inspired me in my studies and life. It has been my great honor to work with such a professional and dedicated mentor.

My gratitude is also extended to the group members at University of Victoria, without whom this research would not have been possible. Special thanks go to Dr. Kunwu Zhang, Tianxiang Lu, Xinxin Shang, Binyan Xu, and Dr. Tianyu Tan for their firm and substantial help throughout my research and manuscript revision. Their willingness to share their experiences and perspectives has enriched the findings and contributed to the broader understanding of the subject matter. I am also grateful to Dr. Songlin Zhuang for his constructive comments and enthusiastic support. I sincerely appreciate the generous help offered by Dr. Henglai Wei and Dr. Changxin Liu in the early stages of my study. I am thankful to Yufan Dai for his precious sharing and close cooperation in completing my Master's program. The time I spent with, Dr. Yukun Shi, Dr. Qian Zhang, Xiang Sheng, Dr. Qi Sun, Dr. Zehua Jia, Yijia Xie, Huiting Wang, Lei Xu, Andy Guevara, Cedar Malim, and the aforementioned group members is always precious to me.

I am deeply thankful to my parents for their unwavering support, encouragement, and understanding. Their steadfast belief in me has been a source of strength throughout this journey. I am also grateful to Menghe Du for her support, patience, and presence in my life.

Acronyms

NCS networked control system

DoS denial-of-service

PID proportional-integral-derivative

MPC model predictive control

OCP optimal control problem

LTI linear time-invariant

FL feedback linearization

SMC sliding mode control

GRPI generalized robust positive invariant

ERPI extended robust positive invariant

S-C sensor-controller

C-A controller-actuator

Chapter 1

Introduction

1.1 Control Methods for Quadrotors

Quadrotors offer a wide range of applications at low costs, such as surveillance, search and rescue, mapping, package delivery, precise farming, disaster recovery, photography, etc. Quadrotors owe their popularity to their excellent maneuverability and hovering ability. Meanwhile, the complexity of tasks and the coupled and nonlinear quadrotor dynamics cast intractable challenges to the controller design.

Many control strategies are developed for quadrotors, such as proportional-integral-derivative (PID) control, feedback linearization (FL), sliding mode control (SMC), and model predictive control (MPC). Their advantages and disadvantages are discussed below. PID is widely applied for quadrotor control due to its easy implementation [1]. However, PID is a model-independent control method, so it is not robust to model uncertainties and usually requires extensive tuning. FL features nonlinearity handling, which is achieved by employing a nonlinear feedback control law such that the closed-loop system can be transformed into a linear system with a new set of state representations [2]. However, the linearization in FL requires a precise nonlinear

model, and thus the robustness of FL against model uncertainties is limited. SMC aims to steer the state to and maintain it on a sliding surface, which is a subset of state space. Then, if the controller is properly designed, the state can be kept on this sliding surface, and the system will eventually be stabilized [3]. Though SMC features robustness against both external disturbances and model uncertainties, it will mostly lead to the chattering phenomenon which deteriorates the control performance.

Compared with the aforementioned three methods, MPC is an optimization-based control method. Apart from the advantage of providing superior control performance, MPC can efficiently handle system constraints which need to be satisfied in many quadrotor applications. However, PID, FL, and SMC may lead to constraint violations, resulting in obstacle collisions, exceeding motor limits, and deviating from the task space in practice. In addition, MPC variants can provide quadrotors with strong robustness against disturbances, model uncertainties, actuator faults, etc. [4, 5].

To summarize, the pros and cons of these four control methods for quadrotors are listed in Table 1.1.

Control Methods	**Advantages**	**Disadvantages**
PID [6, 7]	model-independent	extensive tuning
FL [2, 8]	nonlinearity handling	limited robustness
SMC [3, 8]	robustness, nonlinearity handling	chattering phenomenon
MPC [4, 5]	robustness, constraint handling	heavy computational load

Table 1.1: Comparison of control methods for quadrotors.

Considering the advantages of MPC over the other three methods, we apply MPC and its variants for quadrotors in this thesis. In the next section, we will give a literature review of existing MPC methods for quadrotors.

1.2 Model Predictive Control for Quadrotors

1.2.1 The Introduction to Model Predictive Control

Before proceeding to the review of MPC schemes for quadrtors in Section 1.2.2, we briefly introduce MPC and highlight some essential MPC schemes in this section.

MPC has been a promising control scheme since the 1960s. In early explorations, MPC is studied as receding horizon control [9] or moving horizon control [10], but the essential ideas remain the same. Since then, MPC has been exhibiting the following features:

- **Optimal control input**: By interpreting the control performance indices as the cost function of an optimal control problem (OCP), MPC is able to provide the optimal control input to complete the control task.
- **State prediction**: The equations describing the dynamics are incorporated as constraints of the OCP to provide the predicted state and control input sequences, endowing MPC with abilities to tackle some critical network-induced issues such as packet dropouts and delays.
- **Constraint handling**: Since both predicted states and inputs are decision variables, the state and input constraints that usually appear in control applications can be easily satisfied by imposing these constraints on predicted states or inputs of the OCP. Moreover, the impact of model uncertainties or external disturbances can be mitigated by introducing tightened or additional constraints.

Here we provide an example to explain the aforementioned features. Consider a

constrained linear time-invariant (LTI) system

$$x_{k+1} = Ax_k + Bu_k \tag{1.1}$$

where x_k and u_k are the system state and input at time instant k, respectively. The state and input constraints can be expressed as

$$x_k \in \mathcal{X}, \quad u_k \in \mathcal{U} \tag{1.2}$$

To stabilize the system (1.1), i.e., to steer the system state to the equilibrium, the OCP of MPC can be formulated as

$$\min_{u_k} \quad V_N = \sum_{i=1}^{N-1} x_{k+i|k}^\top Q x_{k+i|k} + u_{k+i|k}^\top R u_{k+i|k} \tag{1.3a}$$

$$\text{s.t.} \quad x_{k|k} = x_k \tag{1.3b}$$

$$x_{k+i+1|k} = Ax_{k+i|k} + Bu_{k+i|k} \quad 0 \le i \le N-1 \tag{1.3c}$$

$$x_{k+i|k} \in \mathcal{X} \quad 0 \le i \le N-1 \tag{1.3d}$$

$$u_{k+i|k} \in \mathcal{U} \quad 0 \le i \le N-1 \tag{1.3e}$$

$$x_{k+N} \in \mathcal{X}_f \tag{1.3f}$$

where Q and R are weighting matrices; k is current time instant; $x_{k+i|k}$ and $u_{k+i|k}$ represent the predicted state and input at $k+i$; (1.6d), (1.6e), and (1.6f) are state, input, and terminal constraints. By solving the OCP above, the control input $u_k = u_{k|k}$ for the current time instant k can be obtained and applied to the system. It can be observed that the prediction starts from the current state, which indicates that the MPC relies on the feedback mechanism. By choosing Q and R, the balance between the control effort and the system performance can be adjusted accordingly.

To guarantee the performance of an MPC controller, it is necessary to guarantee that a feasible solution to the OCP exists at every time instant, along with closed-loop stability. These two requirements motivate the recursive feasibility and stability analysis in theoretical explorations. To guarantee feasibility, one way is to introduce a terminal set [11], in which a state feedback law can be implemented without violating the state and input constraints. Then, based on the state feedback control law, it can be proved that a feasible solution always exists. Another way is to predesign an auxiliary control law without constraint violation. A representative of this strategy is Lyapunov MPC [12, 13], in which the auxiliary control law is involved as a constraint to ensure feasibility. For the stability analysis, the optimal cost function is often chosen as the candidate Lyapunov function, because it keeps decreasing along the optimal predicted state trajectory.

In practical applications, many factors can degrade the control performance or even harm the closed-loop stability, including disturbances, actuator faults, model mismatch, communication delays, etc. Meanwhile, apart from the LTI system in (1.1), the system dynamics can be described by a generalized nonlinear system or stochastic system, which provides a more accurate description of the plant dynamics in certain cases.

Here we provide a brief review of existing robust MPC frameworks which are developed to guarantee feasibility and stability in the presence of model uncertainties and disturbances. A viable solution is tube-based MPC [14, 15, 16]. Since disturbances are not predictable, the prediction is conducted based on a nominal system without involving the disturbances. Based on the previously mentioned LTI system, a perturbed system example can be

$$x_{k+1} = Ax_k + Bu_k + \omega_k \tag{1.4}$$

where $\omega_k \in \mathcal{W}$ denotes the unknown but bounded disturbance at time instant k. The nominal system for prediction is

$$\bar{x}_{k+1} = A\bar{x}_k + B\bar{u}_k \tag{1.5}$$

To mitigate the effect of disturbances, a feedback control policy is developed based on the results of the OCP such that the deviation between the nominal system state in prediction and the actual perturbed system state can be explicitly bounded by a robust positively invariant set $\mathcal{Z}$ [17], i.e., $x_k - \bar{x}_k \in \mathcal{Z}$ for all $k \geq 0$. All possible realizations of the disturbance ω_k are considered in the design. Thus, along the state trajectory, this set serves as a tube to wrap the actual state trajectory and the nominal state trajectory. For nonlinear systems, similar invariant sets can be developed to keep the actual state within a neighborhood of the nominal state trajectory [18, 19].

In tube-based MPC, the control input is obtained when all possible realizations of disturbances are considered. Alternatively, the effect of disturbances can be mitigated when the control input is generated to stabilize the system in the worst case, which is min-max MPC. Also, min-max MPC is suitable to handle the parameter uncertainties that appear in modeling. The OCP is formulated in a min-max form, where disturbances and parameter uncertainties are chosen to maximize the cost, and the control input sequence with minimum cost will be employed. A typical formulation of min-max MPC is

$$\min_{u_k} \max_{\omega_{k:k+N-1}\in\mathcal{W}} \quad J(x_{k:k+N}, u_{k:k+N-1}, \omega_{k:k+N-1}) \tag{1.6a}$$

$$\text{s.t.} \quad x_{k|k} = x_k \tag{1.6b}$$

$$x_{k+i+1|k} = Ax_{k+i|k} + Bu_{k+i|k} + \omega_{k+i} \quad 0 \le i \le N-1 \tag{1.6c}$$

$$x_{k+i|k} \in \mathcal{X} \quad 0 \le i \le N-1 \tag{1.6d}$$

$$u_{k+i|k} \in \mathcal{U} \quad 0 \le i \le N-1 \tag{1.6e}$$

$$x_{k+N} \in \mathcal{X}_f \tag{1.6f}$$

Some representative results can be found in [20, 21]. However, the OCP in min-max form results in high computational complexity. Thus, many strategies are developed to reduce the computation burden, such as solution approximation [22], event-triggered min-max MPC [23], and self-triggered min-max MPC [24].

In MPC design for nonlinear systems, the terminal region design usually relies on the assumption that the linearized system around the equilibrium is stabilizable, which may not be satisfied in applications [25]. Moreover, how to handle the nonlinearity between the original system and the linearized one is also an intractable problem. To address these issues, Lyapunov MPC is developed for nonlinear systems [26]. Different from the tube-based MPC, the terminal constraint is discarded, and an additional constraint is introduced to characterize the decay rate of the Lyapunov function value. Specifically, the Lyapunov function value of the closed-loop system should decay faster than that under a predesigned auxiliary control law. This constraint is imposed on the first element of the predicted input sequence only, since only the first element will be applied to the plant. To guarantee feasibility, the auxiliary control law is able to stabilize the system without violating state and input constraints. In practical applications, the plant is usually a nonlinear system, thus

Lyapunov MPC is widely employed in process systems [27], unmanned aerial vehicles [13], autonomous underwater vehicles [28], etc.

The aforementioned MPC schemes give rise to various adoptions in academia and industries, which also inspire the investigation of controller design for quadrotors in this thesis.

1.2.2 Literature Review of MPC for Quadrotors

Since the dynamics of quadrotors are nonlinear and highly coupled, how to design an efficient MPC framework is challenging. Moreover, how to mitigate the effect of disturbances is still an open problem. One way is to develop a linear quadrotor model, which greatly simplifies the controller design. Firstly, the translation and attitude control is decomposed by neglecting the rotational dynamics. Then, the translational dynamic model is linearized based on the assumption that the roll, pitch, and yaw angles vary within a small range. To stabilize the linear system in the presence of disturbances, the simplest form of linear MPC can be utilized [4, 29, 30], which relies on the inherent robustness of MPC. Alternatively, well-developed robust MPC schemes, such as linear tube-based MPC, can be employed to effectively handle the disturbances [5]. Since the linear model cannot explicitly characterize the nonlinear system behavior, the nonlinear model is directly used in MPC design, and both translational and rotational dynamics are considered [31].

To improve the computation efficiency and further simplify the controller design, the dual-loop control framework is developed, as shown in Figure 1.1. Usually, four motors are installed vertically with respect to the body frame, so the attitude needs to be adjusted before moving horizontally. Meanwhile, the motor body cannot rotate against the frame, so the attitude adjustment is achieved by thrust differences among the four motors. Thus, the attitude control loop is the inner one. For quadrotor

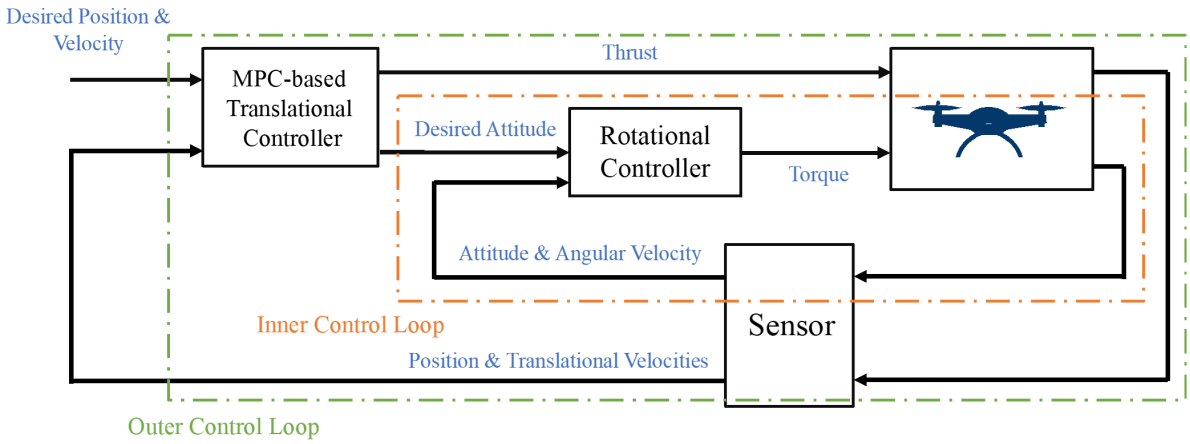

Figure 1.1: Dual-loop control scheme for quadrotors.

control, a typical strategy is to employ a simple and efficient control scheme as the inner-loop attitude controller, such as sliding mode control or PID control, while the advanced algorithm development mainly focuses on the outer-loop controller design, such as MPC. The reason behind dual-loop control is that the attitude control loop requires a higher input updating frequency than that of position control. The dual-loop scheme is applied in [32, 33, 34] and MPC controllers are designed and demonstrate inherent robustness against disturbances, such as wind gusts. To provide the stability guarantee, constraint tightening can be utilized to mitigate the effect of disturbances [35, 36]. The efficiency of robust MPC schemes for quadrotors is validated in vast applications, such as min-max MPC for tracking the moving ground vehicle [37] and tube-based MPC for load transportation [38].

In dual-loop control, most existing results assume that the sampling frequencies of the inner and outer loops are the same. On one hand, compared with the translational dynamics, the rotational dynamics should converge faster. On the other hand, the computation time of controllers in two control loops is usually different. Therefore, it is not necessary to choose the same sampling rate in dual-loop control. However, different sampling rates will greatly affect the control performance and even the sta-

bility, so how to choose the sampling rate and how the dual sampling rate affects the control performance require more investigations. In [39], for a given sampling ratio of two control loops, a sufficient condition for finding the minimum sampling frequency is provided. Also, a similar minimum sampling rate is given to ensure the closed-loop stability of a multi-rate quadrotor control framework with three control loops [40]. However, how control performance varies for different choices of dual sampling rates is still an open problem.

1.3 Networked Quadrotor Control Systems

1.3.1 Networked Control for Quadrotors

The fast dynamic of the quadrotor requires high computation speed, i.e., the control input needs to be generated and employed with high frequency. Meanwhile, due to the limited payload of quadrotors, the onboard devices cannot afford heavy computational load in many scenarios. Hence, a popular framework is that a ground station receives the sensor measurements from the quadrotor and provides control inputs back to the quadrotor.

An example is shown in Figure 1.2. The position, velocity, attitude, and other motion parameters are obtained from onboard sensors such as the inertia measurement unit (IMU), global positioning system (GPS), and altimeter. Then, the measurement results are sent to the ground station via the communication network. Based on these motion parameters, the controller provides the control input and transmits it to the quadrotor by the network. The quadrotor control systems under this networked framework can be considered as networked control systems (NCSs), and the quadrotor control systems may encounter the same issues as NCSs. Therefore, it is necessary to briefly introduce the existing problems in NCSs and corresponding solutions.

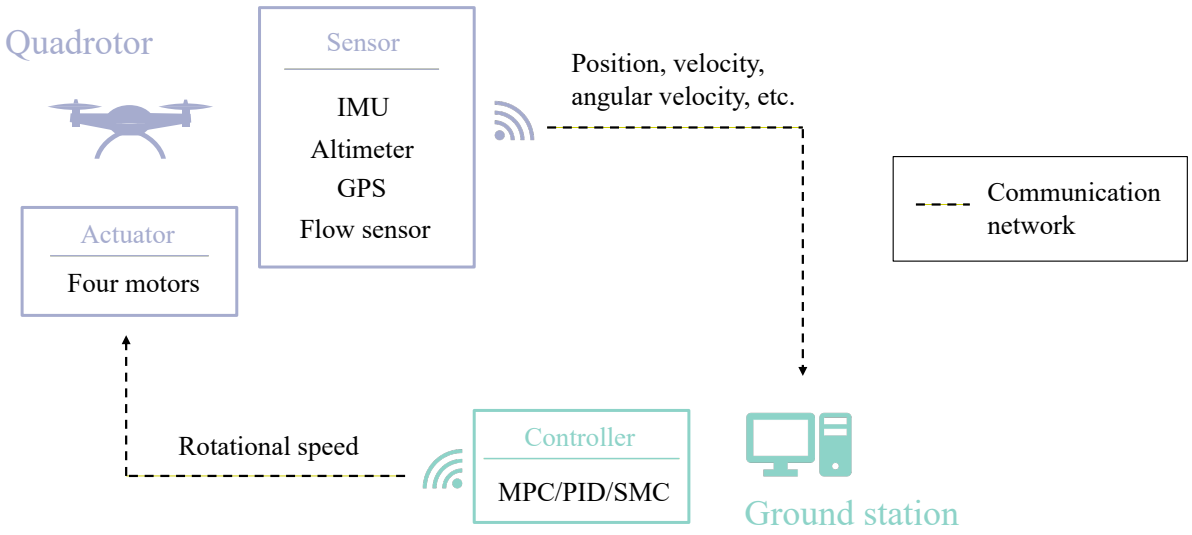

Figure 1.2: Networked quadrotor control system.

1.3.2 Existing Network-induced Issues

Networked control systems (NCSs) are defined as closed-loop control systems whose components are connected via networks [41]. With substantial developments in optimization, communication technology, and computing power, NCSs exhibit great scalability, resource reduction, easy maintenance, and diagnostics. Many applications can be found in smart grids [42], automobiles [43], teleoperations [44]. However, due to the introduction of the networked architecture, the communication channels between different components in NCSs are inherently subject to network-induced issues, which are listed as follows:

- **Network-induced delays**: In practical applications, delays always exist in the data transmissions between components of an NCS due to limited bandwidth, communication protocol, or traffic conditions. For NCSs with a single plant, there are mainly two types of delays, i.e., controller-actuator delays and sensor-controller delays [45]. The first one leads to delayed measurements of the system state or output, and the second one results in mismatches between the input

commands and system states. Thus, the control performance and the closed-loop stability are inevitably affected. To address this problem, many strategies are proposed, and some representative ones are discussed below. Based on the known or partially known dynamic model, a predictor can be developed to estimate the current state in the presence of delays [46]. Alternatively, a buffer can be utilized on the actuator side to store the most recent control signal [47]. To simplify the derivation of the stability criterion, the NCS subject to delays can be described by a model with the augmented state [48]. Moreover, the upper bound of delays that a controller can tolerate also draws significant attention [49]. For multi-agent system control, the existence of communication delays between agents is also an intractable problem. In addition to the stability issue of each agent, the connectivity of the multi-agent network can also be destroyed [50]. To address these delay-related problems in NCSs, delays are usually assumed to be upper-bounded. MPC [51], SMC [52], and other methods can be adopted to handle these delay-related issues.

- **Packet dropouts**: Since the network links all components in NCSs, the nature of the network mechanism determines that all information is transmitted discretely in terms of packets. Under certain traffic conditions, the packet may be lost in transmissions. If there is no handshake mechanism, the transmitter has no information about which packet is lost during transmissions, and consequently, the lost packets will not be sent again, which is different from delays. Fortunately, many strategies have been developed to handle packet dropouts. Due to the random features of packet dropouts, packet dropouts are usually assumed to be a Bernoulli process [53, 54] or a Markov process [55, 56]. In NCSs, packet dropouts may happen in the controller-actuator and sensor-controller channels. The first case means the packet dropouts occur when the controller

transmits control inputs to the actuator, and a typical solution is to compensate for lost control inputs [53]. The second results in intermittent measurements of state or system outputs, and how to stabilize the system is a major concern. An effective solution is to utilize an observer to estimate state, such as Luenburger observer [57] and Kalman filter [58]. Moreover, the packet dropout may happen simultaneously in both controller-actuator and sensor-controller channels, which is even more intractable [59].

- **Security issues**: Another concern that emerges in the applications of NCSs is the security issue, which jeopardizes closed-loop stability and further control performance [60]. The primary cause of the security issue is that the network connections are vulnerable to malicious attacks, which aim to tamper or block the data transmission between the transmitter and receiver, and further affect the system behavior. There are mainly two types of attack, the denial-of-service (DoS) attack and the deception attack. When a DoS attack is launched, the transmission of control and measurement data packets will be interrupted, which results in packet losses. Since the system model and transmitted signals are not necessary to be known for DoS attackers, the DoS attack is easier to initiate compared with the deception attack [61]. The deception attack endeavors to tamper with the signals sent through the communication channels and further affects the control performance [62]. A typical deception attack is the false data injection (FDI) attack. Based on the knowledge of the control system, especially the plant model and the data transmission protocol, false data is generated and injected into the control or measurement signal. In this way, the performance of the control system is degraded and the security is inevitably affected. Though the prerequisites of launching the FDI attack are much more demanding than that of the DoS attack, the FDI attack is harder to detect and defend [60].

Consequently, significant efforts have been devoted to the attack design and the resilient controller design respectively. The combat between them seems endless, and the techniques to improve system resilience are yet worth investigating.

The above-mentioned issues will degrade the control performance or even lead to instability. On the one hand, classical control solutions that tackle the uncertainties including disturbances and model uncertainties are no longer viable when the delay, packet dropout, and attack in NCSs appear. On the other hand, network-induced issues in NCSs cannot be addressed by information technology and network security solutions alone. Thus, new control strategies need to be developed for these exclusive problems in NCSs. In this thesis, we focus on how to mitigate the effect of packet dropouts, especially for networked quadrotor control systems. Thus, it is necessary to discuss the existing solutions to handle packet dropouts.

1.3.3 Model Predictive Control for Network-induced Packet Dropouts

Since the quadrotor control system can be regarded as an NCS when sensor measurements and control inputs are transmitted via communication networks, the packet dropouts in NCSs also exist in networked quadrotor control systems [63, 64], which are caused by not only the adverse network conditions but also the malicious DoS attacks [61]. On the one hand, conventional closed-loop control strategies usually require continuous measurement of the system output, which cannot be guaranteed when packet dropouts occur in the sensor-controller (S-C) channel. On the other hand, no continuous control input can be received by the actuator when packet dropouts exist in the controller-actuator (C-A) channel. Thus, how to stabilize the system in the presence of packet dropouts in both S-C and C-A channels is a challenging problem, especially for systems with unmeasurable states.

In early solutions to handle packet dropouts, the state or output feedback controller design is a popular trend [65, 66]. Though the closed-loop system in the presence of packet dropouts can be formulated in different forms, such as switched systems, Markov jump systems, and asynchronous dynamical systems, the essential ideas are similar. A typical solution is to derive the stability conditions described by linear matrix inequalities (LMIs) which can then be solved by well-developed LMI algorithms to obtain proper control parameters [41, 67, 68]. By following this framework, [69] gives the maximum packet dropout rate that the closed-loop system can tolerate. Alternatively, the intermittent observation from the lossy S-C channel can be regarded as the sensor fault and addressed by the interaction multiple model approach [70]. The packet dropout problem is also investigated from the perspective of escape time which describes the minimum time for estimation error to leave a specific region [71]. However, the constraints commonly arise in practical applications, such as the actuator saturation and limited task space, which cannot be efficiently handled by the aforementioned control strategies.

Nowadays, among all control schemes for NCSs to tackle packet dropouts, MPC has been gaining significant popularity in practical applications. Owing to the prediction feature, MPC can effectively and efficiently handle the packet dropout in NCSs. Specifically, as shown in [72], by employing a buffer on the actuator side, the predicted control input sequence from MPC can be stored for potential usage when packet dropout happens. This idea is widely utilized in handling the data loss in linear systems [53, 59, 73, 74], nonlinear systems [75], and fuzzy systems [76]. Moreover, the state and input constraints can be satisfied with guarantees by embedding them into the MPC optimization problem [59, 74, 76, 77]. Thus, MPC is widely applied in NCSs to provide promising control solutions to address network-induced packet dropouts.

When it comes to NCSs that have unmeasurable states and are subject to packet dropouts in the S-C channel, existing state feedback MPC strategies cannot be adopted. How to utilize intermittent output measurement to regulate the state in MPC design is yet challenging. An effective solution is to utilize the Luenburger observer or its variants to estimate the state. Then, the estimation result is incorporated in the MPC optimization problem to stabilize the system [56, 57], in which only input or state constraint is considered. Another choice of the observer is the Kalman filter, which is a well-developed method to estimate the state in the presence of random measurement loss [58, 78, 79]. The effectiveness of the Kalman-filter-based output feedback MPC scheme is also demonstrated in [54], but the proposed scheme needs to assume that the plant is Lyapunov stable. Apart from observer-based methods, dynamic output feedback MPC solutions are also employed to handle the packet dropout, in which involved MPC parameters are updated online [77]. However, the state constraint is still not considered in [77]. In all the above-mentioned results, the packet dropout is modeled by a Bernoulli or Markov process, and only the chance constraint on the state or the hard constraint on the input is considered. Table 1.2 summarizes the above-mentioned MPC solutions for packet dropouts.

Existing results	**Lossy channels**		**Unmeasurable state**	**Constraint type**	
	C-A	S-C		Input	State
[53]	✓			✓	
[76]	✓	✓		✓	
[75, 74, 59]	✓	✓		✓	✓
[77]		✓	✓	✓	
[57]		✓	✓		✓
[80]		✓	✓	✓	✓
[56]	✓		✓	✓	
[54]	✓	✓	✓	✓	

Table 1.2: Existing MPC schemes for NCSs subject to packet dropouts.

To fulfill both state and input constraints in the presence of packet dropouts in

the S-C channel, in [80], an output feedback MPC scheme is proposed to stabilize a constrained NCS with intermittent output measurements. Invariant sets are used to characterize the estimation error and facilitate the constraint tightening for constraint satisfaction. In this work, the packet dropouts are assumed to occur periodically in the S-C channel; however, most often, they occur randomly in both C-A and S-C channels. Thus, it is still intractable to guarantee both state and input constraint satisfaction when both S-C and C-A channels are subject to random packet dropouts and the system is affected by external disturbances.

1.4 Motivations and Contributions

Aiming at stabilizing a networked quadrotor control system subject to packet dropouts in S-C and C-A channels and satisfying both state and input constraints, we propose a robust output feedback MPC framework, which consists of a state observer and a state feedback model predictive controller. With the help of the designed observer, the estimation error dynamics can be formulated as a switched system. To provide the explicit bound of the estimation error, a generalized robust positive invariant (GRPI) set is developed based on the switched system formulation, in which all possible realizations of bounded disturbances and packet dropouts are considered. Similarly, an extended robust positive invariant (ERPI) set is constructed to confine the error between the predicted state and the actual state. Further, by utilizing the GRPI and ERPI sets, tightened constraints are imposed on predicted states and inputs in the OCP to guarantee constraint satisfaction in the presence of packet dropouts and disturbances.

- An observer is proposed to estimate the state in the presence of random packet dropouts. Compared with existing probability-based methods [56, 57], the

bound of the estimation error is explicitly provided as a generalized robust positive invariant set.

- Rather than solely considering the chance constraint on the system state [57] or the hard constraint on the control input [54, 56, 77], we take both hard state and input constraints into consideration and propose a robust output feedback MPC scheme, which stabilizes the system while fulfilling both the state and input constraints.

- Recursive feasibility and closed-loop stability of the proposed control scheme are rigorously proved to be guaranteed in the presence of bounded random packet dropouts in both S-C and C-A channels.

To validate the effectiveness of different existing MPC schemes, and explore the impact of disturbances and sampling rates on quadrotor control performance, the comparison results are conducted from the following perspectives:

- The effectiveness of the nominal MPC, tube-based MPC, and Lyapunov MPC are validated on different quadrotor models. The robustness of these MPC schemes against disturbances from wind gusts is also compared.

- The control performance of three MPC schemes is compared in a trajectory tracking problem. Though prediction models are different, the generated control inputs are applied to the same nonlinear quadrotor system as the plant, in which both the rotational and translational dynamics. This setup is to mimic the control process of practical applications.

- The sampling ratio of inner and outer control loops is chosen to be different values to investigate its effect on control performance, which may guide the dual-loop controller design in the future.

1.5 Thesis Organization

The remainder of this thesis is organized as follows:

Chapter 2 proposes a robust output feedback MPC scheme for networked quadrotor control systems to tackle random packet dropouts in both S-C and C-A channels.

Chapter 3 provides the comparison studies of conventional MPC, tube-based MPC, and Lyapunov MPC for quadrotors, which evaluates and compares their effectiveness, robustness, and control performance under the dual-sampling-rate strategy.

Chapter 4 concludes the thesis and highlights potential future work.

Chapter 2

Output-feedback MPC for Networked Quadrotor Control Systems Subject to Random Packet Dropouts

2.1 Overview

As introduced in the previous chapter, MPC enjoys tremendous popularity in handling networked-induced issues, especially packet dropouts that commonly occur in networked quadrotor control systems. However, the existing results for addressing packet dropouts cannot handle the state and input constraints simultaneously when the system state is unmeasurable. In addition to the constraint handling, random packet dropouts in both S-C and C-A channels pose more challenges to the controller design.

In this chapter, aiming at stabilizing the quadrotor subject to packet dropouts

in both S-C and C-A channels and satisfying both state and input constraints, we propose a robust output feedback MPC framework, which consists of a state observer and a state feedback model predictive controller. Firstly, to provide the explicit bound of the estimation error in the presence of packet dropouts and disturbances, a generalized robust positive invariant (GRPI) set is developed, and the estimation error is confined to this set. Then, an extended robust positive invariant (ERPI) set is developed to confine the error between the predicted and estimated states. Tightened constraints that are obtained based on the GRPI and ERPI sets are imposed on predicted states and inputs in the MPC optimization problem to fulfill the state and control input constraints. The recursive feasibility and closed-loop stability are rigorously proved. Simulation results based on a two-dimensional quadrotor model are provided to validate the effectiveness of the proposed method.

Nomenclature: The notations in this chapter are fairly standard. $\mathbb{R}$ stands for real space. Symbols $\mathbb{N}$, $\mathbb{N}_{\geq 0}$, $\mathbb{N}_{>0}$ represent sets of integers, non-negative integers, and positive integers, respectively. Given two sets $\mathcal{X} \subset \mathbb{R}^n$ and $\mathcal{Y} \subset \mathbb{R}^n$, the Minkowski set addition is denoted by $\mathcal{X} \oplus \mathcal{Y} \triangleq \{x + y | x \in \mathcal{X}, y \in \mathcal{Y}\}$, while the Pontryagin set difference is defined as $\mathcal{X} \ominus \mathcal{Y} \triangleq \{z \in \mathbb{R}^n | z + y \in \mathcal{X}, \forall y \in \mathcal{Y}\}$. Given a sequence of sets $\{\mathcal{X}_i \subset \mathbb{R}^n\}$ with $a \leq i \leq b$, $i \in \mathbb{N}$, $a \leq b$, $a \in \mathbb{N}$ and $b \in \mathbb{N}$, we define $\bigoplus_{i=a}^{b} \mathcal{X}_i \triangleq \mathcal{X}_a \oplus \cdots \oplus \mathcal{X}_b$. Given a set $\mathcal{X}$ and a real matrix M with compatible dimension, $M\mathcal{X}$ refers to the set $\{Mx | x \in \mathcal{X}\}$. Given a vector $v \in \mathbb{R}^n$ and a set $\mathcal{X}$, for brevity, $\{v\} \oplus \mathcal{X}$ is written as $v \oplus \mathcal{X}$. A continuous function $\alpha : [0, a) \to [0, \infty)$ is said to belong to class $\mathcal{K}$ if it is strictly increasing and $\alpha(0) = 0$. It is said to belong to class $\mathcal{K}_\infty$ if $a = \infty$ and $\alpha(r) \to \infty$ as $r \to \infty$. A continuous function β: $[0, a) \times [0, \infty) \to [0, \infty)$ is said to belong to class $\mathcal{KL}$ if, for each fixed s, the mapping $\beta(r, s)$ belongs to class $\mathcal{K}$ with respect to r, and, for each fixed r, the mapping $\beta(r, s)$ is decreasing with repect to s and $\beta(r, s) \to 0$ as $s \to \infty$. The distance between a

vector x, $x \in \mathbb{R}^n$ to a set $\mathcal{Y}$, $\mathcal{Y} \subset \mathbb{R}^n$, is denoted by $d(x, \mathcal{Y}) \triangleq \inf_{y \in \mathcal{Y}} ||x - y||$. $\mathcal{B}^n$ stands for the unit hyperball with dimension n.

2.2 Model Description

Consider the following disturbed discrete-time linear time-invariant system

$$\begin{cases} x_{k+1} = Ax_k + Bu_k + \omega_k \\ y_k = Cx_k + v_k \end{cases} \tag{2.1}$$

where $x_k \in \mathbb{R}^{n_x}$, $u_k \in \mathbb{R}^{n_u}$, $y_k \in \mathbb{R}^{n_y}$, $\omega_k \in \mathbb{R}^{n_x}$, and $v_k \in \mathbb{R}^{n_y}$ are the state, control input, output, unknown disturbance, and unknown sensor noise at time instant k, respectively. The state and the control input constraints are

$$x_k \in \mathcal{X} \subseteq \mathbb{R}^{n_x}, \quad u_k \in \mathcal{U} \subseteq \mathbb{R}^{n_u}, \quad \forall k \in \mathbb{N}_{\geq 0} \tag{2.2}$$

Meanwhile, the disturbance ω_k and sensor noise v_k are bounded by sets $\mathcal{W} \subset \mathbb{R}^{n_x}$ and $\mathcal{V} \subset \mathbb{R}^{n_y}$, respectively. $\mathcal{X}$, $\mathcal{U}$, $\mathcal{W}$, and $\mathcal{V}$ are compact sets including the origin as an interior point. Here, the quadrotor model is obtained based on the symmetric structure of the quadrotor, and the translational dynamics in two vertical planes are decomposed based on a small-angle assumption. More details of the modeling process can be found in Chapter 3. The utilization of the linear quadrotor model can be found in [4, 29, 5].

To address the random packet dropouts, external disturbances, and sensor noise, an output feedback MPC scheme is proposed as shown in Figure 2.1. The controller and the sensor are connected by a communication network, where the measurement dropout occurs randomly. In order to characterize the packet loss and design an observer, an assumption is needed:

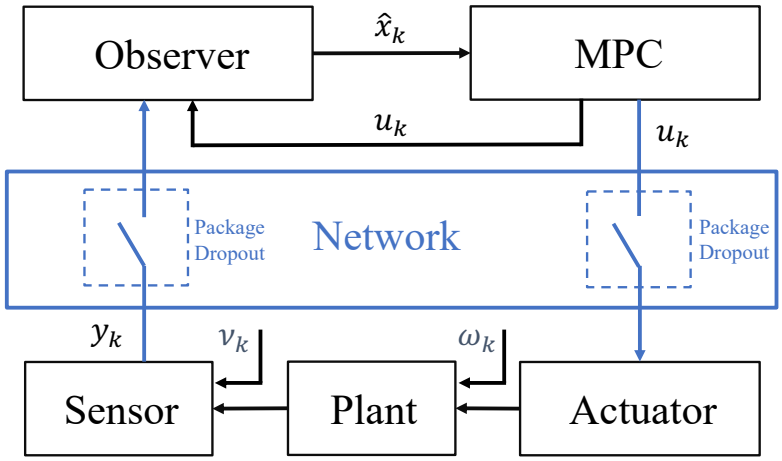

Figure 2.1: Output feedback MPC scheme.

Assumption 1: The maximum length of consecutive dropouts in the sensor-controller channel is T, and the minimum length of consecutive measurement is τ, where $T \in \mathbb{N}_{>0}$, and $\tau \in \mathbb{N}_{>0}$.

Remark 1: In the literature, random packet dropouts are usually modeled by i.i.d. Bernoulli processes with a probability p [53, 54, 57, 59, 77], or a time-homogeneous binary Markov process with certain transition probabilities [55, 56, 81, 82, 83]. The i.i.d. Bernoulli process can be regarded as a special case of the time-homogeneous Markov process, and consequently, the Markov process is more general. The time-homogeneous Markov process for describing the random packet dropout has the following properties [55]:

$$\mathbf{Pr}\{k_{i+1} - k_i = j\} = \begin{cases} q & \text{if } j = 1 \\ (1-q)(1-p)p^{j-2} & \text{if } j \geq 2 \end{cases} \tag{2.3}$$

where $\mathbf{Pr}\{\Omega\}$ stands for the probability of an event Ω. $k_i \in \mathbb{N}_{\geq 0}$ stands for ith time instant that there is no packet dropout. p and q are real numbers between 0 and 1. More details can be found in [55]. j can be regarded as the event of $j-1$ consecutive dropouts. From Eq. (2.3), it can be observed that, as j increases, the probability of

such an event keeps decreasing, which relates to the probability of $j-1$ consecutive measurements. Thus, by proper approximations, the assumption described by the Markov process can be converted to the upper bound of the dropouts in *Assumption 1*. A similar approximation can be found in [84]. Also, the periodic packet dropout assumption in [80], which is a type of assumption that differs from the probability-based assumption, is a special case of *Assumption 1*.

2.3 Observer Design

Consider a Luenberger observer with the following form:

$$\begin{cases} \hat{x}_{k+1} = A\hat{x}_k + Bu_k + L(\hat{y}_k - y_k) \\ \hat{y}_k = C\hat{x}_k \end{cases} \tag{2.4}$$

where $\hat{x}$ is estimated state and L is the observer gain that needs to be designed. However, consecutive measurements of output y_k can not be guaranteed due to random packet dropouts. Thus, instead of achieving the convergence of the estimation error, our objective is to confine the estimation error in an invariant set. When the output measurement is not available due to packet dropouts, the estimation process becomes:

$$\begin{cases} \hat{x}_{k+1} = A\hat{x}_k + Bu_k \\ \hat{y}_k = C\hat{x}_k \end{cases} \tag{2.5}$$

By combining Eq. (2.4) and Eq. (2.5) according to the occurrence of packet dropouts, the observer is designed as follows to estimate the state in the presence of random

packet dropouts:

$$\begin{cases} \hat{x}_{k+1} = A\hat{x}_k + Bu_k + L(C\hat{x}_k - y_k) & \text{if } y_k \text{ is measurable} \quad (2.6a) \\ \hat{x}_{k+1} = A\hat{x}_k + Bu_k & \text{if } y_k \text{ is not measurable} \quad (2.6b) \end{cases}$$

Define the estimation error at time instant k as $e_k \triangleq x_k - \hat{x}_k$. The error dynamics can be obtained by subtracting Eq. (2.6) from Eq. (2.1).

$$\begin{cases} e_{k+1} = A_1 e_k + \omega_{1,k} & \text{if } y_k \text{ is measurable} \quad (2.7a) \\ e_{k+1} = A_2 e_k + \omega_{2,k} & \text{if } y_k \text{ is not measurable} \quad (2.7b) \end{cases}$$

where $A_1 \triangleq A + LC$, $A_2 = A$, $\omega_{1,k} = \omega_k + Lv_k$, and $\omega_{2,k} = \omega_k$. Disturbances $\omega_{1,k}$ and $\omega_{2,k}$ are bounded by

$$\omega_{1,k} \in \mathcal{W}_1 \triangleq \mathcal{W} \oplus L\mathcal{V} \quad (2.8)$$

$$\omega_{2,k} \in \mathcal{W}_2 \triangleq \mathcal{W} \quad (2.9)$$

respectively. Though the system matrix A_2 may not be stable, bounding the estimation error can be achieved by choosing proper values of A_1 since the estimation error evolves by two dynamic equations in (2.7a) and (2.7b). Thus, Eq. (2.7a) and Eq. (2.7b) can be regarded as two subsystems of a switched system, which can be rewritten as

$$e_{k+1} = A_{\sigma(k)} e_k + w_{\sigma(k),k} \quad (2.10)$$

where $\sigma(k) : \mathbb{N}_{\geq 0} \to \{1, 2\}$ is a time-dependent switching signal representing the activated subsystem at time instant k. The switching sequences, $\{\sigma(0), \sigma(1), \sigma(2), \ldots, \sigma(k), \ldots\}$, are unknown *a priori*, but are known instantly when the switching happens. k_n, $n \in \mathbb{N}_{\geq 0}$, denotes switching instants, which are the time instants when a subsystem is

switched to another subsystem. When $k \in [k_n,\, k_{n+1})$, the system matrix of the subsystem is $A_{\sigma(k_n)}$. Based on the notations above, *Assumption 1* can be expressed as: if $\sigma(k_n) = 1$, $k_{n+1} - k_n \geq \tau$; if $\sigma(k_n) = 2$, $k_{n+1} - k_n \leq T$.

To compute the invariant set for the dynamic system (2.10), we define the *admissible* switching sequence as below, which satisfies *Assumption 1*:

Definition 1: An admissible switching sequence of the system (2.10), $\xi_{[\tau,T]}(k) \triangleq \{\sigma(0),\, \sigma(1),\, \ldots,\, \sigma(k-1)\}$, with switching instants $k_0,\, k_1,\, \ldots, k_n$, satisfies

$$k_{n+1} - k_n \geq \tau \qquad \text{if } \sigma(k_n) = 1 \tag{2.11}$$

$$k_{n+1} - k_n \leq T \qquad \text{if } \sigma(k_n) = 2 \tag{2.12}$$

for all $n \in \mathbb{N}_{\geq 0}$. $\Xi_{[\tau,T]}$ is defined as the set containing all admissible switching sequences for given τ and T.

Remark 2: To explain the definition of the admissible switching sequence, several examples are provided here. Suppose $\tau = 2$ and $\bar{T} = 3$, then, for the system (2.10), $\xi_{[2,3]}(7) = \{1,\, 1,\, 2,\, 2,\, 2,\, 1,\, 1\}$ is an admissible sequence. However, $\bar{\xi}_{[2,3]}(7) = \{1,\, 1,\, 2,\, 2,\, 2,\, 2\}$ is not admissible because $k_2 - k_1 > \bar{T}$ and thus the constraint (2.12) is violated. Note that $\xi_{[\tau,\bar{T}]}(k)$ for any k less than τ is also not an admissible sequence.

Similar to [85], a *phase* is defined as the interval composed of the running time of subsystem (2.7a), and a jointed running time of subsystem (2.7b), which is illustrated in Figure 2.2. The initial instant of the p-th phase is represented by k_{s_p}. Before the initial instant of the first phase, k_{s_1}, a dwell time of subsystem (2.7b) satisfying (2.12) may exist.

The objective of observer design is to describe all possible estimation errors by certain sets with the existence of disturbances and random dropouts. After formulating the estimation error dynamics as a switched system and developing basic concepts

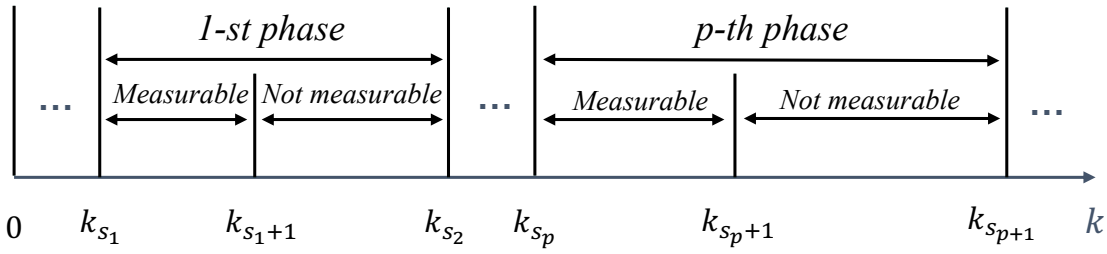

Figure 2.2: Illustration of phases.

to describe the switched system in the last section, it becomes possible to utilize the invariant set to describe the estimation error if the observer gain L satisfies certain conditions. The invariant set is defined below.

Definition 2: A set $\mathcal{O} \subseteq \mathbb{R}^n$ is said to be a generalized robust positive invariant (GRPI) set for system (2.10) with constraints (2.11) (2.12), if $e_0 \in \mathcal{O}$ implies $e_k \in \mathcal{O}$ for every admissible sequence $\xi_{[\tau,T]}$ and for every allowable disturbance sequence.

For brevity, we define two sets $\Theta_1 \triangleq \{\tau, \tau+1, \ldots, 2\tau-1\}$, $\Theta_2 \triangleq \{0, 1, \ldots, T\}$. To develop the stability theorem of the switched system, we describe the system (2.10) as the perturbed switched system, and the system

$$\bar{e}_{k+1} = A_{\sigma(k)}\bar{e}_k \tag{2.13}$$

as the nominal switched system, where the system matrices of two systems are identical. To describe the stability of switched systems, the following definitions are required. For the nominal switched system, we have

Definition 3: System (2.13) is globally uniformly asymptotically stable (GUAS) under certain switching signals σ if for initial condition e_0, there exists a class of $\mathcal{KL}$ function β such that the solution of the system in (2.13) satisfies the inequality $||e_k|| \leq \beta(||e_0||, k)$, $\forall k \in \mathbb{N}_{\geq 0}$.

For the perturbed switched system, the stability is defined as

Definition 4: System (2.10) is globally robustly uniformly asymptotically stable (GRUAS) under certain switching signals σ if for all $k \in \mathbb{N}_{\geq 0}$, $d(e_k, \mathcal{O}) \leq \kappa(d(e_0, \mathcal{O}))$ and $d(e_k, \mathcal{O}) \to 0$ as $k \to \infty$, where $\kappa \in \mathcal{K}_\infty$.

The distance between the state and the GRPI set also reveals the stability of a perturbed switched system:

Definition 5: A GRPI set $\mathcal{O} \subseteq \mathbb{R}^n$ is said to be GUAS for system (2.10) with constraints (2.11) (2.12), if for all $k \in \mathbb{N}_{\geq 0}$, $d(e_k, \mathcal{O}) \leq \kappa(d(e_0, \mathcal{O}))$ and $d(e_k, \mathcal{O}) \to 0$ as $k \to \infty$, where $\kappa \in \mathcal{K}_\infty$.

To guarantee the convergence of the estimation error, we start by analyzing the stability of switched systems (2.10) and (2.13).

Theorem 1: System (2.13) is GUAS if and only if system $\hat{q}_{i+1} = \hat{A}\hat{q}_i$ is asymptotically stable under arbitrary switching signals, where $\hat{A} \in \mathcal{A}_{\tau,T} \triangleq \{A_2^\beta A_1^\alpha, \alpha \in \Theta_1, \beta \in \Theta_2\}$.

Proof. Necessity: The state evolution between initial instants of two consecutive phases is

$$e_{s_{p+1}} = A_2^\beta A_1^\alpha e_{s_p} \tag{2.14}$$

where $\alpha \in \Theta_1$, $\beta \in \Theta_2$, which is align with system $\hat{q}_{k+1} = \hat{A}\hat{q}_k$. Since system (2.13) is GUAS, there exists a $\mathcal{KL}$ function f such that the solution of system (2.13) satisfies $||e_k|| \leq f(||e_0||, k)$, $\forall k \in \mathbb{N}_{\geq 0}$. Thus, $||e_{s_p}|| \leq f(||e_{s_0}||, p)$, $\forall k \in \mathbb{N}_{\geq 0}$, which means $||\hat{q}_i|| \leq f(||\hat{q}_0||, i)$, $\forall i \in \mathbb{N}_{\geq 0}$. It implies that system $\hat{q}_{i+1} = \hat{A}\hat{q}_i$ is asymptotically stable under arbitrary switching signals.

Sufficiency: The asymptotical stability under arbitrary switching indicates that there exists a $\mathcal{KL}$ function g such that $||e_{s_p}|| \leq g(||e_{s_0}||, p)$. Though the length of an actual

phase can be infinite, an actual phase can be regarded as a sequence of phases with finite lengths, no longer than $T+(2\tau-1)$. Due to the fact that $||e_k||$, $k \in [k_{s_p}, k_{s_{p+1}}]$, are bounded, there also exists a $\mathcal{KL}$ function g' for the solution of system (2.13) such that $||e_k|| \leq g'(||e_0||, k)$, $\forall k \in \mathbb{N}_{\geq 0}$. □

Based on Theorem 1, the relation between the existence of the invariant set and the stability of a switched system is revealed by the following theorem.

Theorem 2: Consider the swtiched system in (2.10) with an admissible switching sequence set $\Xi_{[\tau,T]}$. The following two statements are equivalent:

a) The switched system in (2.13) is GUAS with $\xi_{[\tau,T]} \in \Xi_{[\tau,T]}$.

b) A GRPI set $\mathcal{O}_{[\tau,T]}$ exists for system (2.10).

Proof. Proof of (a) ⇒ (b): For the system (2.10), let $\mathcal{O}_v$ be the set of the initial state of v-th phase. Consider sets of the state at two initial instants of two consecutive phases

$$\mathcal{O}_{v+1} \triangleq co\{A_2^\beta A_1^\alpha \mathcal{O}_v \oplus \bigoplus_{i=0}^{\alpha-1} A_2^\beta A_1^i \mathcal{W}_1 \oplus \bigoplus_{j=0}^{\beta-1} A_2^j \mathcal{W}_2 : \alpha \in \Theta_1, \beta \in \Theta_2\}$$

where $\mathcal{O}_0$ is $\Lambda \triangleq co\left\{\bigoplus_{\beta=0}^{T-1} A_2^\beta \mathcal{W}_2\right\}$ or $\{0\}$. When $\mathcal{O}_0 = \Lambda$, it means there exist consecutive dropouts satisfying (2.12) before the first phase. Let $\mathcal{R} \triangleq co\{\bigoplus_{i=0}^{\alpha-1} A_2^\beta A_1^i \mathcal{W}_1 \oplus \bigoplus_{j=0}^{\beta-1} A_2^j \mathcal{W}_2 : \alpha \in \Theta_1, \beta \in \Theta_2\}$. $\mathcal{O}_{v+1}$ satisfies

$$\mathcal{O}_{v+1} \subseteq co\left\{A_2^\beta A_1^\alpha \mathcal{O}_v \oplus \mathcal{R} : \alpha \in \Theta_1, \beta \in \Theta_2\right\} \tag{2.15}$$

Iterating from v to 0 yields

$$\mathcal{O}_v \subseteq \Phi_v \triangleq co\{A_2^{\beta_h}A_1^{\alpha_h}A_2^{\beta_m}A_1^{\alpha_m}\dots A_2^{\beta_n}A_1^{\alpha_n}A_2^{\beta_k}A_1^{\alpha_k}\mathcal{O}_0 \oplus A_2^{\beta_h}A_1^{\alpha_h}A_2^{\beta_m}A_1^{\alpha_m}\dots A_2^{\beta_n}A_1^{\alpha_n}\mathcal{R}\oplus\dots\oplus A_2^{\beta_h}A_1^{\alpha_h}\mathcal{R}\oplus\mathcal{R}: \alpha_d\in\Theta_1, d\in\mathbb{N}_{[1,v]}, \beta_b\in\Theta_2, b\in\mathbb{N}_{[1,v]}\}$$

Since the system (2.13) is GUAS, the system $\hat{q}_{k+1} = \hat{A}\hat{q}_k$ is asymptotically stable under arbitrary switching, where $\hat{A}\in\mathcal{A}_{\tau,T}\triangleq\{A_2^{\beta}A_1^{\alpha}, \alpha\in\Theta_1, \beta\in\Theta_2\}$. Therefore, there exists a constant $\epsilon\in(0,1)$ and $\eta>0$ satisfying $\mathcal{R}\subseteq\eta\mathcal{B}^n$ such that $\hat{A}\mathcal{R}\subseteq\eta\epsilon\mathcal{B}^n$. Note that $\Lambda\subseteq\mathcal{R}\subseteq\eta\mathcal{B}^n$. Then

$$\mathcal{O}_v\subseteq\Phi_v\subseteq\eta(\epsilon^n+\epsilon^{n-1}+\dots+\epsilon+1)\mathcal{B}^n \tag{2.16}$$

where $n=v$ when $\mathcal{O}_0=\Lambda$, or $n=v-1$ when $\mathcal{O}_0=\{0\}$. Eqn. (2.15) and (2.16) imply that $\mathcal{O}_v\subseteq\mathcal{O}_{v+1}$, and $\mathcal{O}_v$ is bounded by $(\eta/(1-\epsilon))\mathcal{B}^n$ as $v\to\infty$. Therefore, for the system (2.10), when $e_0\in\mathcal{O}_{[\tau,T]}\triangleq\mathcal{O}_\infty$, $e_k\in\mathcal{O}_{[\tau,T]}$ always holds for system under any admissible switching sequence $\xi_{[\tau,T]}$.

Proof of (b) $\Rightarrow$ (a): The existence of the invariant set $\mathcal{O}_{[\tau,T]}$ implies that

$$A_2^{\beta}A_1^{\alpha}\mathcal{O}_{[\tau,T]}\subset\mathcal{O}_{[\tau,T]} \tag{2.17}$$

for all $\alpha\in\Theta_1$ and $\beta\in\Theta_2$.

Consequently, for any $\epsilon>0$ satisfying $\mathcal{O}_{[\tau,T]}\subseteq\epsilon\mathcal{R}^n$, there always exists a $\delta>0$ satisfying $\delta\mathcal{R}^n\in\mathcal{O}_{[\tau,T]}$ and $A_1^{\alpha}\delta\mathcal{R}^n\in\mathcal{O}_{[\tau,T]}$ for all $\alpha\in\{0,1,\dots,\tau-1\}$, such that for the nominal switched system (2.13), $\forall\bar{e}_0\in\delta\mathcal{R}_n$, $\bar{e}_k\in\epsilon\mathcal{R}^n$. When ϵ is chosen as $\{\epsilon\mathcal{R}^n\cap\mathcal{O}_{[\tau,T]}\}\neq\mathcal{O}_{[\tau,T]}$, there always exists a $\delta>0$ and a $\lambda\in(0,1)$ satisfying $\delta\mathcal{R}^n\subseteq\lambda\mathcal{O}_{[\tau,T]}$ and $A_1^{\alpha}\lambda\mathcal{O}_{[\tau,T]}\subseteq\epsilon\mathcal{R}^n$ for all $\alpha\in\{0,1,\dots,\tau-1\}$, such that $\forall\bar{e}_0\in\delta\mathcal{R}_n$,

$\bar{e}_k \in \epsilon\mathcal{R}^n$, according to (2.17).

In general, it is proved that for any $\epsilon > 0$, there always exists a $\delta > 0$, such that for all initial state of the system (2.13) satisfying $\bar{e}_0 \in \delta\mathcal{R}^n$, $\bar{e}_k \in \epsilon\mathcal{R}^n$ for all $k \geq 0$. Thus, the system (2.13) is stable.

Then, we will prove that for the arbitrary initial state $\bar{e}_0$, $\bar{e}_k \to 0$ as $k \to \infty$. According to (2.17), there exists a $\mu \in (0, 1)$ such that $\hat{A}\mathcal{O}_{[\tau,T]} \in \mu\mathcal{O}_{[\tau,T]}$. Thus, for the admissible switching sequence $\xi_{[\tau,T]}$, the state at time k can be expressed as $\bar{e}_k = \hat{A}^n\bar{e}_0$, where n is the number of phases. There exists a $\gamma \geq 0$ satisfying $\bar{e}_0 \in \gamma\mathcal{O}_{[\tau,T]}$. Thus, $\bar{e}_k \in \mu^n\gamma\mathcal{O}_{[\tau,T]}$. The length of instants that are not incorporated in a single phase is no longer than τ, so there exists a $\rho \in (0, \infty)$ such that $\forall k \in [k_{s_n}, k_{s_{n+1}})$, $\bar{e}_k \in \rho\mu^n\gamma\mathcal{O}_{[\tau,T]}$. When $n \to \infty$, $\rho\mu^n\gamma\mathcal{O}_{[\tau,T]} \to \{0\}$, which implies that $\forall\hat{e}_0$, $\hat{e}_k \to 0$ as $k \to \infty$. System (2.13) is GUAS. □

It is proved that the global uniform asymptotical stability of the nominal switched system (2.13) is equivalent to the existence of the invariant set for the perturbed switched system (2.10). Thus, according to Definition 4, system (2.10) is GRUAS, which is the third equivalent statement.

An algorithm is provided to compute the GRPI set for the switched system (2.10) with switching instants constraints (2.11) and (2.12):

Algorithm 1: GRPI set $\mathcal{O}_\infty$ algorithm.

Input: T, τ, A_1, A_2, $\mathcal{W}_1$, $\mathcal{W}_2$, $\mathcal{O}_0$;

Initialization: $v = 0$;

while $\mathcal{O}_{v+1} \neq \mathcal{O}_v$ **do**

$\mathcal{O}_{v+1} = co\{A_2^\beta A_1^\alpha \mathcal{O}_v \oplus \bigoplus_{i=0}^{\alpha-1} A_2^\beta A_1^i \mathcal{W}_1 \oplus \bigoplus_{j=0}^{\beta-1} A_2^j \mathcal{W}_2 :$

$\alpha \in \Theta_1, \beta \in \Theta_2\}$;

$v = v + 1$;

end

$\mathcal{O}_\infty = \mathcal{O}_v$;

Output: $\mathcal{O}_\infty$

Remark 3: While designing the observer, i.e., choosing the proper value of observer

gain L, it is not convenient to verify the stability of the switched system. However, it is possible to verify the existence of the invariant set by utilizing the GRPI set algorithm. If $\mathcal{O}_\infty$ is obtained, the perturbed switched system is GRUAS based on Theorem 2.

However, set $\mathcal{O}_{[\tau,T]}$ only describes the estimation error e_k for system (2.10) with admissible switching sequences. To incorporate the sequences that are not admissible, we develop the following corollary:

Corollary 1: There exists a set $\mathcal{E}_{[\tau,T]}$

$$\mathcal{E}_{[\tau,T]} \triangleq co\left\{ A^j \mathcal{O}_{[\tau,T]} \oplus \bigoplus_{i=0}^{j} A^i \mathcal{W}_1,\ j \in \{0, 1, \ldots, \tau - 1\} \right\} \tag{2.18}$$

such that $\forall k \in \mathbb{N}_{\geq 0}$, $e_k \in \mathcal{E}_{[\tau,T]}$, if and only if system (2.10) is GRUAS.

2.4 Robust Output Feedback MPC Design

When the packet dropout happens in the C-A channel, the actuator will not receive any control input from the controller. To tackle this problem, the control input sequence after solving the optimal control problem will be sent to and stored in the actuator. To ensure the continuity of control actions on the actuator side, the input from the previously stored input sequence is employed when communication between the controller and actuator interrupts. Meanwhile, a robust MPC scheme and the corresponding algorithm are provided with rigorous proofs of feasibility and stability.

2.4.1 Bounding the Estimation and Control Errors

Since the state is not measurable, a robust model predictive controller is designed to stabilize the observer system. The estimated state evolution in (2.6) can be written

as

$$\begin{cases} \hat{x}_{k+1} = A\hat{x}_k + Bu_k + d_k \\ \hat{y}_k = C\hat{x}_k \end{cases} \tag{2.19}$$

where

$$d_k = \begin{cases} L(\hat{y}_k - y_k) = -LCe_k - Lv_k & \text{if } y_k \text{ is measurable} \\ 0 & \text{if } y_k \text{ is not measurable} \end{cases} \tag{2.20}$$

and d_k is regarded as the *artificial disturbance* [15], which incorporates the estimation error and the sensor noise. The nominal system for prediction is,

$$\bar{x}_{k+i+1|k} = A\bar{x}_{k+i|k} + B\bar{u}_{k+i|k} \tag{2.21}$$

where $i \in \{0, 1, \ldots, N-1\}$ and N is the prediction horizon. $\bar{x}_{k+i|k}$ denotes predicted states obtained at time k.

The proposed observer design confines the estimation error e_k to the set $\mathcal{E}_{[\tau,T]}$, i.e., $e_k \in \mathcal{E}_{[\tau,T]}$, $\forall k \geq 0$. Thus, the artificial disturbance set $\mathcal{D}$ can be obtained:

$$\mathcal{D} = -LC\mathcal{E}_{[\tau,T]} - L\mathcal{V} \tag{2.22}$$

Similar to the tube-based MPC design in [15], the control input is designed as

$$u_k = \bar{u}_{k|k} + K\tilde{e}_k \tag{2.23}$$

where $\tilde{e}_k \triangleq \hat{x}_k - \bar{x}_{k|k}$. If there is no packet dropout in the controller-actuator channel, the evolution of $\tilde{e}_k$ is

$$\tilde{e}_{k+1} = \Phi_K \tilde{e}_k + d_k \tag{2.24}$$

where $\Phi_K \triangleq A+BK$, and Φ_K is stable. Such a control law is shown to be an effective solution to cope with external disturbances in [15]. However, when the packet dropout happens, the control input u_k cannot be sent to the actuator. To address this problem, the input at the current time instant in the most recent received input sequence is employed. In general, the applied input is dependent on the communication status as

$$u_{k+p} = \begin{cases} \bar{u}_{k+p|k+p} + K(\hat{x}_{k+p} - \bar{x}_{k+p|k+p}), & \text{if } u_{k+p} \text{ is received} \\ \bar{u}_{k+p|k}, & \text{if } u_{k+p} \text{ is not received} \end{cases} \tag{2.25}$$

where $k+p$ is the current time instant and k is the last time that the optimization problem of MPC is solved. p indicates the length of the consecutive packet dropouts. Consequently, the evolution of $\tilde{e}_k$ is governed by

$$\tilde{e}_{k+1} = \begin{cases} \Phi_K \tilde{e}_k + d_k & \text{if } u_k \text{ is received} \\ A\tilde{e}_k + d_k, & \text{if } u_k \text{ is not received} \end{cases} \tag{2.26}$$

Apparently, the deviation between the nominal state and estimated state increases when packet dropouts happen. To confine $\tilde{e}_k$ to a bounded set, the following assumption is needed.

Assumption 2: The maximum length of consecutive dropouts in the sensor-controller channel is T^+, and the minimum length of consecutive measurement is τ^+, where $T^+ \in \mathbb{N}_{>0}$, and $\tau^+ \in \mathbb{N}_{>0}$.

Note that T^+ and τ^+ may equal or not equal T and τ, respectively. Based on this assumption, it can be observed that the dynamics of (2.26) and (2.10) are similar. Thus, the techniques used in the observer design can be adopted to find a compact set to which $\tilde{e}_k$ is confined. To this end, we define an extended robust positively

invariant set as follows.

Definition 6: A set $\mathcal{S}_{[\tau^+,T^+]} \subseteq \mathbb{R}^n$ is said to be an extended robust positive invariant (ERPI) set for system (2.26) with constraints imposed by *Assumption 2*, if $\tilde{e}_0 \in \mathcal{S}_{[\tau^+,T^+]}$ implies $\tilde{e}_k \in \mathcal{S}_{[\tau^+,T^+]}$ for every $k \in \mathbb{N}_{\geq 0}$ and for every allowable disturbance sequence.

Remark 4: Different from the GRPI set, we require that the invariance property of an ERPI set is retained at every time instant. All switching sequences including unadmissible ones are considered.

Similar to *Algorithm 1*, we define $\Theta_1^+ \triangleq \{\ \tau^+, \tau^+ + 1, \ldots, 2\tau^+ - 1\}$, $\Theta_2^+ \triangleq \{0, 1 \ldots, T^+\}$ and provide *Algorithm 2* to compute the ERPI set $S_{[\tau^+,T^+]}$. Additionally, we define $\Theta_0^+ = \{1, \ldots, \tau^+ - 1\}$.

Algorithm 2: ERPI set $\mathcal{S}_{[\tau^+,T^+]}$ algorithm.

Input: T^+, τ^+, Φ_K, A, $\mathcal{D}$;
Initialization: $v = 0, \mathcal{O}_0 = \{0\}$;
while $\mathcal{O}_{v+1} \neq \mathcal{O}_v$ **do**
  $\mathcal{O}_{v+1} = co\{co\{\Phi_K^\gamma \mathcal{O}_v \oplus \bigoplus_{i=0}^{\gamma-1} \Phi_K^i \mathcal{D} : \gamma \in \Theta_0^+\}$
    $co\{A^\beta \Phi_K^\alpha \mathcal{O}_v \oplus \bigoplus_{i=0}^{\alpha-1} A^\beta \Phi_K^i \mathcal{D} \oplus \bigoplus_{j=0}^{\beta-1} A^j \mathcal{D} :$
    $\alpha \in \Theta_1, \beta \in \Theta_2\}\}$;
  $v = v + 1$;
end
$\mathcal{S}_{[\tau^+,T^+]} = \mathcal{O}_v$;
Output: $\mathcal{S}_{[\tau^+,T^+]}$

With this set, the following theorem can be developed:

Theorem 3: If $\tilde{e}_0 = \hat{x}_0 - \bar{x}_0 \in \mathcal{S}_{[\tau^+,T^+]}$ is satisfied, and *Algorithm 2* converges, where the initial estimated state is $\hat{x}_0$ and the initial nominal system state is $\bar{x}_0$, then $\tilde{e}_k = \hat{x}_k - \bar{x}_k \in \mathcal{S}_{[\tau^+,T^+]}$ for all admissible disturbances ω_k and v_k, $k \in \mathbb{N}_{\geq 0}$.

The proof of *Theorem 3* is similar to *Theorem 2*, thus it is omitted here. The difference between these two theorems/algorithms is that, in iterations for each stage, we involve the switching sequences $\{1, 2, 3, \ldots, \tau^+\}$ in *Theorem 2* that are not admis-

sible. By using $S_{[\tau^+,T^+]}$, the optimization problem for robust output feedback MPC can be developed.

2.4.2 Robust Output Feedback MPC

After bounding the deviation between the nominal state and the estimated state with the existence of the random packet dropout, we are able to construct the optimal control problem of the robust output feedback MPC. To mitigate the effects of the sensor noise, disturbances, and random packet dropouts in both sensor-controller and controller-actuator channels, tightened constraints are imposed on predicted state and input sequences:

$$\bar{u}_k \in \mathcal{U} \ominus K\mathcal{S}_{[\tau^+,T^+]} \tag{2.27}$$

$$\hat{x}_k \in \mathcal{X} \ominus \mathcal{E}_{[\tau,T]} \tag{2.28}$$

$$\bar{x}_k \in \mathcal{X} \ominus \mathcal{E}_{[\tau,T]} \ominus \mathcal{S}_{[\tau^+,T^+]} \tag{2.29}$$

where $\hat{\mathcal{X}} \triangleq \mathcal{X} \ominus \mathcal{E}_{[\tau,T]}$. The existence of a feasible input sequence requires the following assumption:

Assumption 3: The estimation error set $\mathcal{E}_{[\tau,T]}$ and the robust positively invariant set $\mathcal{S}_{[\tau^+,T^+]}$ satisfy $\mathcal{E}_{[\tau,T]} \oplus \mathcal{S}_{[\tau^+,T^+]} \subset \mathcal{X}$ and $K\mathcal{S}_{[\tau^+,T^+]} \subset \mathcal{U}$.

This assumption can be satisfied if the disturbance set $\mathcal{W}$ and the sensor noise set $\mathcal{V}$ are sufficiently small.

To ensure that the state constraint $x_k \in \mathcal{X}$ and the input constraint $u_k \in \mathcal{U}$ are satisfied, the following tightened constraints are imposed on predicted states and

inputs:

$$\bar{u}_k \in \mathcal{U} \ominus K\mathcal{S}_{[\tau^+,T^+]} \tag{2.30}$$

$$\hat{x}_k \in \mathcal{X} \ominus \mathcal{E}_{[\tau,T]} \tag{2.31}$$

$$\bar{x}_k \in \mathcal{X} \ominus \mathcal{E}_{[\tau,T]} \ominus \mathcal{S}_{[\tau^+,T^+]} \tag{2.32}$$

For brevity, we rewrite the nominal state constraint as $\bar{x}_k \in \bar{\mathcal{X}} \triangleq \mathcal{X} \ominus \mathcal{E}_{[\tau,T]} \ominus \mathcal{S}_{[\tau^+,T^+]}$ and the nominal input constraint as $\bar{u}_k \in \bar{\mathcal{U}} \triangleq \mathcal{U} \ominus K\mathcal{S}_{[\tau^+,T^+]}$. With these state and input constraints, the optimal control problem is designed as

$$\min_{\bar{x}_k, \bar{\boldsymbol{u}}_k} \quad V_N(\bar{x}_k, \bar{\boldsymbol{u}}_k) = \sum_{i=0}^{N-1} l(\bar{x}_{i+k|k}, \bar{u}_{i+k|k}) + V_f(\bar{x}_{N+k|k}) \tag{2.33}$$

$$\text{s.t.} \quad \bar{x}_{k+i+1|k} = A\bar{x}_{k+i|k} + B\bar{u}_{k+i|k} \quad 0 \le i \le N-1 \tag{2.34}$$

$$\hat{x}_k \in \bar{x}_{k|k} \oplus S_{[\tau^+,T^+]} \tag{2.35}$$

$$\bar{x}_{k+i|k} \in \bar{\mathcal{X}} \quad 0 \le i \le N-1 \tag{2.36}$$

$$\bar{u}_{k+i|k} \in \bar{\mathcal{U}} \quad 0 \le i \le N-1 \tag{2.37}$$

$$\bar{x}_{k+N|k} \in \mathcal{X}_f \tag{2.38}$$

where $N \ge T^+$ is the prediction horizon; $V_f(\cdot)$ and $l(\cdot)$ denote the terminal cost function and the stage cost function, respectively. They are defined as

$$l(x,u) \triangleq \tfrac{1}{2}(x^T Q x + u^T R u) \tag{2.39}$$

$$V_f(x) \triangleq \tfrac{1}{2} x^T P x \tag{2.40}$$

where P, Q and R are chosen to be positive definite. $\mathcal{X}_f$ represents the terminal set,

which satisfies

$$\Phi_K \mathcal{X}_f \subset \mathcal{X}_f, \quad \mathcal{X}_f \subset \bar{\mathcal{X}}, \quad K\mathcal{X}_f \subset \bar{\mathcal{U}} \tag{2.41}$$

Meanwhile, the terminal cost function $V_f(\cdot)$ satisfies

$$V_f(\Phi_K x) + l(x, Kx) \leq V_f(x), \quad \forall x \in \mathcal{X}_f \tag{2.42}$$

Note that the initial nominal state $\bar{x}_{k|k} = \bar{x}_k$ and input sequence $\bar{\boldsymbol{u}}_k$ are decision variables in the optimization problem (2.33). Here, the use of terminal region and the ERPI set $S_{[\tau^+,T^+]}$ aims to guarantee recursive feasibility, which is demonstrated as follows.

2.4.3 Feasibility Analysis

The recursive feasibility is an essential requirement in the application of MPC to guarantee that a control input can always be obtained whenever the optimization problem is solved. Based on mathematical induction, the following theorem is developed:

Theorem 4: Suppose the optimization problem (2.33) is feasible at initial time instant $k = 0$, then it is also feasible for all time instants that the control input can be transmitted successfully.

Proof. Without loss of generality, we assume the optimization problem (2.33) is feasible and solved at time instant k. The obtained state and control input sequences are

$$\bar{\boldsymbol{x}}_k = \{\bar{x}_{k+0|k}, \bar{x}_{k+1|k}, \ldots, \bar{x}_{k+N|k}\} \tag{2.43}$$

$$\bar{\boldsymbol{u}}_k = \{\bar{u}_{k+0|k}, \bar{u}_{k+1|k}, \ldots, \bar{u}_{k+N-1|k}\} \tag{2.44}$$

respectively. Due to the existence of packet dropouts, we assume that the next time instant that the optimization problem (2.33) is solved is $k+p$. Next, we provide a candidate solution $\tilde{\boldsymbol{u}}_{k+p}$ and further demonstrate it is feasible for (2.33). $\tilde{\boldsymbol{u}}_{k+p}$ is constructed as

$$\tilde{\boldsymbol{u}}_{k+p} = \{\bar{u}_{k+p|k}, \bar{u}_{k+p+1|k}, \ldots, \bar{u}_{k+N-1|k}, K\bar{x}_{k+N|k}, \\ K\Phi_K\bar{x}_{k+N|k}, \ldots, K\Phi_K^{p-1}\bar{x}_{k+N|k}\}$$

Since the dynamic equations (2.21) are incorporated as constraints in the optimization problem, the corresponding suboptimal state sequence is

$$\tilde{\boldsymbol{x}}_{k+p} = \{\bar{x}_{k+p|k}, \bar{x}_{k+p+1|k}, \ldots, \bar{x}_{k+N|k}, \Phi_K\bar{x}_{k+N|k}, \\ \Phi_K^2\bar{x}_{k+N|k}, \ldots, \Phi_K^p\bar{x}_{k+N|k}\}$$

According to *Theorem 3*, $\hat{x}_{k+p} - \bar{x}_{k+p|k} \in \mathcal{S}_{[\tau^+, T^+]}$. Thus, the constraint (2.35) is satisfied.

Since $\bar{\boldsymbol{x}}_k$ and $\bar{\boldsymbol{u}}_k$ are obtained by solving the optimization problem, the first $N-p+1$ items in $\tilde{\boldsymbol{x}}_{k+p}$ and the first $N-p$ items in $\tilde{\boldsymbol{u}}_{k+p}$ satisfy the state constraint (2.36) and the input constraint (3.23e), respectively. Meanwhile, considering $\bar{x}_{k+N|k} \in \mathcal{X}_f$ and (2.41), we can conclude that $\{\bar{x}_{k+p|k},\ \tilde{\boldsymbol{u}}_k\}$ is a feasible solution of the optimal control problem. □

Now, it has been shown that the OCP is recursively feasible if it is feasible at $k=0$. Then, the stability of the closed-loop system can be evaluated.

2.4.4 Stability Analysis

The stability of the closed-loop system is studied in this subsection. By choosing the optimal value of the cost function as the Lyapunov function, the following theorem is conducted based on the Lyapunov stability theory.

Theorem 5: Suppose that Assumptions 1-3 hold. For the system (**??**) with constraint (2.2), if Theorems 1-3 are satisfied, i.e., $\mathcal{E}_{[\tau,T]}$ and S exist, then the system state exponentially converges to compact set $\mathcal{E}_{[\tau,T]} \times \mathcal{S}_{[\tau^+,T^+]}$ in the presence of disturbances, sensor noise and random packet dropouts.

Proof. Since $(\bar{x}_{k+p|k}, \tilde{\boldsymbol{u}}_{k+p})$ is a suboptimal solution at $k+p$, we have $V_N^*(\hat{x}_{k+p}) \leq V_N(\bar{x}_{k+p}, \tilde{\boldsymbol{u}}_{k+p})$. Meanwhile, (2.42) implies that

$$V_N(\bar{x}_{k+p|k}, \tilde{\boldsymbol{u}}_{k+p}) \leq V_N^*(\hat{x}_k) - \sum_{i=0}^{p-1} l(\bar{x}_{k+i|k}, \bar{u}_{k+i|k}) \tag{2.45}$$

Let $V_N^*(\hat{x}_k)$, the optimal value of the cost function, be the candidate Lyapunov function. From (2.39), (2.40), and (2.42), we obtain

$$V_N^*(\hat{x}_k) \geq c_1 |\bar{x}_{k|k}|^2, \tag{2.46}$$

$$V_N^*(\hat{x}_{k+p}) - V_N^*(\hat{x}_k) \leq -\sum_{i=0}^{p-1} l(\bar{x}_{k+i|k}, \bar{u}_{k+i|k}) \leq c_1 |\bar{x}_{k|k}|^2, \tag{2.47}$$

$$V_N^*(\hat{x}_k) \leq c_2 |\bar{x}_{k|k}|^2 \tag{2.48}$$

Combining (2.46), (2.47), and (2.48), we obtain $V_N^*(\hat{x}_{k+p}) \leq \gamma^p V_N^*(\hat{x}_k)$, where $\gamma = (1 - c_1/c_2) \in (0,1)$. Hence, $|\bar{x}_{k|k}| \leq c\delta^k |\bar{x}_{0|0}|$ for all feasible $\hat{x}_0$ and some $c \leq \infty$, where $\delta = \sqrt{\gamma}$. Obviously, $|\bar{x}_{0|0}| \to 0$ as $k \to \infty$. Since $\hat{x}_k \in \bar{x}_0^*(\hat{x}_k) \oplus \mathcal{S}_{[\tau^+,T^+]}$ and $x_k \in \bar{x}_0^*(\hat{x}_k) \oplus \mathcal{S}_{[\tau^+,T^+]} \oplus \mathcal{E}_{[\tau,T]}$, $\mathcal{E}_{[\tau,T]} \times \mathcal{S}_{[\tau^+,T^+]}$ is robustly exponentially stable for the controlled system.

□

Now, *Theorem 3* provides the guarantee of the closed-loop stability. Then, a numerical example is provided to validate the effectiveness of the proposed MPC scheme.

2.5 Numerical Example

Consider an unstable quadrotor linear system

$$x_{k+1} = Ax_k + Bu_k + \omega_k$$
$$y_k = Cx_k + v_k$$

where

$$A = \begin{bmatrix} 1 & 0.02 \\ 0 & 1 \end{bmatrix},\ B = \begin{bmatrix} 0.002 \\ 0.196 \end{bmatrix},\ C = \begin{bmatrix} 1 \\ 0 \end{bmatrix} \tag{2.49}$$

with state and input constraints:

$$||x_1||^2 \leq 10,\ ||x_2||^2 \leq 10,\ ||u||^2 \leq 10 \tag{2.50}$$

The external disturbances and measurement noise are bounded by $||\omega|| \leq 0.001$ and $||v|| \leq 0.01$, respectively. The maximum length of consecutive dropouts in two channels is chosen to be the same $T = T^+ = 3$, while the minimum length of consecutive measurement in two channels is $\tau = \tau^+ = 2$. For the MPC optimization problem, the weighting matrix Q is chosen as an identity matrix, and R is 0.1. The results of 50 iterations are shown in this section. Random packet dropouts in two channels are generated randomly but satisfy the constraints in Assumptions 1 and 2. The

simulation starts with the initial state $x_0 = [2 \quad 2]^\top$. The initial estimation error is assumed to be within the GRPI set $\mathcal{O}_{[\tau=2,T=3]}$.

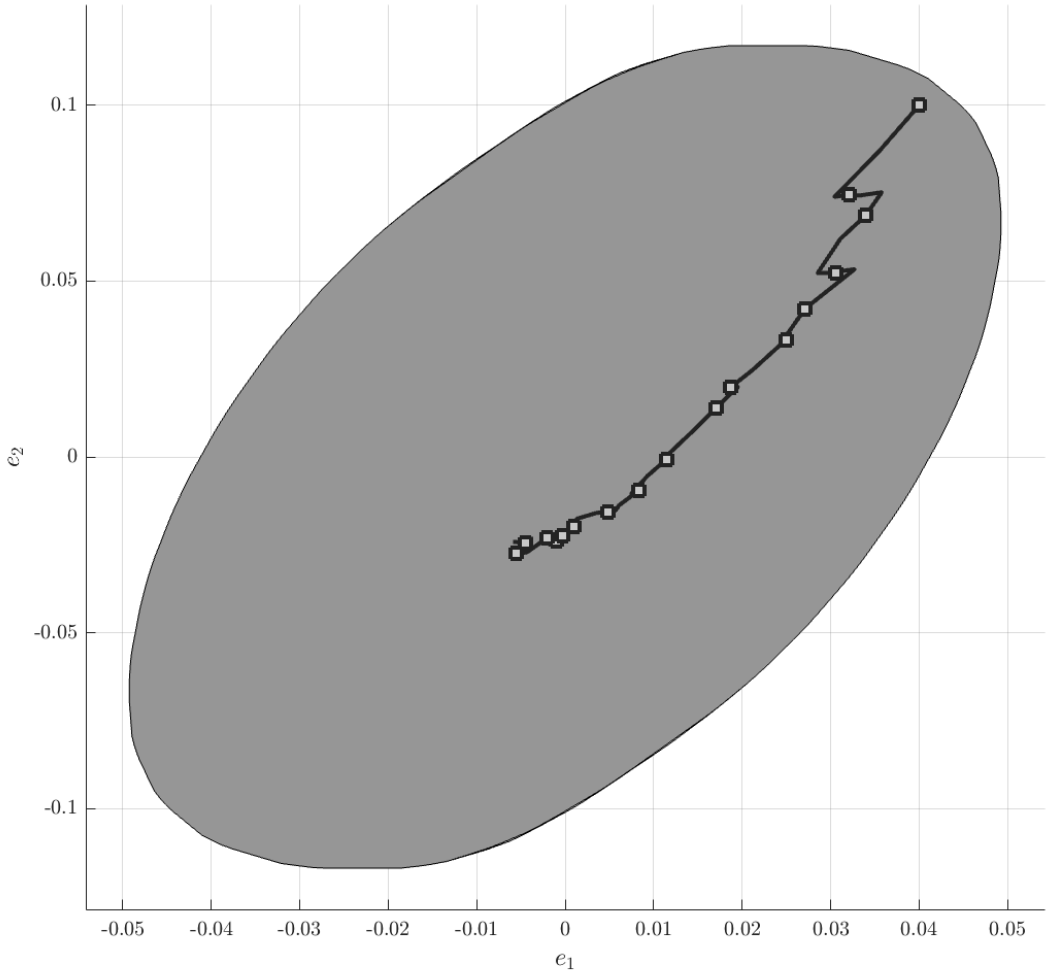

Figure 2.3: GRPI set of the estimation error.

By using Algorithm 1, a GRPI set is obtained and shown in Figure 2.3. The gray set represents the GRPI set $\mathcal{O}_{[\tau=2,T=3]}$. The initial estimation error is set to be $e_0 = [0.04 \quad 0.1]^\top$. It can be observed that estimation errors are confined to the GRPI set for all admissible packet dropouts as expected. Since $\mathcal{O}_{[\tau=2,T=3]} \subset \mathcal{E}_{[\tau=2,T=3]}$, estimation errors at every time instant remain within $\mathcal{E}_{[\tau=2,T=3]}$. Real, estimated, and nominal state trajectories are illustrated in Figure 2.4. Since the nominal state is an

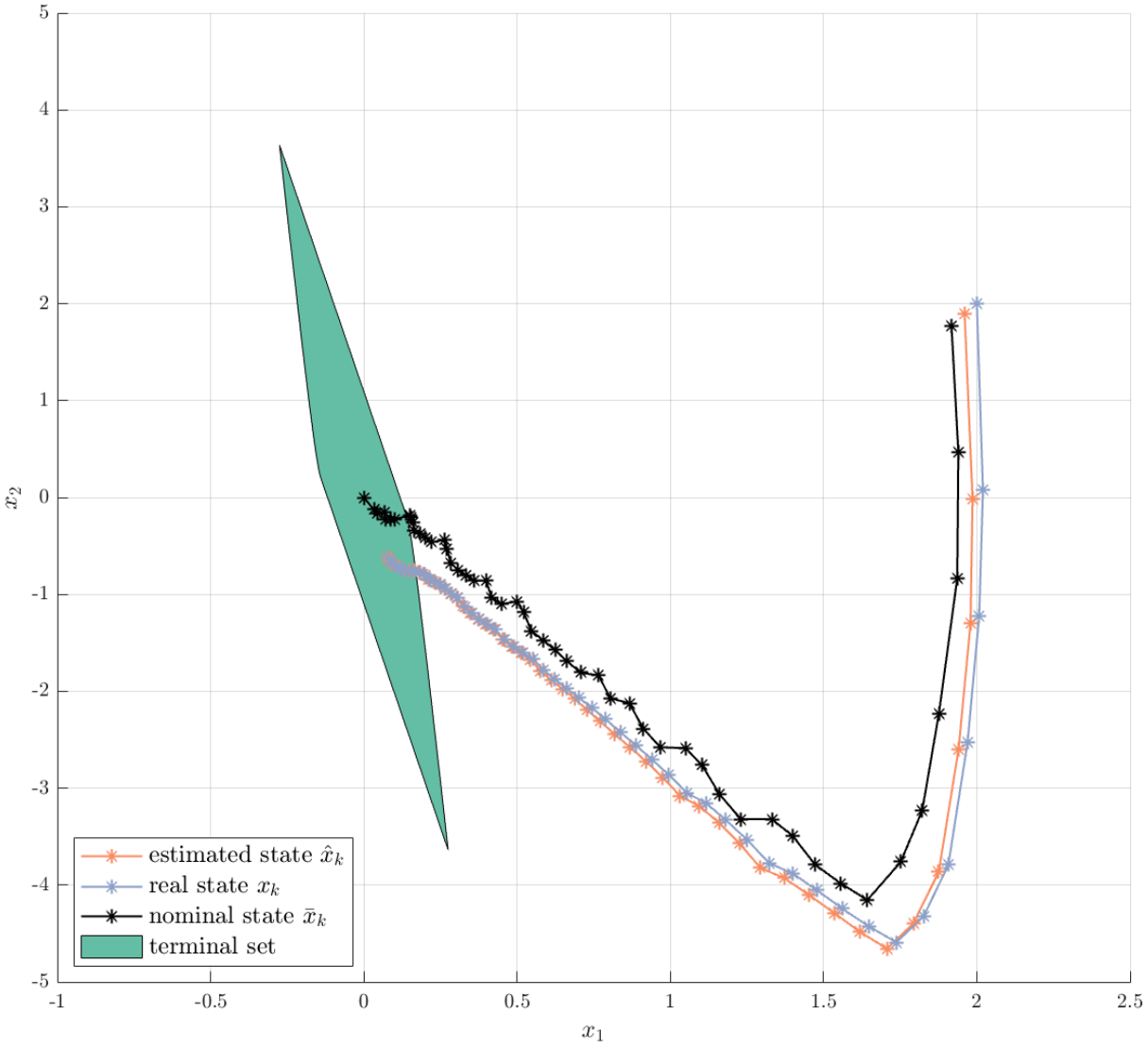

Figure 2.4: State trajectories.

optimization variable, deviations between the nominal state and the estimated state always exist but are bounded by the set $\mathcal{S}_{[\tau^+,T^+]}$. Eventually, the nominal state enters the terminal set and reaches the equilibrium. Due to the existence of disturbances and packet dropouts, the real state is steered to the set $\mathcal{S}_{[\tau^+,T^+]} \oplus \mathcal{E}_{[\tau,T]}$.

To illustrate the impact of packet losses, a comparison simulation is conducted based on the MPC method proposed in [15]. Two groups of simulation results are obtained:

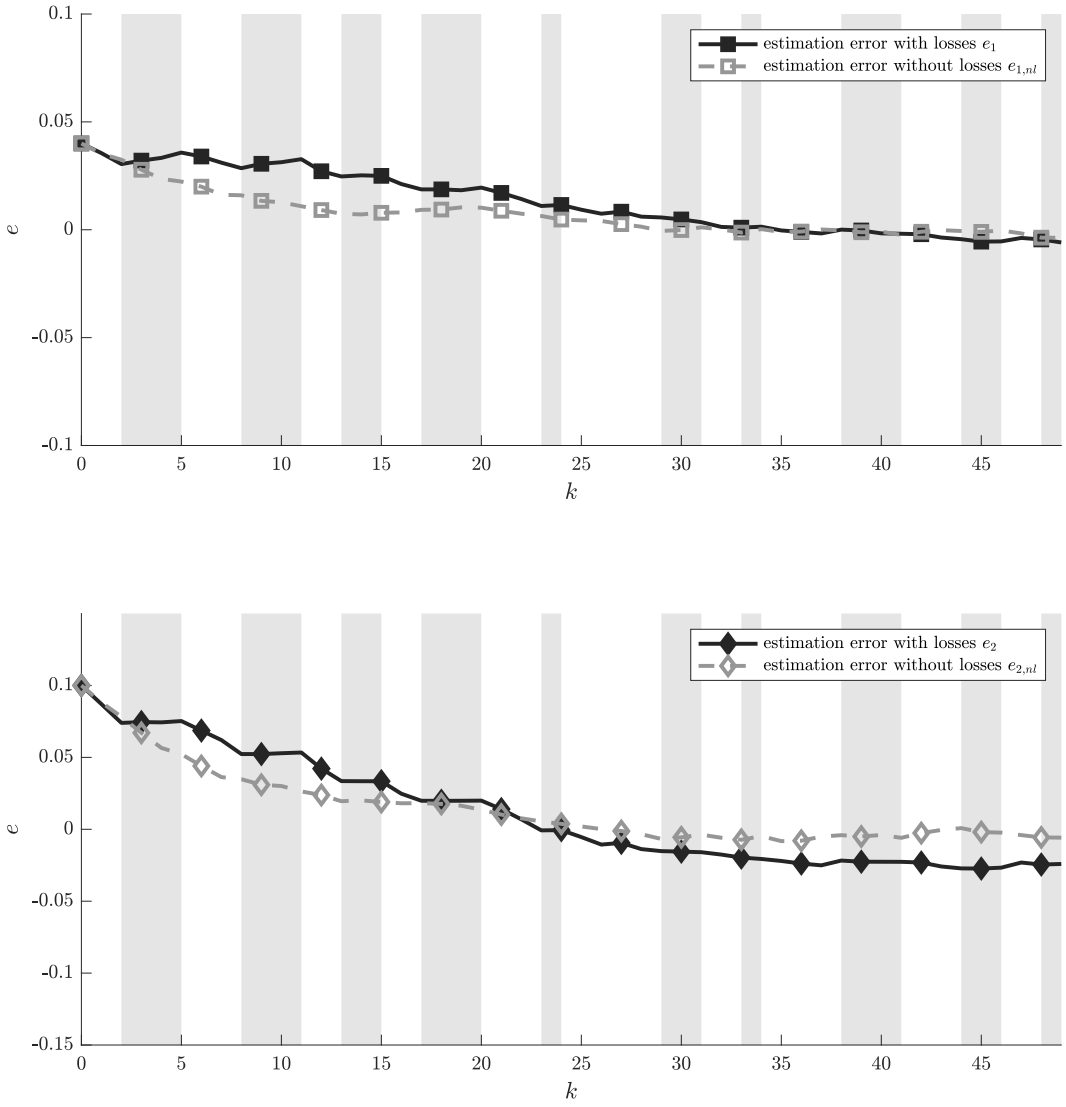

Figure 2.5: Estimation error comparison.

Group A: Results of the proposed method based on the above simulation setup.

Group B: Results of the robust output-feedback MPC method proposed in [15] based on identical simulation setups without S-C packet dropouts.

In Figure 2.5, dash lines represent the estimation error of Group B, while the solid lines stand for the estimation error in Group A when random dropouts happen, which is the same as the evolution in Figure 2.3. Two state trajectories originate from the

same initial state, and the output is measurable in the first two iterations in both cases. Thus, the obtained control input and state evolution under two communication settings in the first two iterations are similar. However, the output packet losses happen since the third iteration, and the estimation error in Group A becomes larger than that of Group B consequently. Eventually, the estimation errors of the two groups fluctuate around zero.

Results in Figure 2.6 examine the system behavior to highlight the effectiveness of the compensation strategy. In the simulation of Group B, when packet dropouts occur in the C-A channel, there is no compensated control input available, and therefore the control inputs are zero. It can be observed that the state of Group A converges faster than that of Group B, which verifies the effectiveness of the proposed compensation strategy.

In summary, the stability and recursive feasibility are validated by simulation results when the networked quadrotor control system endures 40% packet dropouts. A comparative simulation is also conducted to demonstrate the impact of random packet dropouts.

2.6 Conclusions

In this chapter, a robust output-feedback MPC scheme is proposed for networked quadrotor control systems considering the following aspects: (1) external disturbances and observation noise, (2) random packet dropouts, and (3) state and input constraints. Based on the designed observer, the bound for estimation error is explicitly obtained, which is the GRPI set. Similarly, the ERPI set is developed as the bound for deviations between the predicted state and estimated state. With the help of these sets, tightened constraints are constructed and incorporated into the OCP of

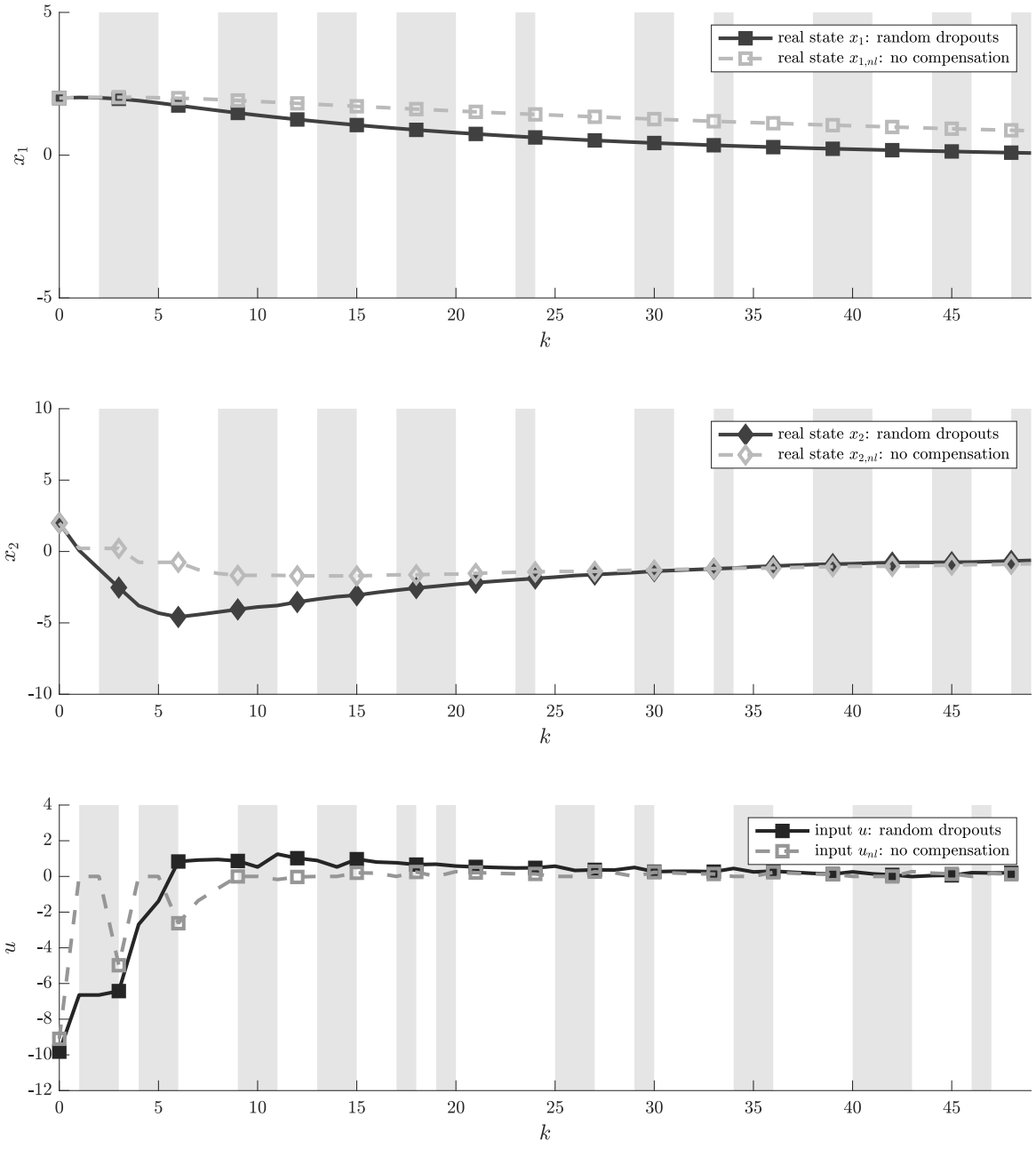

Figure 2.6: Real state and input sequences comparison.

the proposed robust output-feedback MPC strategy to ensure constraint satisfaction. Based on a two-dimensional quadrotor model, the simulation results are conducted to verify the effectiveness of the proposed method.

Chapter 3

Model Predictive Control for Quadrotors

3.1 Overview

The quadrotor model for controller design ranges from the linear model to the nonlinear model, resulting in great variations in the control strategies. When it comes to MPC for quadrotors, the difference between linear MPC and nonlinear MPC is even more evident. As introduced in Chapter 1, many well-developed MPC strategies can be utilized for quadrotor control, such as the tube-based MPC [5] based on linear models and the Lyapunov MPC [39] for nonlinear models. However, these methods are developed based on different models and techniques, and their effectiveness on the same quadrotor has not been compared.

In this chapter, we evaluate the efficiencies of different MPC schemes by comparing their performances on the same quadrotor. Firstly, we develop linear and nonlinear models of the quadrotor in detail. Then, three MPC strategies for quadrotors are introduced: The conventional MPC and tube-based MPC based on a linear quadrotor

model, and Lyapunov MPC for a nonlinear quadrotor model.

In practical applications, the quadrotor usually relies on the dual-loop control framework, and the inner loop control can be achieved by embedded commercial controllers. Firstly, to compare their efficiencies in quadrotor control, three MPC strategies are employed in the translation control loop while the rotational dynamics are neglected. Moreover, since wind gusts are the most common disturbance exerted on the quadrotor, the robustness against wind gusts of three MPC schemes is provided and compared. Then, we take both translational and rotational dynamics into consideration. By using a dual-loop control framework, the control inputs generated by three MPC schemes are applied to the same nonlinear quadrotor model to simulate the practical application. Lastly, we investigate the impact of different sampling ratios of the outer and inner control loops on the control performance, which provides potential research topics in both practical applications and theoretical studies.

3.2 Model Description

In general, the quadrotor dynamics can be described by different linear and nonlinear systems with varying assumptions for simplification, but all these models originate from the same nonlinear model. In this section, a nonlinear model and a simplified linear model for the quadrotor are developed. Though different MPC schemes are designed based on linear or nonlinear models, the MPC schemes we aim to compare in this chapter will be tested on the same nonlinear model. Before proceeding to the model development, we briefly discuss the principle for operations of the quadrotor.

For a quadrotor, four identical motors are usually installed vertically on the quadrotor's airframe. Since the motor's body cannot move with respect to the airframe, the quadrotor operation relies on the difference between torques generated by

four motors. Figure (3.1) illustrates the typical layout of a quadrotor. To maintain the hovering without rotations, the default rotation direction of the two motors on the diagonal is different from the two on the anti-diagonal. A viable layout can be motors 1 and 3 rotate clockwise while motors 2 and 4 rotate counterclockwise, such that the total moment exerted on the airframe can be zero when four motors rotate at the same speeds. To change the position and orientation of the quadrotor from hovering, the rotation speeds are modified accordingly. For example, to move along the axis b_1, the rotation speeds of motors 1 and 2 decrease at the same rate while that of motors 3 and 4 increase in a similar way. Then the pitch angle is changed and the horizontal component of the thrust is nonzero and along the axis b_1, which brings the acceleration along this axis. In general, the movement of the quadrotor that we are usually interested in relies on angular rotation. Meanwhile, the translational movement and the angular rotation are strongly coupled. Thus, our primary focus is on developing a model that establishes a relationship between the thrust of each motor and the translational and rotational motions.

3.2.1 Nonlinear Quadrotor Model

Here we follow the conventional way, i.e., Netwon-Euler formalism, to construct the nonlinear quadrotor model. The following assumptions are needed: 1) The quadrotor is a rigid body; 2) The quadrotor has a symmetric structure. The first assumption is a prerequisite for applying Netwon-Euler equations, the second one is utilized to simplify the inertia matrix. To describe the position and orientation of a quadrotor, an inertial frame $\boldsymbol{\mathcal{F}}_I$ is defined with axes $\{\boldsymbol{x}_I, \boldsymbol{y}_I, \boldsymbol{z}_I\}$, and a body fixed frame $\boldsymbol{\mathcal{F}}_B$ with axes $\{\boldsymbol{x}_B, \boldsymbol{y}_B, \boldsymbol{z}_B\}$. The origin of $\boldsymbol{\mathcal{F}}_B$ coincides with the Center of Mass of the quadrotor. The orientation of the quadrotor is parameterized by Euler angles, roll ϕ, pitch θ, and yaw ψ, which also represent the orientation of $\boldsymbol{\mathcal{F}}_B$ with respect to $\boldsymbol{\mathcal{F}}_I$.

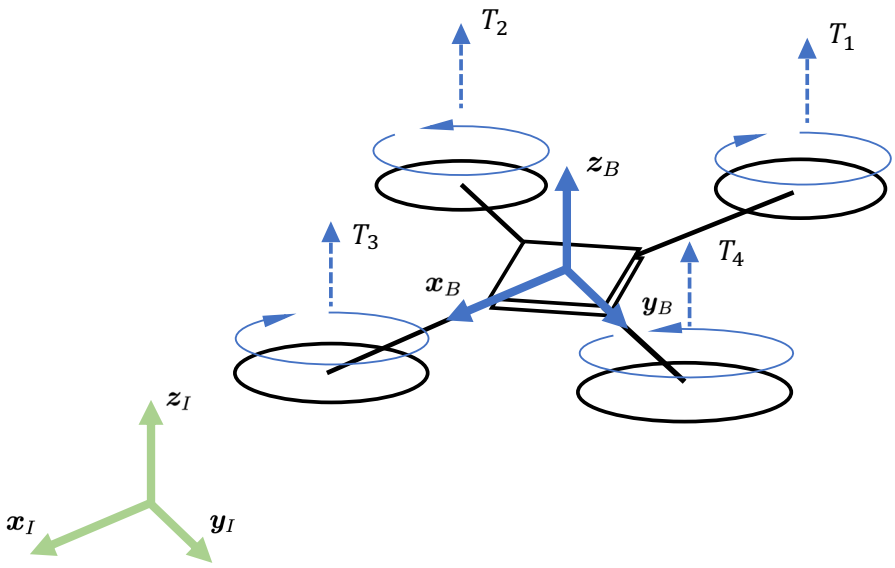

Figure 3.1: Quadrotor configuration and reference frames.

The coordinate transformation matrix from $\boldsymbol{\mathcal{F}}_B$ to $\boldsymbol{\mathcal{F}}_I$ is

$$\boldsymbol{R}_B^I = \begin{bmatrix} \mathrm{c}\theta\mathrm{c}\psi & \mathrm{s}\phi\mathrm{s}\theta\mathrm{c}\psi - \mathrm{c}\phi\mathrm{s}\psi & \mathrm{c}\phi\mathrm{s}\theta\mathrm{c}\psi + \mathrm{s}\phi\mathrm{s}\psi \\ \mathrm{c}\theta\mathrm{s}\psi & \mathrm{s}\phi\mathrm{s}\theta\mathrm{s}\psi + \mathrm{c}\phi\mathrm{c}\psi & \mathrm{c}\phi\mathrm{s}\theta\mathrm{s}\psi - \mathrm{s}\phi\mathrm{c}\psi \\ -\mathrm{s}\theta & \mathrm{s}\phi\mathrm{c}\theta & \mathrm{c}\phi\mathrm{c}\theta \end{bmatrix} \tag{3.1}$$

where s and c denote sine and cosine functions. Then the following Netwon-Euler equations are utilized to analyze the motion of the rigid quadrotor in the space:

$$\boldsymbol{F} = m\boldsymbol{\mathcal{I}}_{3\times 3}\dot{\boldsymbol{v}} \tag{3.2}$$

$$\boldsymbol{\tau} = \boldsymbol{I}\dot{\boldsymbol{\omega}} + \boldsymbol{\omega} \times \boldsymbol{I}\boldsymbol{\omega} \tag{3.3}$$

where $\boldsymbol{F}$ and $\boldsymbol{\tau}$ denote the external force and torque respectively that are exerted on the rigid body; $\boldsymbol{\mathcal{I}}_{3\times 3}$ denotes a 3×3 identity matrix; $\boldsymbol{I}$ represents the moment of inertial about the center of the mass; $\boldsymbol{v}$ and $\boldsymbol{\omega}$ stand for the translational velocity and

angular velocity of the rigid body in the inertial frame; m denotes the mass of the quadrotor. Obviously, the dynamics of a rigid body can be divided into translational dynamics and rotational dynamics.

When the quadrotor operates near the ground, the efficiency of the motor will increase and the extra thrust will be generated, which is called the ground effect. Since we focus on the motion control of the quadrotor that is operating far away from the ground, the ground effect is neglected. When the axis of the motor rotates, the gyroscopic torque will appear, but it is also neglected here. Then, the quadrotor model can be obtained as below.

$$m\ddot{x} = (\mathrm{c}\phi\mathrm{s}\theta\mathrm{c}\psi + \mathrm{s}\phi\mathrm{s}\psi)T_{sum} \tag{3.4a}$$

$$m\ddot{y} = (\mathrm{c}\phi\mathrm{s}\theta\mathrm{s}\psi - \mathrm{s}\phi\mathrm{c}\psi)T_{sum} \tag{3.4b}$$

$$m\ddot{z} = (\mathrm{c}\phi\mathrm{c}\theta)T_{sum} - mg \tag{3.4c}$$

$$I_{xx}\dot{\omega}_x = (I_{yy} - I_{zz})\omega_y\omega_z + \tau_\phi \tag{3.4d}$$

$$I_{yy}\dot{\omega}_y = (I_{zz} - I_{xx})\omega_x\omega_z + \tau_\theta \tag{3.4e}$$

$$I_{zz}\dot{\omega}_z = (I_{xx} - I_{yy})\omega_x\omega_y + \tau_\psi \tag{3.4f}$$

where I_{xx}, I_{yy}, and I_{zz} are moments of inertia about $\boldsymbol{x}_B$, $\boldsymbol{y}_B$, and $\boldsymbol{z}_B$ respectively; ω_x, ω_y, and ω_z are angular velocities in $\boldsymbol{\mathcal{F}}_B$. T_{sum}, τ_x, τ_y, and τ_z denote the sum of thrusts and torques generated by four motors:

$$T_{sum} = \sum_{i=1}^{4} T_i \tag{3.5a}$$

$$\tau_x = (-T_2 + T_4)l \tag{3.5b}$$

$$\tau_y = (T_1 - T_3)l \tag{3.5c}$$

$$\tau_z = (M_1 - M_2 + M_3 - M_4) \tag{3.5d}$$

where T_i and M_i for $i \in \{1, 2, 3, 4\}$ are thrusts and torques produced by four motors and l is the arm length. The thrust and the torque depend on the rotational speed of the motor. Moreover, both the thrust and torque can be approximated by scaling the squared rotation speed [86]. Thus, the thrust and the torque exhibit a linear relationship, and for given T_{sum}, τ_x, τ_y, and τ_z, the required rotation speed of four motors can be determined explicitly. Here, we delve no further into the dynamics of motors and regard T_{sum}, τ_x, τ_y, and τ_z as independent control inputs.

It can be observed that the quadrotor model 3.4 is highly nonlinear and has many coupled terms, which is still computationally intractable and needs more simplifications. To this end, the following derivations are provided.

The angular velocity transformation from $\boldsymbol{\mathcal{F}}_I$ to $\boldsymbol{\mathcal{F}}_B$ can be obtained by

$$\begin{bmatrix} \omega_x \\ \omega_y \\ \omega_z \end{bmatrix} = \begin{bmatrix} 1 & 0 & -\mathrm{s}\theta \\ 0 & \mathrm{c}\phi & \mathrm{s}\phi\mathrm{c}\theta \\ 0 & -\mathrm{s}\phi & \mathrm{c}\phi\mathrm{c}\theta \end{bmatrix} \begin{bmatrix} \dot{\phi} \\ \dot{\theta} \\ \dot{\psi} \end{bmatrix} \tag{3.6}$$

where t denotes the tangent function. By assuming that the quadrotor operates near the hovering state and Euler angles are small, we have

$$\begin{cases} \omega_x = \dot{\phi} - \theta\dot{\psi} \\ \omega_y = \dot{\theta} - \phi\dot{\psi} \\ \omega_z = -\phi\dot{\theta} + \dot{\psi} \end{cases} \tag{3.7}$$

Here, the product of the small angle and angular velocity can be regarded as zero. Thus, we have

$$\omega_x = \dot{\phi}, \quad \omega_y = \dot{\theta}, \quad \omega_z = \psi \tag{3.8}$$

For brevity, the following notations are used: $\boldsymbol{p} = [x \quad y \quad z]^\top$, $\boldsymbol{v} = [\dot{x} \quad \dot{y} \quad \dot{z}]^\top$,

$\boldsymbol{\tau} = [\tau_x \quad \tau_y \quad \tau_z]^\top$, $\boldsymbol{q} = [\phi \quad \theta \quad \psi]^\top$, $\boldsymbol{\omega} = [\tau_x \quad \tau_y \quad \tau_z]^\top$, $T = T_{sum}$. Then, the quadrotor model becomes

$$\begin{cases} \dot{\boldsymbol{p}} = \boldsymbol{v} \\ m\dot{\boldsymbol{v}} = -m\boldsymbol{g} + \boldsymbol{r}(\boldsymbol{q})T \end{cases} \tag{3.9}$$

$$\begin{cases} \dot{\boldsymbol{q}} = \boldsymbol{\omega} \\ \boldsymbol{I}\dot{\boldsymbol{\omega}} = -\boldsymbol{\omega} \times \boldsymbol{I}\boldsymbol{\omega} + \boldsymbol{\tau} \end{cases} \tag{3.10}$$

where $\boldsymbol{r}(\boldsymbol{q}) = [\mathrm{c}\phi\mathrm{s}\theta\mathrm{c}\psi + \mathrm{s}\phi\mathrm{s}\psi \quad \mathrm{c}\phi\mathrm{s}\theta\mathrm{s}\psi - \mathrm{s}\phi\mathrm{c}\psi \quad \mathrm{c}\phi\mathrm{c}\theta]^\top$ and $\boldsymbol{g} = [0 \quad 0 \quad g]^\top$. It can be observed that the model can be divided into two subsystems, translational dynamics (3.9) and rotational dynamics (3.10). Thus, a widely applied dual-loop control scheme is developed, which consists of the outer loop for the translation control and the inner loop for the rotation control. More details can be found in Chapter 1. By assuming that the reference signal is slowly varying, the Euler angles $\boldsymbol{q}$ can be approximated by the reference angles $\boldsymbol{q}^r = [\phi^r \ \theta^r \ \psi^r]^\top$. In this manner, the translational dynamics can be simplified to be

$$\begin{cases} \dot{\boldsymbol{p}} = \boldsymbol{v} \\ m\dot{\boldsymbol{v}} = -m\boldsymbol{g} + \boldsymbol{r}(\boldsymbol{q}^r)T \end{cases} \tag{3.11}$$

To compare different robust control methods, we only consider their implementations on the outer loop, because the inner loop system can be stabilized by many embedded commercial controllers in practical implementations.

3.2.2 Linear Quadrotor Model

In this subsection, a simplified linear model is obtained based on the simplified nonlinear model (3.11). In many applications, the translational position and velocity receive more attention than the angular position and velocity. Specifically, lateral movement is our major interest, which can be achieved by adjusting the pitch and

roll angles without involving the yaw. Thus, we treat the yaw angle as fixed. In this manner, the yaw angle has no impact on pitch and roll, i.e., the angular dynamics of the quadrotor. Meanwhile, when the quadrotor is hovering, the body frame is placed such that $\boldsymbol{x}_I$ and $\boldsymbol{y}_I$ coincides with $\boldsymbol{x}_B$ and $\boldsymbol{y}_B$, respectively. In this way, the yaw angle remains zero.

Here, only gravity and thrust are considered to be exerted on the airframe. The gravity vector always points along the axe $\boldsymbol{z}_I$. To decouple translational movements, we assume that the vertical component of the total thrust is identical to the gravity, leaving angles between the thrust vector and the verticle planes $\boldsymbol{x}_I - \boldsymbol{z}_I$, $\boldsymbol{y}_I - \boldsymbol{z}_I$ as our concern. Thus, the translational dynamics can be decomposed to two lateral horizontal dynamics in the $\boldsymbol{x}_I - \boldsymbol{z}_I$ plane and $\boldsymbol{y}_I - \boldsymbol{z}_I$ plane respectively. Meanwhile, we assume that the quadrotor is symmetric with respect to the vertical planes $\boldsymbol{x}_B - \boldsymbol{z}_B$ and $\boldsymbol{y}_B - \boldsymbol{z}_B$, respectively. Thus, the two horizontal dynamics in two vertical planes are identical.

To obtain a linear model, the quadrotor is assumed to be a point mass model. The lateral acceleration is generated by the horizontal projection of the total thrust T, which is always aligned with $\boldsymbol{z}_B$. The vertical component of T determines the acceleration in the vertical direction. When we consider the lateral dynamics, the thrust dynamics are assumed to be sufficiently fast such that the quadrotor is at its vertical equilibrium, i.e., the vertical component of the thrust is equal to the gravity. Based on the above descriptions, the lateral dynamics in axis $\boldsymbol{x}_I$ can be obtained as follows:

$$\begin{bmatrix} \dot{x} \\ \ddot{x} \end{bmatrix} = \begin{bmatrix} 0 & 1 \\ 0 & 0 \end{bmatrix} \begin{bmatrix} x \\ \dot{x} \end{bmatrix} + \begin{bmatrix} 0 \\ g \end{bmatrix} \theta^r \tag{3.12}$$

The lateral dynamics in axis $\boldsymbol{y}_I$ can be obtained in a similar way. In vertical dynamics,

the Euler angles and angular velocities are not involved, and it can be modeled as

$$\begin{bmatrix} \dot{z} \\ \ddot{z} \end{bmatrix} = \begin{bmatrix} 0 & 1 \\ 0 & 0 \end{bmatrix} \begin{bmatrix} z \\ \dot{z} \end{bmatrix} + \begin{bmatrix} 0 \\ K_T \end{bmatrix} u_T - \begin{bmatrix} 0 \\ g \end{bmatrix} \tag{3.13}$$

where K_T is the thrust-to-command ratio. In the application, the employed control input u_T compensates the gravity, i.e., $u_T = u_T^* + g/K_T$, where u_T^* denotes the control input generated based on the linear model:

$$\begin{bmatrix} \dot{z} \\ \ddot{z} \end{bmatrix} = \begin{bmatrix} 0 & 1 \\ 0 & 0 \end{bmatrix} \begin{bmatrix} z \\ \dot{z} \end{bmatrix} + \begin{bmatrix} 0 \\ K_T \end{bmatrix} u_T^* \tag{3.14}$$

For brevity, we still u_T to denote the control input u_T^* in the linear model above. In summary, the linear translational model for the quadrotor is

$$\begin{bmatrix} \dot{x} \\ \ddot{x} \\ \dot{y} \\ \ddot{y} \\ \dot{z} \\ \ddot{z} \end{bmatrix} = \begin{bmatrix} 0 & 1 & 0 & 0 & 0 & 0 \\ 0 & 0 & 0 & 0 & 0 & 0 \\ 0 & 0 & 0 & 1 & 0 & 0 \\ 0 & 0 & 0 & 0 & 0 & 0 \\ 0 & 0 & 0 & 0 & 0 & 1 \\ 0 & 0 & 0 & 0 & 0 & 0 \end{bmatrix} \begin{bmatrix} x \\ \dot{x} \\ y \\ \dot{y} \\ z \\ \dot{z} \end{bmatrix} + \begin{bmatrix} 0 & 0 & 0 \\ g & 0 & 0 \\ 0 & 0 & 0 \\ 0 & -g & 0 \\ 0 & 0 & 0 \\ 0 & 0 & K_T \end{bmatrix} \begin{bmatrix} \theta^r \\ \phi^r \\ u_T \end{bmatrix} \tag{3.15}$$

This equation can be rewritten as

$$\dot{\boldsymbol{x}}_l = \boldsymbol{A}_l \boldsymbol{x}_l + \boldsymbol{B}_l \boldsymbol{u}_l \tag{3.16}$$

where $\boldsymbol{x}_l = [x\ \dot{x}\ y\ \dot{y}\ z\ \dot{z}]^\top$ and $\boldsymbol{u}_l = [\theta^r\ \phi^r\ u_T]^\top$.

3.2.3 Disturbance Model

For quadrotors, the main disturbance that emerges in practical applications is the wind gust, which will be modeled and involved in simulations. When the wind gust appears, the forces and torques generated by motors will be affected, and the state will not evolve as predicted in MPC. Though the disturbance forces and torques originate from each of the four motors, we consider them in a compact form T_d and $\boldsymbol{\tau}_d$, which is similar to the forms of control inputs in the nonlinear quadrotor model (3.4). Here we use the wind gust model in [87] and assume that the disturbance force T_d and disturbance torque $\boldsymbol{\tau}_d$ are proportional to the speed of the wind gust $\boldsymbol{v}_d$:

$$\begin{aligned} T_d &= \boldsymbol{M}_1 \boldsymbol{v}_d \\ \boldsymbol{\tau}_d &= \boldsymbol{M}_2 \boldsymbol{\tau}_d \end{aligned} \tag{3.17}$$

where $\boldsymbol{M}_1$ and $\boldsymbol{M}_2$ are coefficient matrices. kth element of $\boldsymbol{v}_d$ is described by

$$v_{d,k}(t) = v_{d,k}^0 + \sum_{i=1}^{n_k} a_{i,k} sin(\bar{\omega}_{i,k} t + \alpha_{i,k}) \tag{3.18}$$

where $v_{d,k}^0$ represents the static wind speed, n_k is the number of sinusoids. $a_{i,k}$, $\bar{\omega}_{i,k}$, and $\alpha_{i,k}$ determine the amplitudes, frequencies, and phase shifts of the sinusoids. $v_{d,k}^0$, $a_{i,k}$, $\bar{\omega}_{i,k}$, and $\alpha_{i,k}$ are randomly chosen to mimic the randomness of wind gusts. Additionally, we denote the upper bound of the disturbance force by $\bar{T}_d$.

3.3 Model Predictive Control Formulations

In this section, we will introduce three MPC methods for quadrotors: conventional MPC, tube-based MPC, and Lyapunov MPC. Note that the prediction models in OCPs of conventional MPC and tube-based MPC are the same linear quadrotor

model, while that of Lyapunov MPC is a nonlinear quadrotor model. Since we use the dual-loop control framework, the controllers discussed in this section are utilized for translation control in the outer loop.

3.3.1 Conventional Model Predictive Control

The conventional MPC is the simplest form of the MPC, in which the OCP is formulated as

$$\min_{\boldsymbol{u}_{k:k+N-1|k}} \quad \sum_{i=0}^{N-1} \boldsymbol{x}_{k+i|k}^{\top} \boldsymbol{Q} \boldsymbol{x}_{k+i|k} + \boldsymbol{u}_{k+i|k}^{\top} \boldsymbol{R} \boldsymbol{u}_{k+i|k} \tag{3.19a}$$

$$\text{s.t.} \quad \boldsymbol{x}_{k+i+1|k} = \boldsymbol{A} \boldsymbol{x}_{k+i|k} + \boldsymbol{B} \boldsymbol{u}_{k+i|k} \quad 0 \leq i \leq N-1 \tag{3.19b}$$

$$\boldsymbol{x}_{k+i|k} \in \mathcal{X} \quad 0 \leq i \leq N-1 \tag{3.19c}$$

$$\boldsymbol{u}_{k+i|k} \in \mathcal{U} \quad 0 \leq i \leq N-1 \tag{3.19d}$$

$$\boldsymbol{x}_{k+N|k} \in \mathcal{X}_f \tag{3.19e}$$

where k is the current time instant; $\boldsymbol{x}_{k+i|k}$ and $\boldsymbol{u}_{k+i|k}$ are predicted states and inputs at $k+i$; $\mathcal{X}$ and $\mathcal{U}$ denote state and input constraints; $\mathcal{X}_f$ represents the terminal constraint; $\boldsymbol{Q}$ and $\boldsymbol{R}$ are weighting matrices. As one of the constraints, the prediction model (3.19b) can be obtained by discretizing (3.15) with the zero-order hold strategy:

$$\boldsymbol{A} = e^{\boldsymbol{A}_l \delta t}, \quad \boldsymbol{B} = \int_0^{\delta t} e^{\boldsymbol{A}_l \tau} \mathrm{d}\tau \boldsymbol{B}_l \tag{3.20}$$

which yields the discrete-time quadrotor model:

$$\begin{bmatrix} x_{k+1} \\ \dot{x}_{k+1} \\ y_{k+1} \\ \dot{y}_{k+1} \\ z_{k+1} \\ \dot{z}_{k+1} \end{bmatrix} = \begin{bmatrix} 1 & \delta t & 0 & 0 & 0 & 0 \\ 0 & 1 & 0 & 0 & 0 & 0 \\ 0 & 0 & 1 & \delta t & 0 & 0 \\ 0 & 0 & 0 & 1 & 0 & 0 \\ 0 & 0 & 0 & 0 & 1 & \delta t \\ 0 & 0 & 0 & 0 & 0 & 1 \end{bmatrix} \begin{bmatrix} x_k \\ \dot{x}_k \\ y_k \\ \dot{y}_k \\ z_k \\ \dot{z}_k \end{bmatrix} + \begin{bmatrix} g\delta t^2/2 & 0 & 0 \\ g\delta t & 0 & 0 \\ 0 & -g\delta t^2/2 & 0 \\ 0 & -g\delta t & 0 \\ 0 & 0 & K_T\delta t^2/2 \\ 0 & 0 & K_T\delta t \end{bmatrix} \begin{bmatrix} \theta_r \\ \phi_r \\ u_T \end{bmatrix} \tag{3.21}$$

By solving the OCP (3.19), the optimal control input u_k is generated and applied to the system at every sampling instant. The task space of quadrotors can be formulated as the state constraint, while the input constraint defines the range of reference angles. For conventional MPC, there is no guarantee of recursive feasibility and stability. However, compared with tube-based MPC and Lyapunov MPC, the OCP of conventional MPC (3.19) incorporates minimum constraints, enabling it to be solved with the fastest speed. Especially, when $\mathcal{X}$, $\mathcal{U}$, and $\mathcal{X}_f$ are convex sets, the OCP becomes a convex optimization problem, which can be efficiently handled by well-developed convex algorithms.

3.3.2 Tube-based Model Predictive Control

Tube-based MPC, as a robust MPC scheme, is able to stabilize the system in the presence of bounded disturbances. The perturbed quadrotor model is formulated as

$$\boldsymbol{x}_{k+1} = \boldsymbol{A}\boldsymbol{x}_k + \boldsymbol{B}\boldsymbol{u}_k + \boldsymbol{\omega}_k \tag{3.22}$$

where $\boldsymbol{\omega}_k$ denotes the disturbance at time instant k, and it is bounded by the disturbance set $\mathcal{W}$, i.e., $\boldsymbol{\omega}_k \in \mathcal{W}$. Tube-based MPC introduced here is developed based on [14], and the corresponding OCP is

$$\min_{\bar{\boldsymbol{u}}_{k:k+N-1|k}, \bar{\boldsymbol{x}}_{k|k}} \quad \sum_{i=0}^{N-1} \bar{\boldsymbol{x}}_{k+i|k}^{\top} \boldsymbol{Q} \bar{\boldsymbol{x}}_{k+i|k} + \bar{\boldsymbol{u}}_{k+i|k}^{\top} \boldsymbol{R} \bar{\boldsymbol{u}}_{k+i|k} + \bar{\boldsymbol{x}}_{k+N|k}^{\top} \boldsymbol{P} \bar{\boldsymbol{x}}_{k+N|k} \tag{3.23a}$$

$$\text{s.t.} \quad \bar{\boldsymbol{x}}_{k|k} \in \boldsymbol{x}_k \oplus \mathcal{Z} \tag{3.23b}$$

$$\bar{\boldsymbol{x}}_{k+i+1|k} = \boldsymbol{A} \bar{\boldsymbol{x}}_{k+i|k} + \boldsymbol{B} \bar{\boldsymbol{u}}_{k+i|k} \quad 0 \leq i \leq N-1 \tag{3.23c}$$

$$\bar{\boldsymbol{x}}_{k+i|k} \in \bar{\mathcal{X}} \quad 0 \leq i \leq N-1 \tag{3.23d}$$

$$\bar{\boldsymbol{u}}_{k+i|k} \in \bar{\mathcal{U}} \quad 0 \leq i \leq N-1 \tag{3.23e}$$

$$\bar{\boldsymbol{x}}_{k+N|k} \in \mathcal{X}_f \tag{3.23f}$$

where $\bar{\boldsymbol{x}}_{k+i|k}$ and $\bar{\boldsymbol{u}}_{k+i|k}$ are ith predicted state and input obtained at time instant k; $\bar{\mathcal{X}}$ and $\bar{\mathcal{U}}$ are state and input constraints; $\mathcal{X}_f$ is the terminal set; $\mathcal{Z}$ represents the robust positively invariant set. The nominal quadrotor model for prediction (3.23c) is also the discrete-time linear quadrotor model (3.21). Note that the initial nominal state $\bar{\boldsymbol{x}}_{k|k}$ is also a decision variable. At every time instant, $\bar{\boldsymbol{u}}_{k|k}$ is obtained by solving (3.23). Then, the actual control input $\boldsymbol{u}_k$ is generated based on the control law

$$\boldsymbol{u}_k = \bar{\boldsymbol{u}}_{k|k} + \boldsymbol{K}(\boldsymbol{x}_k - \bar{\boldsymbol{x}}_{k|k}) \tag{3.24}$$

where $\boldsymbol{K}$ is the feedback gain.

Since disturbances are not predictable, the prediction is conducted based on the nominal system (3.23c), and the impact of disturbances is mitigated by introducing the set $\mathcal{Z}$, which bounds the deviation between the predicted state $\bar{\boldsymbol{x}}_{k|k}$ and actual state $\boldsymbol{x}_k$, as expressed in (3.23b). The robust positively invariant set $\mathcal{Z}$ is calculated

as

$$\mathcal{Z} = \bigoplus_{i=0}^{\infty} (\boldsymbol{A} + \boldsymbol{B}\boldsymbol{K})^i \mathcal{W} \tag{3.25}$$

where $\oplus$ represents the Minkowski set addition as introduced in Chapter 2. In this way, the effect of disturbances on the system state can be explicitly characterized by $\mathcal{Z}$, in which all possible realizations of disturbances are considered. Thus, to ensure constraint satisfaction, the tightened constraints are imposed on predicted states and inputs:

$$\bar{\mathcal{X}} = \mathcal{X} \ominus \mathcal{Z} \tag{3.26a}$$

$$\bar{\mathcal{U}} = \mathcal{U} \ominus K\mathcal{Z} \tag{3.26b}$$

Combined with terminal set $\mathcal{X}_f$, tube-based MPC provides guarantees of recursive feasibility and closed-loop stability as proved in [14].

3.3.3 Lyapunov Model Predictive Control

The linear quadrotor model greatly simplifies the controller design, but it cannot fully characterize the nonlinear dynamics of quadrotors. However, it is challenging to design a similar terminal set in tube-based MPC for nonlinear systems. Thus, to design an MPC controller for a nonlinear quadrotor model, Lyapunov MPC is utilized in this subsection. Without the terminal set, Lyapunov MPC is able to stabilize the nonlinear system with guaranteed feasibility and stability by introducing an auxiliary control law and a stability constraint. Firstly, we provide a general form of the OCP

in Lyapunov MPC:

$$\min_{\boldsymbol{u}(\cdot)} \quad \int_{k_0}^{k_0+N\delta t} \left(x(t)^\top Q x(t) + u(t)^\top R u(t)\right) \mathrm{d}t \tag{3.27a}$$

$$\text{s.t.} \quad \dot{x}(t) = f(x(t), u(t)) \quad k_0 \leq t < k_0 + N\delta t \tag{3.27b}$$

$$x_{k+i|k} \in \mathcal{X} \quad k_0 \leq t < k_0 + N\delta t \tag{3.27c}$$

$$u(t) \in \mathcal{U} \quad k_0 \leq t < k_0 + N\delta t \tag{3.27d}$$

$$\frac{\partial V}{\partial x} f(x(k_0), u(k_0)) \leq \frac{\partial V}{\partial x} f(x(k_0), h(x(k_0))) \tag{3.27e}$$

where δt denotes the sampling period and k_0 is the current time instant. $V(\cdot)$ is the predefined Lyapunov equation and $h(\cdot)$ is the auxiliary control law. The auxiliary control law is a predesigned control law that can stabilize the system without constraint violation. However, the auxiliary control law is usually not optimal. To ensure closed-loop stability, the stability constraint (3.27e) is developed based on the auxiliary control law. In this constraint, the decay rate of the Lyapunov function value of the closed-loop system under the Lyapunov MPC should be less than that under the auxiliary control law. In this way, the closed-loop stability can be guaranteed.

To develop a Lyapunov MPC controller for quadrotors, the auxiliary control law should be designed first, which facilitates the development of the stability constraint. Here, an SMC control law is established to stabilize the translation based on the method proposed in [39]. For the translational dynamics (3.11), the sliding surface is designed as

$$\boldsymbol{s}_p = \lambda_p \boldsymbol{p} + \boldsymbol{v} = \boldsymbol{0} \tag{3.28}$$

where λ_p is chosen properly such that $s + \lambda_p$ is Hurwitz. When the system state $\boldsymbol{p}$ and $\boldsymbol{v}$ are on the sliding surface $\boldsymbol{s}_p = \boldsymbol{0}$, $\boldsymbol{p}$ approaches the equilibrium as t approaches infinity. Therefore, the control objectives of SMC are to drive the state to the sliding

surface and keep the state on this sliding surface. By differentiating $\boldsymbol{s}_p$ along the translational dynamics (3.11), we have

$$\dot{\boldsymbol{s}}_p = \lambda_p \boldsymbol{v} - \boldsymbol{g} + \frac{1}{m}\boldsymbol{r}(\boldsymbol{q}^r)T \tag{3.29}$$

It can be observed that both $\boldsymbol{r}(\boldsymbol{q}^r)$ and T are control inputs of the outer-loop control system, and they appear as a product in the equation above. Thus, a virtual control input $\boldsymbol{u}_{vir}$ is designed:

$$\boldsymbol{u}_{vir} \triangleq \boldsymbol{r}(\boldsymbol{q}^r)T = -c_p \boldsymbol{s}_p - \lambda_p \boldsymbol{v} + \boldsymbol{g} \tag{3.30}$$

where c_p is a constant and $c_p > 0$. To evaluate the closed-loop stability of the outer-loop control system, a Lyapunov function candidate is chosen:

$$V_p = \frac{1}{2}||\boldsymbol{s}_p||^2 \tag{3.31}$$

By differentiating V_p with respect to the time and utilizing (3.29), we have

$$\dot{V}_p = \boldsymbol{s}_p^\top(\lambda_p \boldsymbol{v} - \boldsymbol{g} + \frac{1}{m}\boldsymbol{r}(\boldsymbol{q}^r)T) \tag{3.32}$$

Replacing $\boldsymbol{r}(\boldsymbol{q}^r)T$ by $\boldsymbol{u}_{vir}$ yields

$$\dot{V}_p \leq -c_p||\boldsymbol{s}_p||^2 \tag{3.33}$$

Thus, by employing the virtual control input $\boldsymbol{u}_{vir}$, the system state will be driven to the sliding surface $\boldsymbol{s}_p = \boldsymbol{0}$ and eventually approach the equilibrium. It should be noted that the inner loop controller requires the reference Euler angles $\boldsymbol{q}^r$, and it cannot be obtained from the virtual control input $\boldsymbol{u}_{vir}$. However, the designed sliding

mode controller here only aims to provide the stability guarantee for Lyapunov MPC, therefore, how to determine $\boldsymbol{q}^r$ and T respectively from $\boldsymbol{u}_{vir}$ is not our concern. With the help of the auxiliary control law, the OCP for Lyapunov MPC can be constructed as

$$\min_{\boldsymbol{q}^r(\cdot),T(\cdot)} \quad \int_{k_0}^{k_0+N\delta t} \left(\boldsymbol{s}(t)^\top \boldsymbol{Q}\boldsymbol{s}(t) + \boldsymbol{q}^r(t)^\top \boldsymbol{R}_{\boldsymbol{q}}\boldsymbol{q}^r(t) + (T(t)-mg)R_T(T(t)-mg)\right) \mathrm{d}t \tag{3.34a}$$

$$\text{s.t.} \quad \begin{cases} \dot{\boldsymbol{p}}(t) = \boldsymbol{v}(t) \\ m\dot{\boldsymbol{v}}(t) = -m\boldsymbol{g} + \boldsymbol{r}(\boldsymbol{q}^r(t))T(t) \end{cases} \quad k_0 \le t < k_0 + N\delta t \tag{3.34b}$$

$$\begin{cases} \boldsymbol{p}(t) \in \mathcal{X}_p \\ \boldsymbol{v}(t) \in \mathcal{X}_v \end{cases} \quad k_0 \le t < k_0 + N\delta t \tag{3.34c}$$

$$\begin{cases} \boldsymbol{q}^r(t) \in \mathcal{U}_q \\ T(t) \in \mathcal{U}_T \end{cases} \quad k_0 \le t < k_0 + N\delta t \tag{3.34d}$$

$$\boldsymbol{s}_p(t)^\top \left(\lambda_p \boldsymbol{v}(t) - \boldsymbol{g} + \frac{1}{m}\boldsymbol{r}(\boldsymbol{q}^r(t))T(t)\right) \le -c_p||\boldsymbol{s}(t)||^2 \quad k_0 \le t < k_0 + \delta t \tag{3.34e}$$

3.3.4 Inner-loop Control

The aforementioned conventional MPC, tube-based MPC, and Lyapunov MPC are designed for translational control based on the assumption that the actual Euler angles are identical to the reference angles generated by MPC. Though this assumption is needed for the dual-loop quadrotor control, it cannot be perfectly satisfied in practical applications. To investigate the effects of the angle tracking error in dual-loop control, a sliding mode controller in [39] for the inner-loop rotational control is utilized. Here, the control objective is to minimize the tracking error $\boldsymbol{e}_q \triangleq \boldsymbol{q} - \boldsymbol{q}^r$. Similarly, the

angular velocity error is defined as $\boldsymbol{e}_\omega \triangleq \boldsymbol{\omega} - \ddot{\boldsymbol{q}}^r$. The sliding surface is designed as

$$\boldsymbol{s}_q = \lambda_q \boldsymbol{e}_q + \boldsymbol{e}_\omega \tag{3.35}$$

where λ_q is chosen such that $s + \lambda_q$ is Hurwitz. Differentiating $\boldsymbol{s}_q$ along the rotational dynamics (3.10) delivers

$$\dot{\boldsymbol{s}}_q = \lambda_q \boldsymbol{e}_\omega - \boldsymbol{I}^{-1}(\boldsymbol{\omega} \times \boldsymbol{I}\boldsymbol{\omega}) + \boldsymbol{I}^{-1}\boldsymbol{\tau} - \ddot{\boldsymbol{q}}^r \tag{3.36}$$

Then, the control law is developed as

$$\boldsymbol{\tau} = \boldsymbol{I}\left(\lambda_q \boldsymbol{e}_\omega + \boldsymbol{I}^{-1}(\boldsymbol{\omega} \times \boldsymbol{I}\boldsymbol{\omega} + \ddot{\boldsymbol{q}}^r - c_q \boldsymbol{s}_q)\right) \tag{3.37}$$

Similar to (3.31), we choose the Lyapunov function candidate

$$V_q = \frac{1}{2}||\boldsymbol{s}_q||^2 \tag{3.38}$$

Differentiating V_q with respect to the time and using (3.36) yields

$$\dot{V}_q = \boldsymbol{s}_q^\top \left(\lambda_q \boldsymbol{e}_\omega - \boldsymbol{I}^{-1}(\boldsymbol{\omega} \times \boldsymbol{I}\boldsymbol{\omega}) + \boldsymbol{I}^{-1}\boldsymbol{\tau} - \ddot{\boldsymbol{q}}^r\right) \tag{3.39}$$

By substituting $\boldsymbol{\tau}$ with the designed control input (3.37), we can obtain

$$\dot{V}_p \leq -c_p||\boldsymbol{s}_q||^2 \tag{3.40}$$

which indicates that the state will be steered to the sliding surface with guarantees if (3.37) is employed.

3.4 Simulation Results

In this section, the simulation results of conventional MPC, tube-based MPC, and Lyapunov MPC for quadrotor control are provided. The control performance and the robustness against the wind gusts are examined and compared. Firstly, we employ three MPC schemes to regulate the system state respectively. The quadrotor models are chosen to be prediction models used in three MPC schemes, which aims to validate the effectiveness of the three MPC schemes. Then, the three MPC methods are tested on the same nonlinear quadrotor model to verify their effectiveness in practical applications, in which trajectory tracking is the control objective. Moreover, since practical implementations require a small sampling period such that control inputs can be provided with high frequency. However, in dual-loop control frameworks, solving the control optimization problem of MPC usually requires more computation time than other non-optimization-based methods. This challenge provokes a dual-sampling-rate solution that MPC is employed for outer-loop control with a longer sampling period, and other control methods with less computation time are utilized for inner-loop control with a faster sampling rate. In this section, such a dual-sampling-rate framework is also utilized to investigate the effect of different sampling ratios on the control performance.

3.4.1 State Regulation with Different Quadrotor Models

The quadrotor control in this chapter is achieved by using a dual-loop control framework, and control strategies for inner-loop and outer-loop are different. Thus, to validate the effectiveness of three MPC schemes for translational control, we ignore the rotational dynamics, i.e., assuming that the actual and reference Euler angles are identical. In this subsection, conventional MPC and tube-based MPC are utilized

Parameter	**Value**
I_{xx} - moment of inertia about axis $\boldsymbol{x}_B$	0.043467
I_{yy} - moment of inertia about axis $\boldsymbol{y}_B$	0.043467
I_{zz} - moment of inertia about axis $\boldsymbol{z}_B$	0.063267
m - mass of the quadrotor	2.618
g - gravitational acceleration	9.81
K_T - thrust-to-command ratio	0.7
T - total thrust	$-2 \leq T - mg \leq 2$

Table 3.1: Physical parameters of the quadrotor.

Variables	**Range**
θ^r - reference pitch (rad)	$[-2 \quad 2]$
ϕ^r - reference roll (rad)	$[-2 \quad 2]$
ψ^r - reference yaw (rad)	$[-2 \quad 2]$
$T - mg$ - thrust-gravity difference (N)	$[-2 \quad 2]$
x - position on axis $\boldsymbol{x}_I$ (m)	$[-100 \quad 100]$
$\dot{x}$ - velocity along axis $\boldsymbol{x}_I$ (m/s)	$[-10 \quad 10]$
y - position on axis $\boldsymbol{y}_I$ (m)	$[-100 \quad 100]$
$\dot{y}$ - velocity along axis $\boldsymbol{y}_I$ (m/s)	$[-10 \quad 10]$
z - position on axis $\boldsymbol{z}_I$ (m)	$[-100 \quad 100]$
$\dot{z}$ - velocity along axis $\boldsymbol{z}_I$ (m/s)	$[-10 \quad 10]$

Table 3.2: Constraints in simulation.

to regulate the state of the linear translational model (3.15), and Lyapunov MPC is employed to regulate the state of the nonlinear translational model (3.11). The disturbance generated by the wind gusts is considered.

Firstly, the physical parameters of the quadrotor are provided in Table 3.1. It can be found that $I_{xx} = I_{yy}$, which indicates that the airframe is symmetric about the center of the quadrotor. The sampling interval is set to be $0.02s$. The constraints for the quadrotor are given in Table 3.2.

Note that for both linear and nonlinear translational dynamic systems, reference angles and the total thrust are control inputs. The weighting matrices for conventional MPC and tube-based MPC are chosen to be the same: $\boldsymbol{Q} = \text{diag}\{10, 10, 10, 10, 10, 10\}$,

and $\boldsymbol{R} = \text{diag}\{0.001, 0.001, 0.001\}$. This choice puts more weight on the state than the input, since driving the state to the equilibrium is our primary objective. The feedback gain $\boldsymbol{K}$ in tube-based MPC is chosen as $\boldsymbol{K} = [-5.0333 \quad -5.1343 \quad 5.0333 \quad 5.1343 \quad -1.4141 \quad -1.4563]$, which is the optimal one that minimizes the cost function when state feedback control is employed.

The disturbance from the wind gust is generated in the form of equations (3.17) and (3.18). The coefficient matrices in (3.17) are chosen as $\boldsymbol{M}_1 = \boldsymbol{\mathcal{I}}_{1\times 1}$ and $\boldsymbol{M}_2 = \boldsymbol{\mathcal{I}}_{3\times 1}$. In the simulation, we manually set the upper bounds of the disturbance torques and forces, but the magnitudes $v_{d,k}^0$, frequencies $\bar{\omega}_{i,k}$, and phase shifts $\alpha_{i,k}$ are chosen randomly.

By using the previously mentioned parameters, the following simulation results of the state regulation with different quadrotor models are provided.

State Regulation with Disturbance Bound 0.005

Firstly, the upper bound of the disturbance $\bar{T}_d$ is set to be 0.005. The initial position is chosen as $[0.5 \;\; 0.3 \;\; 0]^\top$ with zero velocity. Three MPC strategies are utilized to drive the quadrotor to the equilibrium. The simulation results are shown as follows. Figure 3.2 illustrates the translational motion of the quadrotor. Since in this subsection, we assume that the reference angle tracking is perfect, the rotational motion control is not included. It can be observed that all three MPC strategies are able to stabilize the quadrotor.

For conventional and tube-based MPC, the same linear model is utilized as the plant, but the state converges faster when tube-based MPC is employed, which can be explained from the perspective of OCP formulation. In the conventional MPC, the first element in the predicted state sequence is equal to the current state. However, the initial predicted state is a decision variable in tube-based MPC, which means the

control input can be chosen from a larger range. Thus, compared with conventional MPC, the tube-based MPC provides more aggressive control commands.

Some fluctuations can be observed in the results of Lyapunov MPC, because rather than directly steering the state to the equilibrium, the designed Lyapunov MPC aims to keep the state on the sliding surface, and therefore the fluctuations around the sliding surface are inevitable in the presence of disturbances.

State Regulation with Disturbance Bound 0.5

To further investigate the robustness of the three MPC schemes, the disturbance upper bound $\bar{T}_d$ is set to be 0.5. Under this setup, the value of the actual velocity may increase or decrease by 0.0981 due to disturbances. The simulation results are shown in Figure 3.3. Larger fluctuations can be found in the vertical motion, which can be inferred from the linear quadrotor model. Motions along three axes of the inertial frame can be decoupled, and the motion along $\boldsymbol{z}_I$ is controlled by the total thrust T. For the nonlinear quadrotor model, when Euler angles are small, the total thrust has the greatest impact on the translational motion along $\boldsymbol{z}_I$. Thus, the effect of disturbances on the translational motion is mainly demonstrated in the third subplot.

Similar to Figure 3.2, tube-based MPC outperforms conventional MPC, and the difference between them becomes more evident in Figure 3.3. The reason is that the larger disturbance upper bound $\bar{T}_d$ results in the larger robust positively invariant set $\mathcal{Z}$ according to (3.25). Consequently, in tube-based MPC, the initial nominal state can be chosen from a larger range compared with the results of $\bar{T}_d = 0.005$.

State Regulation with Disturbance Bound 1.9

To further explore how large the disturbance is that the controller can handle, an estimated maximum value of the upper bound for the disturbance is obtained, which

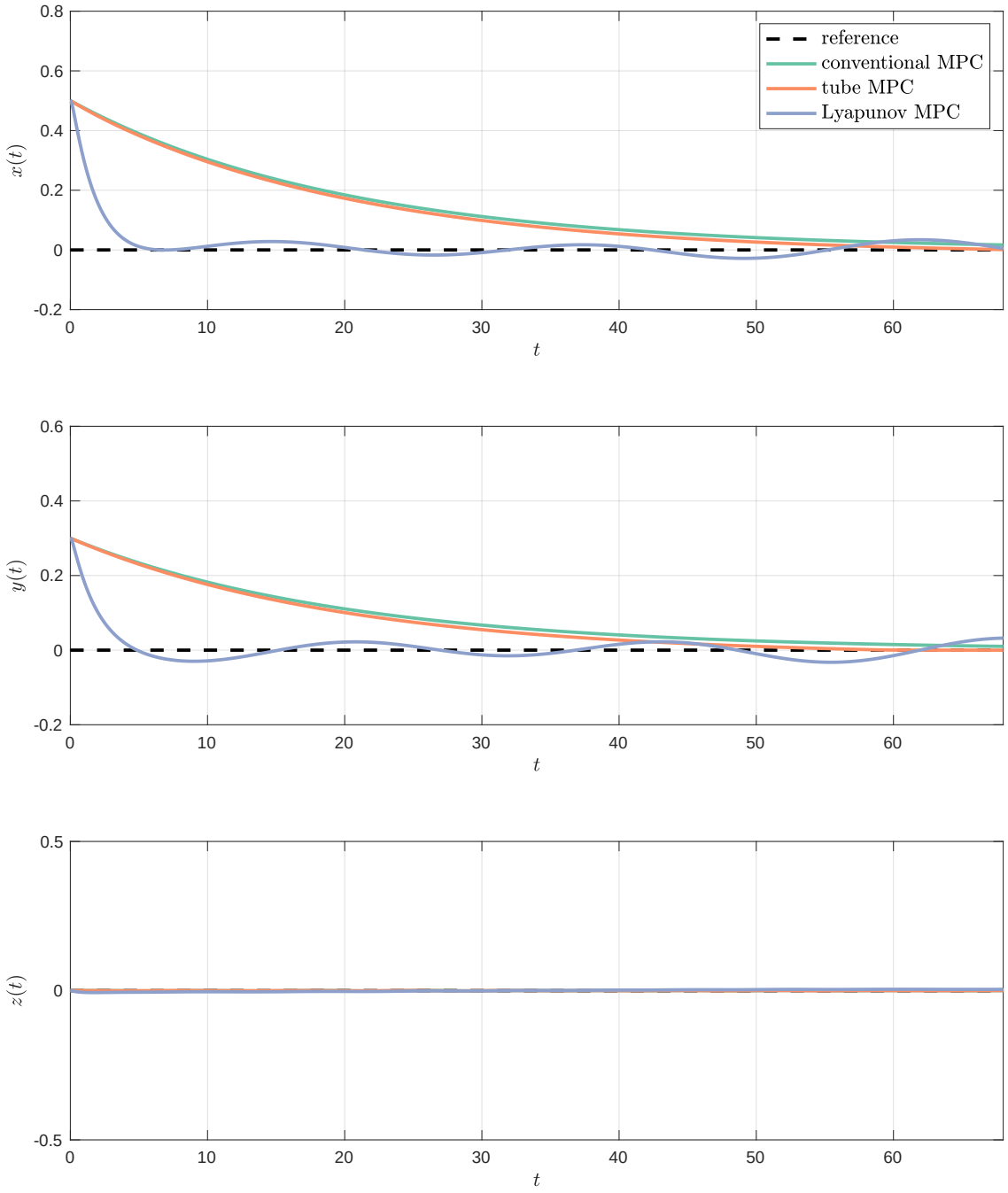

Figure 3.2: Quadrotor translational motion with $\bar{T}_d = 0.005$.

is $\bar{T}_d = 1.9$. The corresponding simulation results are shown in Figure 3.4. Compared with Figure 3.3, the state converges faster when the quadrotor is controlled by tube-

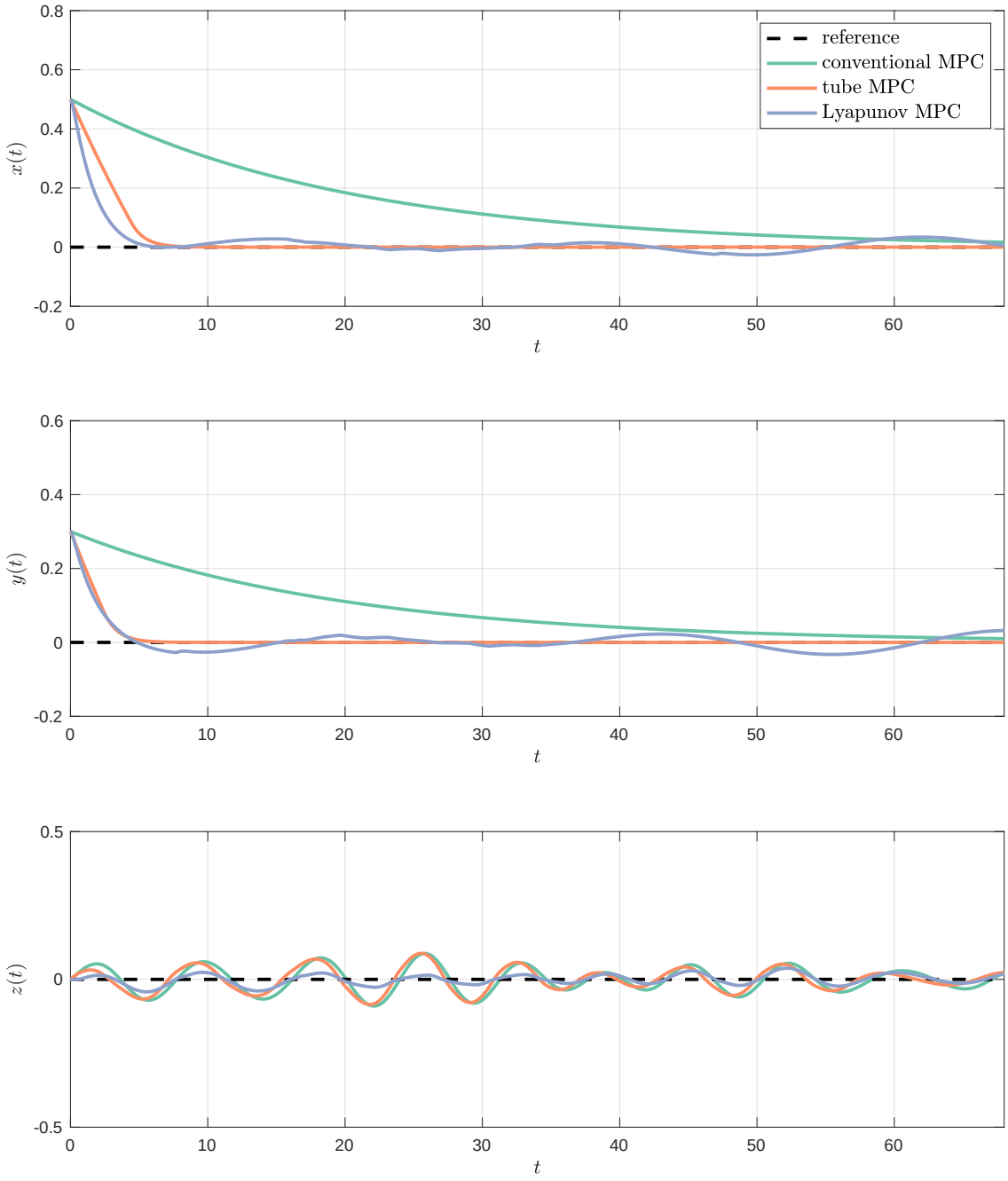

Figure 3.3: Quadrotor translational motion with $\bar{T}_d = 0.5$.

based MPC. However, the larger disturbance upper bound results in smaller tightened constraint sets $\bar{\mathcal{X}}$ and $\bar{\mathcal{U}}$. Thus, the OCP of the tube-based MPC becomes infeasible

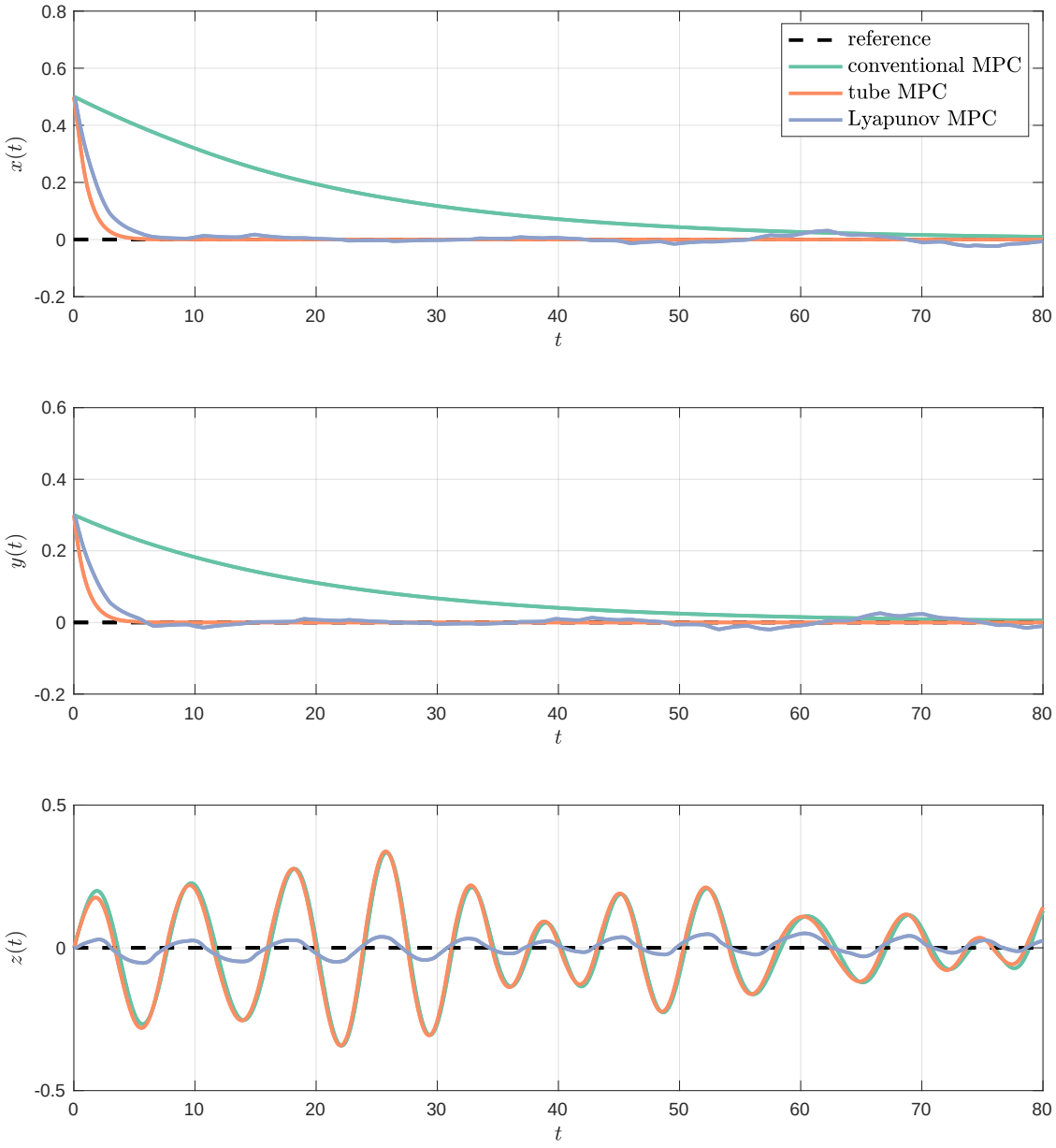

Figure 3.4: Quadrotor translational motion with $\bar{T}_d = 1.9$.

when $\bar{T}_d$ is greater than 1.9. The constant fluctuations exist in vertical movement due to disturbances exerted on thrusts.

In general, all three MPC strategies are able to stabilize the quadrotor and exhibit great robustness against wind gusts.

3.4.2 Reference Tracking with the Same Nonlinear Quadrotor Model

In the previous subsection, the simulations are conducted based on different quadrotor models. However, in practical applications, the control input generated by the controller is applied to the quadrotor with nonlinear dynamics. Thus, to simulate the practical application, three MPC schemes are adopted as the outer-loop controllers in a dual-loop control framework. Both translational and rotational dynamics are considered and the SMC-based inner-loop controller introduced in Section 3.3.4 is utilized. The sampling intervals of both inner and outer control loops are set to be $0.02s$.

Apart from the state regulation, another control objective for quadrotors that commonly appears in applications is trajectory tracking. In this subsection, three MPC schemes are adopted for trajectory tracking, and the following reference trajectory is utilized:

$$x^r(t) = 10\cos(\frac{\pi}{60}t)\cos(\frac{\pi}{15}t) \tag{3.41a}$$

$$y^r(t) = 10\cos(\frac{\pi}{60}t)\sin(\frac{\pi}{15}t) \tag{3.41b}$$

$$z^r(t) = 20\cos(\frac{\pi}{60}t) \tag{3.41c}$$

The corresponding reference velocity and acceleration can be obtained by differentiating x^r, y^r, z^r with respect to t. To adopt the control schemes for tracking, the sliding surface for Lyapunov MPC is changed to be

$$\boldsymbol{s}_p = \lambda_p \boldsymbol{e}_p + \boldsymbol{e}_v = \boldsymbol{0} \tag{3.42}$$

where $\boldsymbol{e}_p \triangleq \boldsymbol{p} - \boldsymbol{p}^r$ and $\boldsymbol{e}_v \triangleq \boldsymbol{v} - \boldsymbol{v}^r$. Accordingly, the virtual control law (3.30)

becomes

$$\boldsymbol{u}_{vir} \triangleq \boldsymbol{r}(\boldsymbol{q}^r)T = -c_p\boldsymbol{s}_p - \lambda_p\boldsymbol{e}_v + \boldsymbol{g} - \ddot{\boldsymbol{p}}^r \tag{3.43}$$

Similarly, the linear quadrotor model becomes

$$\boldsymbol{e}_{k+1} = A\boldsymbol{e}_k + B\boldsymbol{u}_k - \boldsymbol{x}^r_{k+1} \tag{3.44}$$

By using the same quadrotor nonlinear model (3.11) and the same control parameters in the last subsection, the simulation results of three MPC for trajectory tracking with nonlinear translational model (3.11) and nonlinear rotational model (3.10) are obtained.

The initial position is $[11 \quad 0 \quad 20]^\top$, and the initial velocity is $[0 \quad 2 \quad 0]^\top$. Disturbances are also involved and the disturbance upper bound is set to be $\bar{T}_d = 0.5$. Figure 3.5 illustrates the translational motion of the quadrotor. It can be observed that the conventional MPC and the Lyapunov MPC are able to track the given reference path, but the tube-based MPC fails. The OCP of tube-based MPC becomes infeasible at around $12.5s$. The rotational motion in Figure 3.6 shows the same phenomenon, in which the dot lines represent the reference angles generated by the outer-loop controller. In Figure 3.6, the fluctuations in rotational motion of conventional and tube-based MPC are caused by the model mismatch and disturbances. Since the tube-based MPC provides more aggressive control inputs, the variations of reference angles generated by the tube-based MPC (red dot line) are too large such that the inner-loop controller fails to track. Thus, the OCP of tube-based MPC eventually becomes infeasible.

One may notice that the yaw changes with small amplitudes. The reason is that due to the symmetric structure, $I_{xx} = I_{yy}$, the rotational dynamics about the $\boldsymbol{z}_B$ becomes $I_{zz}\ddot{\psi} = \tau_\psi$ such that the variation of yaw is induced by the disturbance

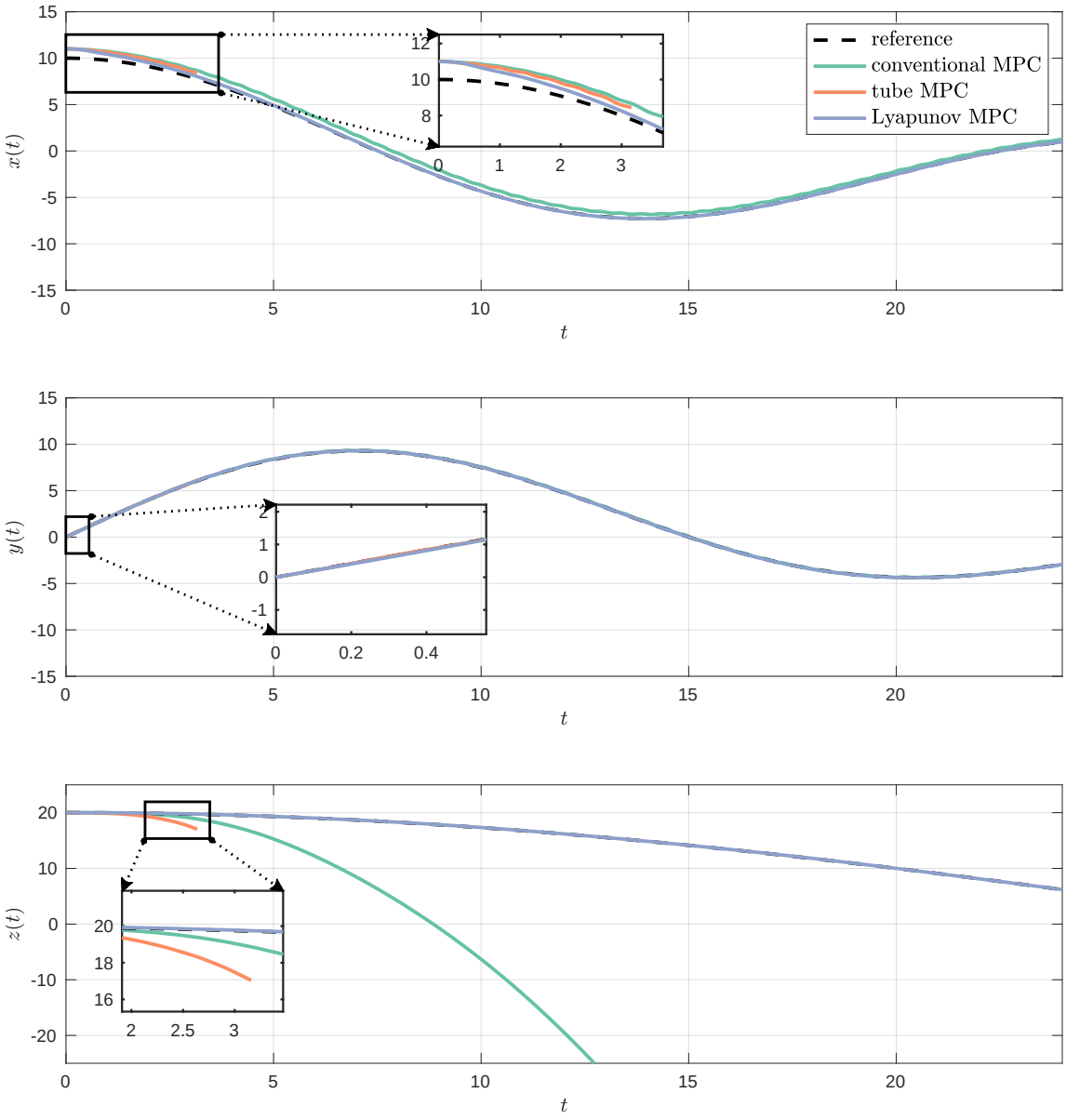

Figure 3.5: Translational motion of the quadrotor in Section 3.4.2.

torque only.

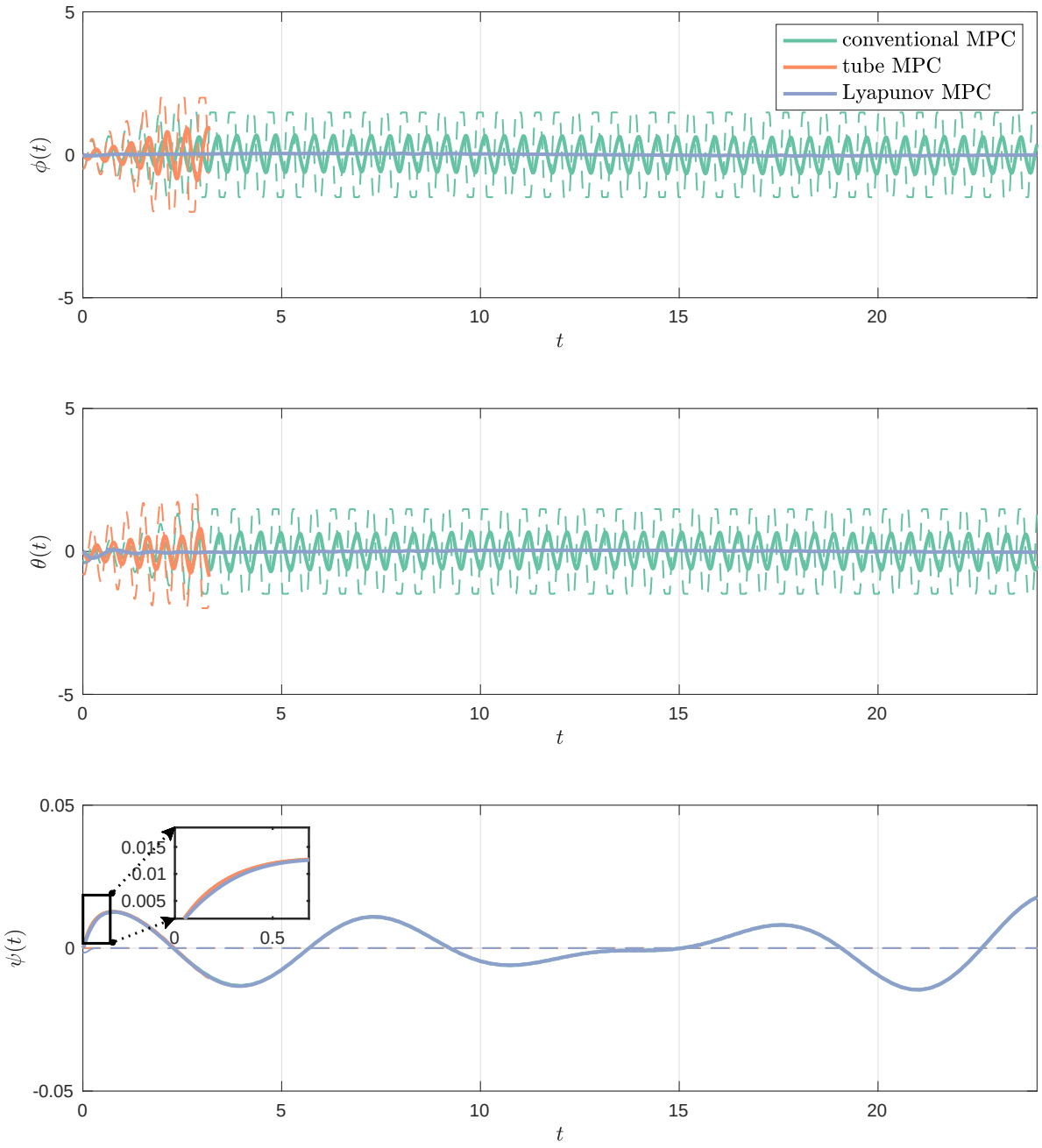

Figure 3.6: Rotational motion of the quadrotor in Section 3.4.2.

3.4.3 Reference Tracking with Dual-rate Sampling

In the last subsection, the simulation is conducted based on the same sampling period in inner-loop and outer-loop control. This setup may bring two issues. Firstly,

the control command can be generated on either the onboard microcontroller or the ground station. To expand the task space, the onboard controller is preferred. However, the limited computation resource may not be able to provide the control command within the small sampling instant. Secondly, in the dual-loop control framework, the outer-loop controller is usually designed based on the assumption that the inner-loop controller is able to track the reference angles. However, this assumption cannot be easily satisfied in practical applications.

To tackle these issues, a solution for dual-loop control is to utilize a dual-sampling-rate strategy, i.e., the sampling period for the outer loop is greater than that of the inner loop. To test the control performance under the dual-sampling-rate settings, the simulation results are conducted in this subsection.

Reference Tracking with Sampling Ratio 3

Firstly, the sampling periods are set to be $0.02s$ for the inner loop and $0.06s$ for the outer loop. The results are shown in Figure 3.7 and 3.6. Other parameters in simulations are chosen to be the same as previous setups. Compared with the results in the previous subsection, all three MPC strategies are able to track the reference trajectory under the dual-sampling-rate framework. For the tube-based MPC, the control optimization problem becomes feasible at all sampling instants. However, in Figure 3.8, fluctuations of the reference angles still appear. Though the magnitude of the fluctuation keeps decreasing over time, it may not be acceptable in practical applications.

Reference Tracking with Sampling Ratio 5

Next, we set the sampling periods to be $0.02s$ for the inner loop and $0.1s$ for the outer loop. Results are shown in Figure 3.9 and Figure 3.10. It can be found that

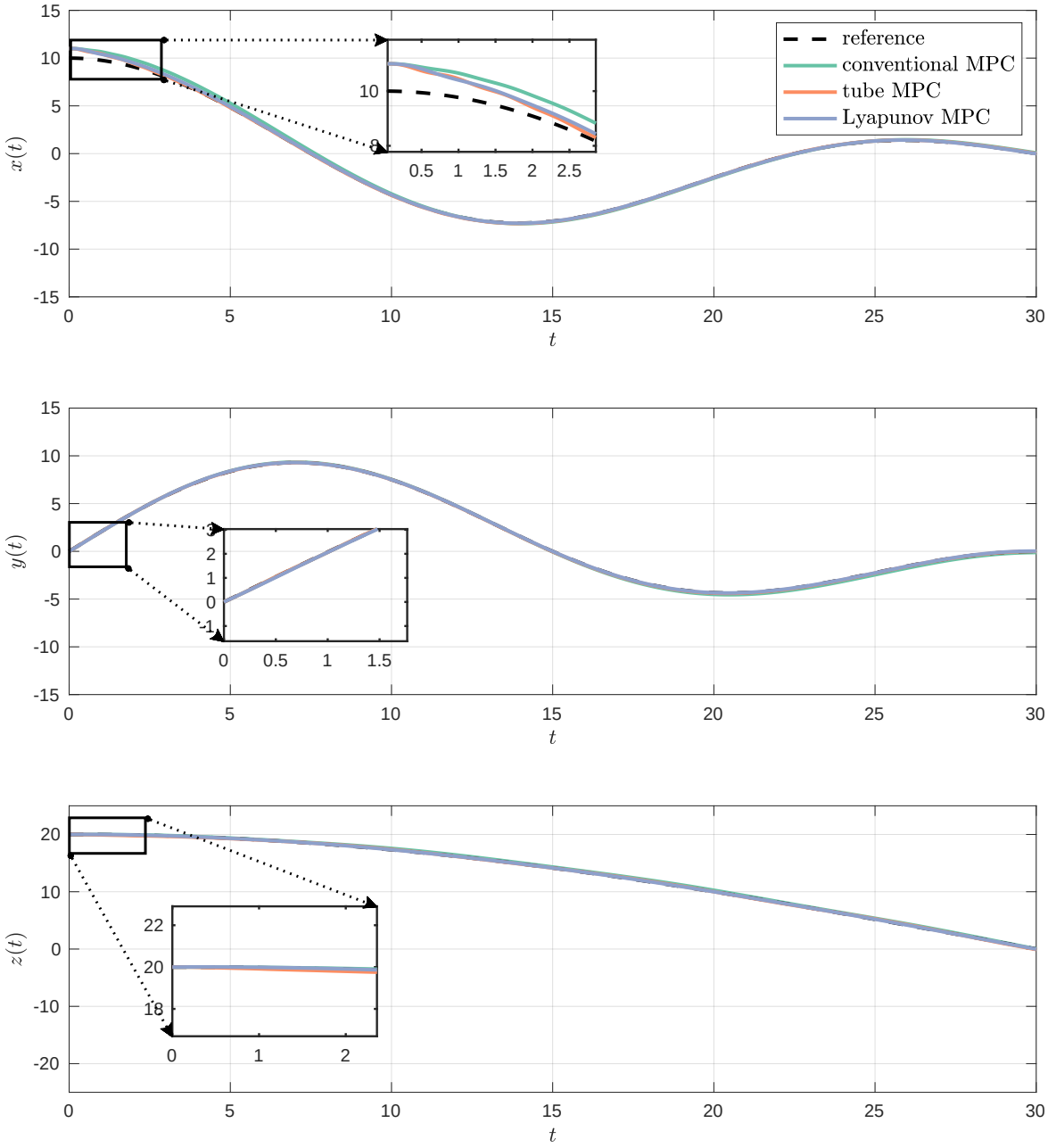

Figure 3.7: Quadrotor translational motion with sampling ratio 3.

the variations of the reference roll and reference pitch are greatly reduced. The magnitude of the reference fluctuation is only half of the magnitude in Figure 3.8 within $0s$ to $10s$. The increased outer-loop sampling period decreases the updating

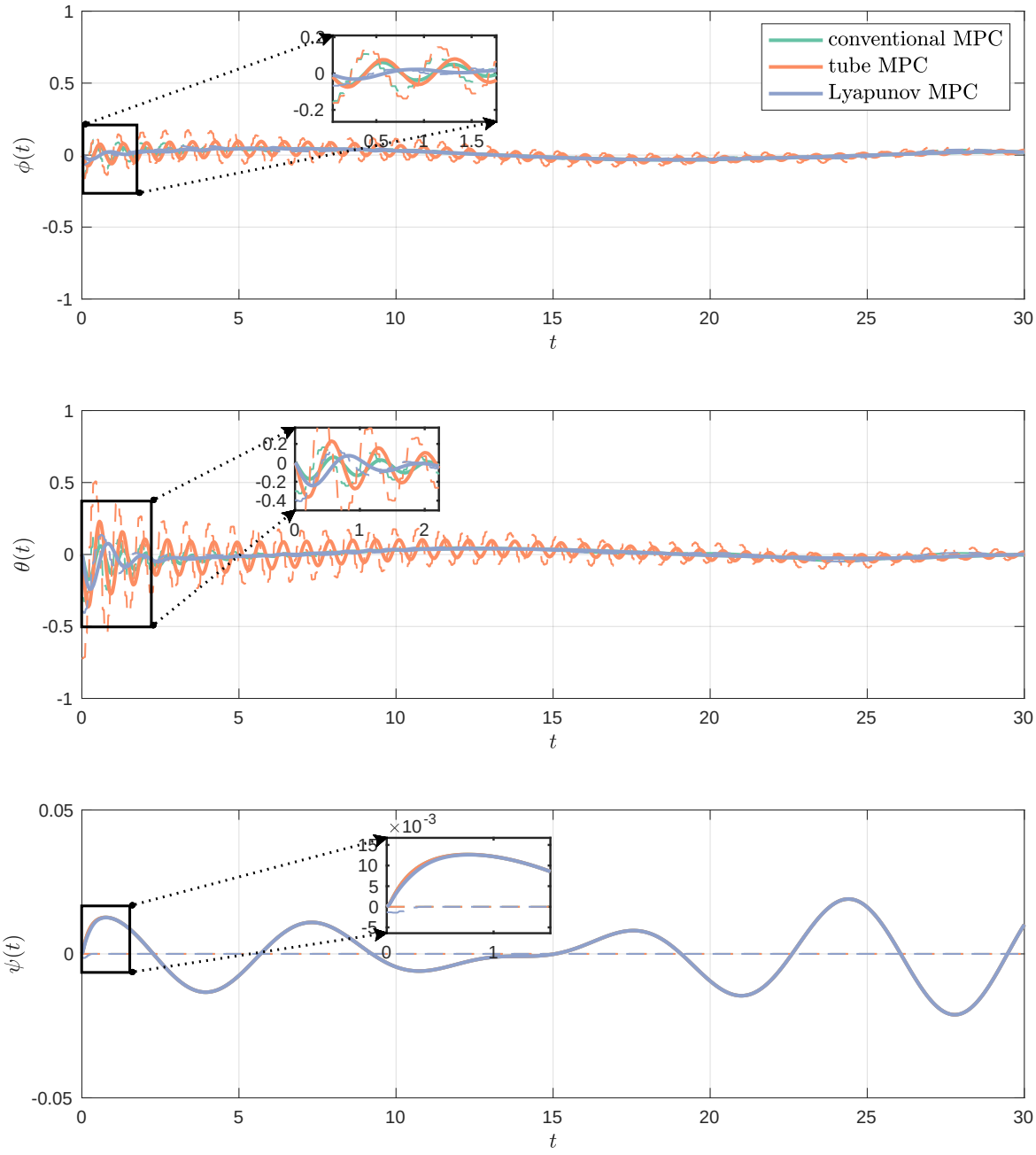

Figure 3.8: Quadrotor rotational motion with sampling ratio 3.

rate of reference angles and provides more time for the inner-loop system to track, which improves the control performance.

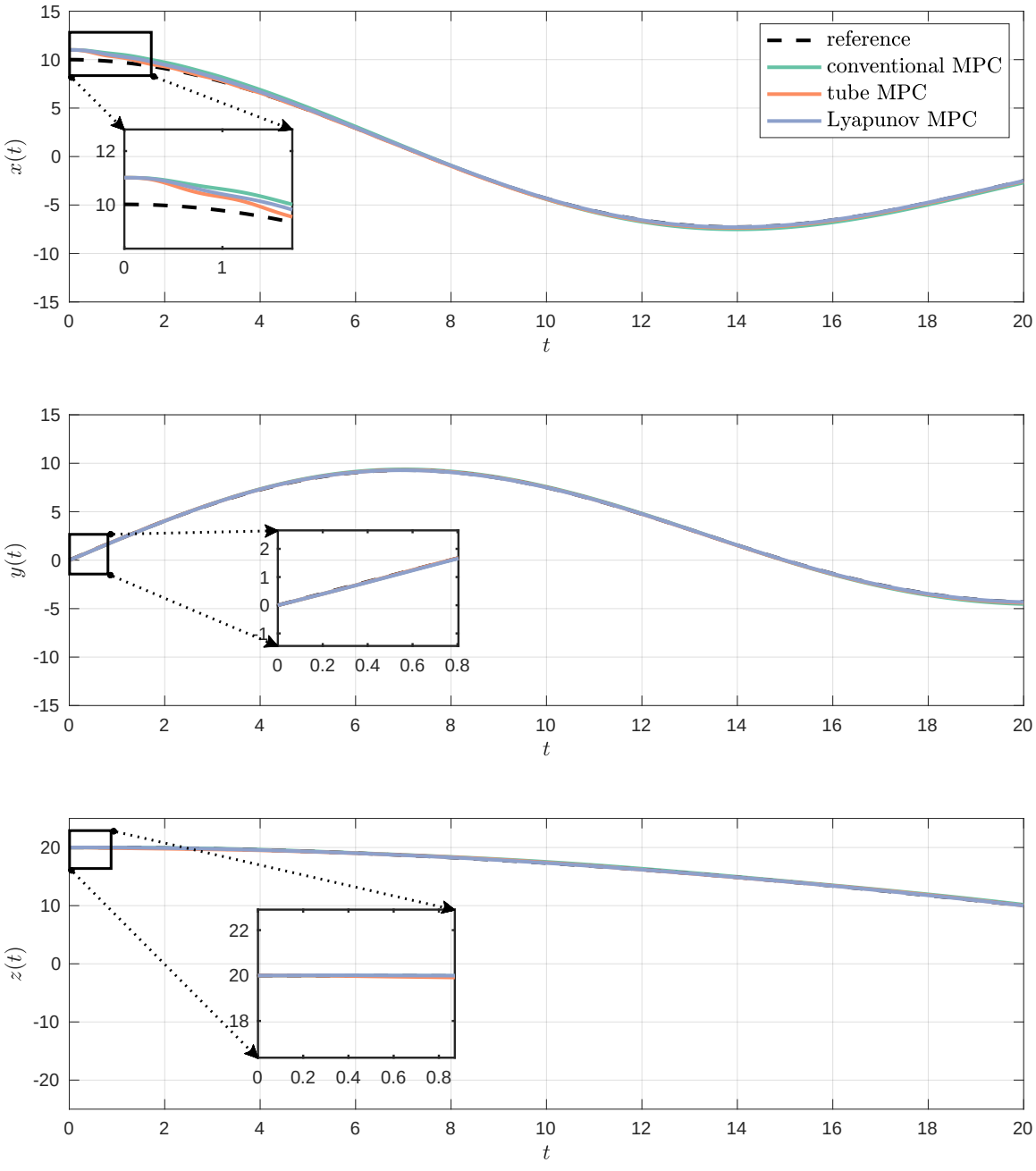

Figure 3.9: Quadrotor translational motion with dual sampling ratio 5.

Reference Tracking with Sampling Ratio 20

According to the obtained simulation results, it can be observed that as the sampling ratio of the outer and inner loop increases, the fluctuations of attitude signals decrease,

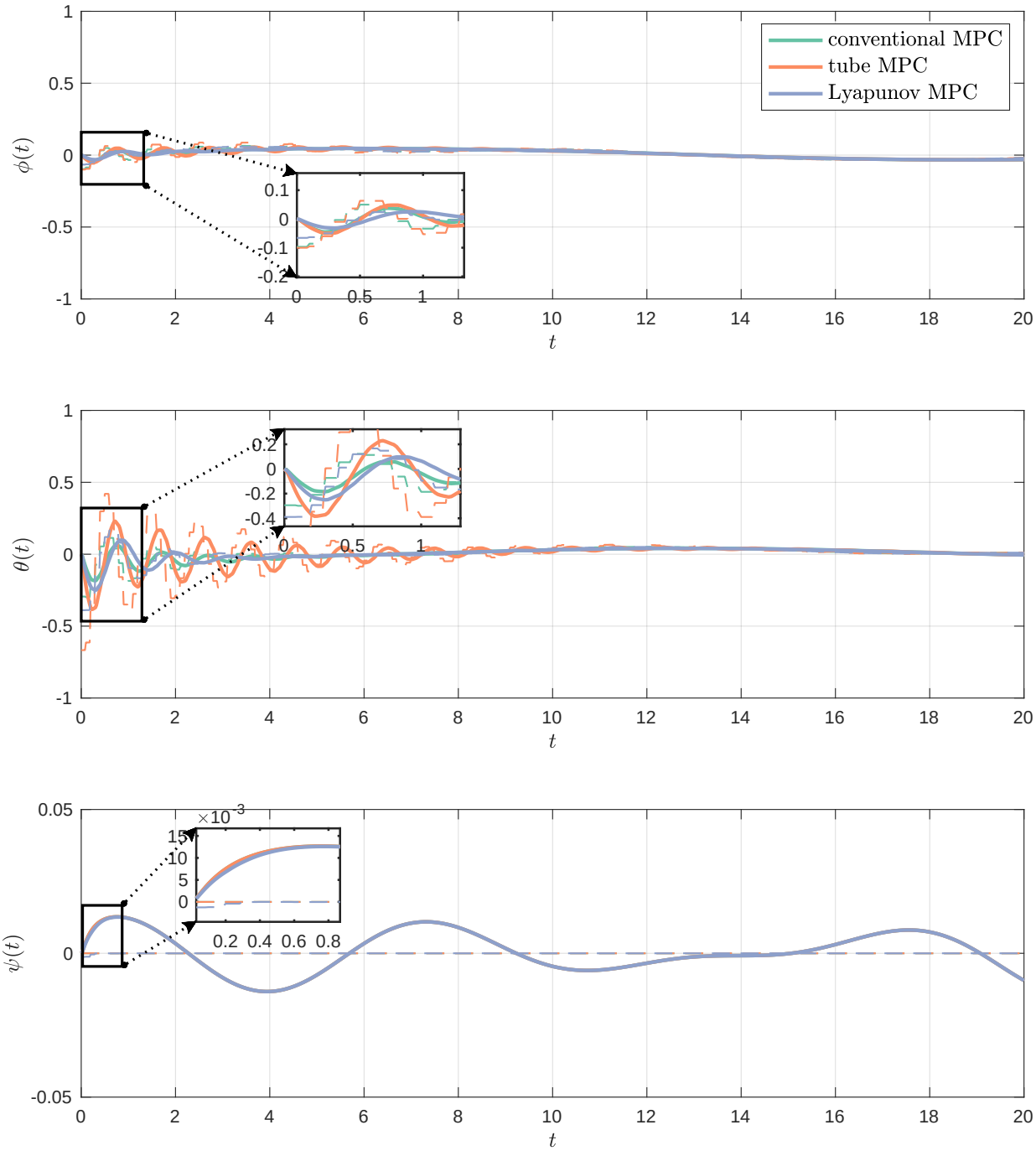

Figure 3.10: Quadrotor rotational motion with dual sampling ratio 5.

and the control performance becomes better. However, a higher sampling ratio does not always imply improved control performance. Figure 3.11 and Figure 3.12 illustrate

the output of the system when sampling periods are chosen to be 0.02 for the inner loop, and 0.4 for the outer loop. Under this setup, more fluctuations of three angles appear, and the OCP of Lyapunov MPC becomes infeasible eventually. The reason is that the variations of reference angles between two consecutive sampling instants are too large, resulting in the tracking failure of the inner-loop controller.

In general, one can conclude that the dual-sampling-rate structure can improve the control performance of the quadrotor if the sampling ratio is properly chosen. Moreover, the quadrotor system is stable only if the sampling ratio is within a certain range.

3.5 Conclusions

In this chapter, we first derive the nonlinear and linear quadrotor models. Then, based on the obtained quadrotor models, conventional MPC, tube-based MPC, and Lyapunov MPC are adopted for translational control.

To validate the effectiveness of the three MPC schemes, they are utilized as the outer-loop controller to regulate the state in the presence of wind gusts as disturbances. All three MPC schemes are able to stabilize the system and exhibit great robustness against the simulated wind gusts. Then, to simulate the practical applications, the control inputs generated by three MPC controllers are applied to the same nonlinear quadrotor model, and both the translational and rotational dynamics are considered. Though Lyapunov MPC and conventional MPC controllers are designed based on different quadrotor models, they are able to track the given trajectory. Due to the existence of reference angle fluctuations induced by model mismatch and disturbances, tube-based MPC cannot provide satisfying performance. Further, we investigate the control performance of the three MPC schemes when the dual-

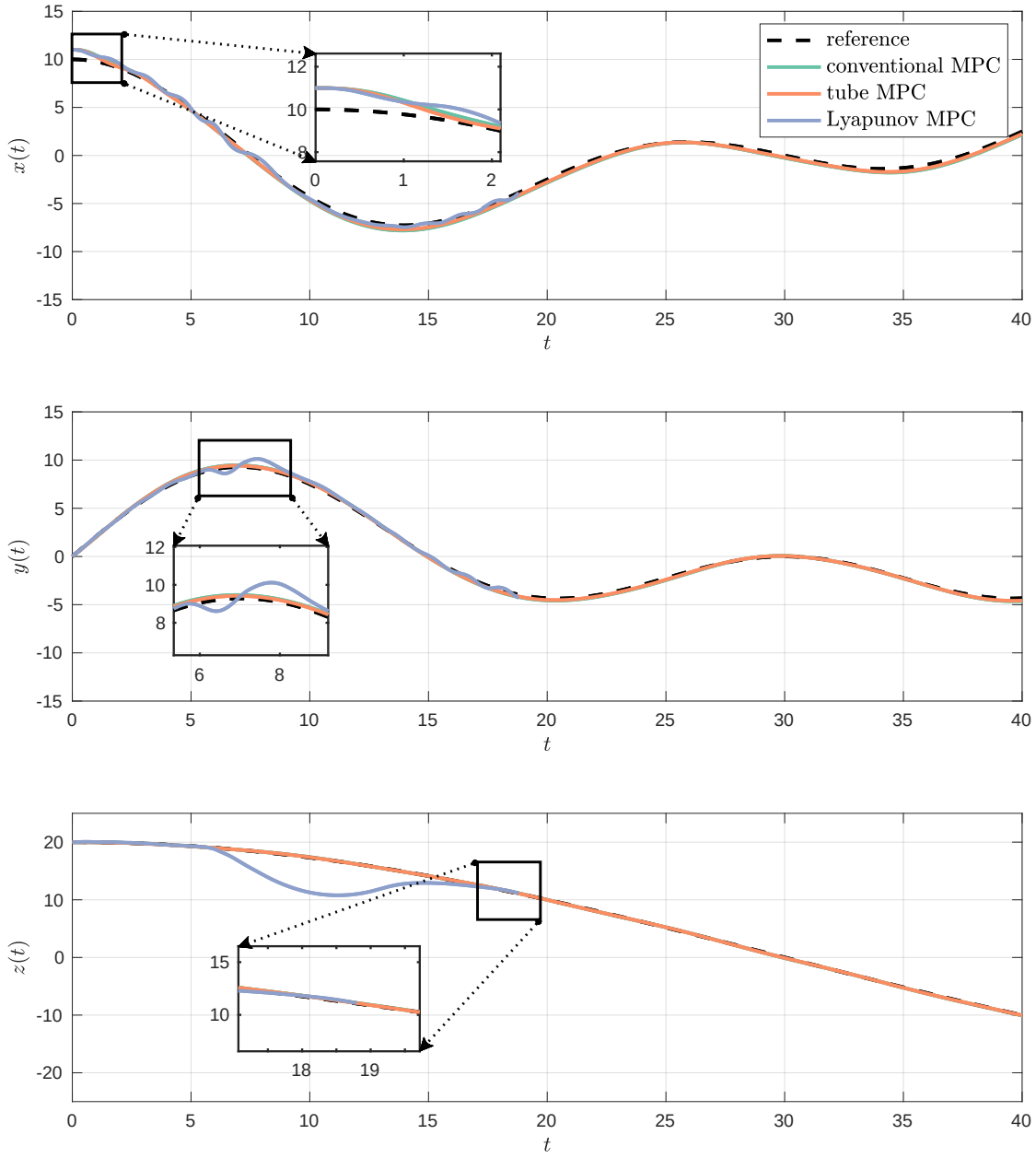

Figure 3.11: Quadrotor translational motion with sampling ratio 20.

sampling-rate strategy is utilized. As the sampling ratio between the outer loop and the inner loop increases, the control performance of the three MPC schemes can be improved. Moreover, the closed-loop system can be stabilized only when the sampling ratio is chosen within a certain range.

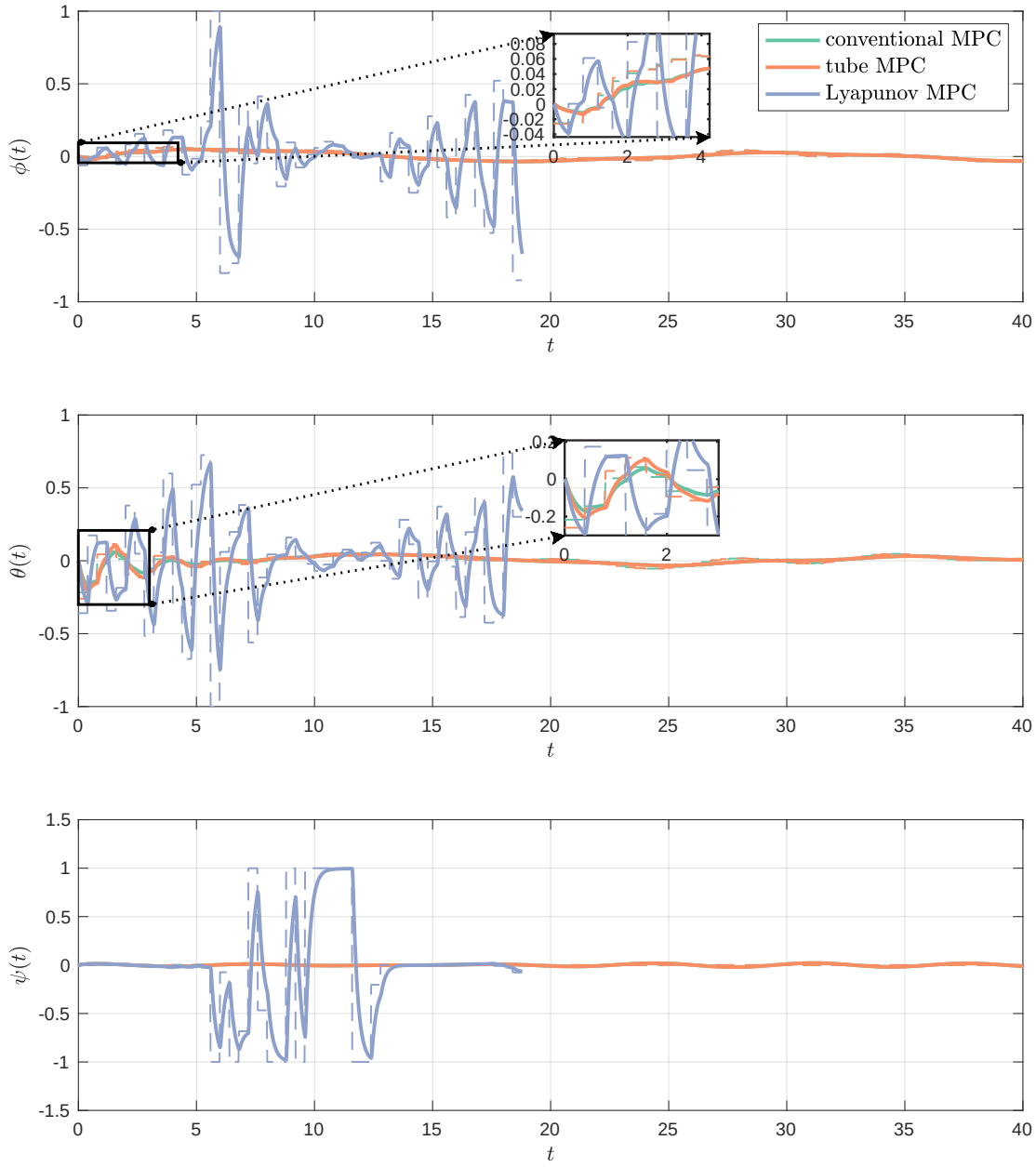

Figure 3.12: Quadrotor rotational motion with sampling ratio 20.

Chapter 4

Conclusions and Future Work

4.1 Conclusions

For the networked quadrotor control systems, we propose a robust output feedback MPC scheme to handle external disturbances, hard state, and input constraints, and random packet dropouts in both controller-actuator and sensor-controller channels. The proposed output feedback MPC scheme consists of a state observer that accommodates the random measurement loss and a state feedback model predictive controller that stabilizes the perturbed system. According to the proposed observer, the estimation error dynamics can be represented by a switched system. By developing a GRPI set under the switched system formulation, the estimation error can be confined in this invariant set, which serves as the explicit error bound of state estimation. Similarly, an ERPI set is developed to confine the deviation between the estimated and predicted states. Then, these sets are utilized to tighten the state and input constraints to alleviate the effects of random packet dropouts and disturbances. By imposing tightened constraints on the predicted states and inputs in the MPC optimization problem, the system can be stabilized by the proposed output feedback

model predictive controller while both state and input constraints are satisfied.

To examine and compare the effectiveness of different MPC schemes for quadrotor control, comparison simulation studies are conducted with conventional MPC, tube-based MPC, and Lyapunov MPC. Firstly, both nonlinear and linear quadrotor models are developed by using Netwon-Euler equations and same-angle assumptions. Then, three MPC schemes are employed to regulate the state of different quadrotor models to validate their effectiveness and robustness in the presence of wind gusts. Moreover, these methods are also tested on the same nonlinear quadrotor model for reference tracking. Additionally, the identical and different sampling periods of the inner control loop and outer control loop are tested. The reference tracking is fulfilled only when the sampling ratio is chosen in a specific range. It can be concluded that conventional MPC, tube-based MPC, and Lyapunov MPC can stabilize the system and drive the quadrotor to track the reference path if the control parameters are properly chosen. All these three algorithms exhibit great robustness against the disturbances caused by wind gusts.

4.2 Future Work

The robust MPC scheme proposed in Chapter 2 is designed based on the tube-based MPC, in which the impact of the disturbances is described by compact sets. Specifically, all possible realizations of the predicted state and the actual state lie in the invariant set in the presence of packet dropouts and disturbances. However, the set computation may result in excessively tightened constraints and thus conservative control performance, especially when the disturbance set is considerably large. Thus, the output feedback stochastic MPC can be utilized to avoid set computation and constraint tightening. How to handle the state and input constraints simultaneously

in stochastic MPC for networked control systems is a remaining problem.

In Chapter 3, the MPC strategies are validated by simulation results without experiments. In simulations, the upper bound for disturbances from the wind gust is assumed to be known, which is hard to obtain in practical implementations. Thus, how to design a robust MPC strategy with unknown disturbance bounds needs further investigation. Meanwhile, the quadrotor model is assumed to be symmetric, but in experiments, the physical parameters cannot be obtained accurately. Thus, how to estimate the unknown parameters and guarantee the stability of the system with model uncertainties is another open problem. Moreover, the simulation results reveal that the dual sampling rate greatly affects the control performance. Thus, how to choose the sampling times for the inner loop and outer loop is crucial in control system design, and further investigation is needed to explore its impact on closed-loop stability.

Bibliography

[1] M. Rinaldi, S. Primatesta, and G. Guglieri, "A comparative study for control of quadrotor UAVs," *Applied Sciences*, vol. 13, no. 6, p. 3464, 2023.

[2] H. Voos, "Nonlinear control of a quadrotor micro-UAV using feedback-linearization," in *Proceedings of IEEE International Conference on Mechatronics*, Malaga, Spain, Apr. 2009, pp. 1–6.

[3] F. Chen, R. Jiang, K. Zhang, B. Jiang, and G. Tao, "Robust backstepping sliding-mode control and observer-based fault estimation for a quadrotor UAV," *IEEE Transactions on Industrial Electronics*, vol. 63, no. 8, pp. 5044–5056, 2016.

[4] E. Soria, F. Schiano, and D. Floreano, "Predictive control of aerial swarms in cluttered environments," *Nature Machine Intelligence*, vol. 3, no. 6, pp. 545–554, 2021.

[5] N. Michel, S. Bertrand, G. Valmorbida, S. Olaru, and D. Dumur, "Design and parameter tuning of a robust model predictive controller for UAVs," in *Proceedings of IFAC World Congress*, Toulouse, France, Jul. 2017.

[6] I. Lopez-Sanchez and J. Moreno-Valenzuela, "PID control of quadrotor UAVs: A survey," *Annual Reviews in Control*, vol. 56, p. 100900, 2023.

[7] F. Goodarzi, D. Lee, and T. Lee, "Geometric nonlinear PID control of a quadrotor UAV on SE(3)," in *Proceedings of European Control Conference (ECC)*, Zurich, Switzerland, Jul. 2013, pp. 3845–3850.

[8] D. Lee, H. Jin Kim, and S. Sastry, "Feedback linearization vs. adaptive sliding mode control for a quadrotor helicopter," *International Journal of Control, Automation and Systems*, vol. 7, pp. 419–428, 2009.

[9] D. Mayne and H. Michalska, "Receding horizon control of nonlinear systems," in *Proceedings of IEEE Conference on Decision and Control (CDC)*, Austin, TX, USA, Dec. 1988, pp. 464–465 vol.1.

[10] W. H. Kwon, A. M. Bruckstein, and T. Kailath, "Stabilizing state-feedback design via the moving horizon method," *International Journal of Control*, vol. 37, no. 3, pp. 631–643, 1983.

[11] H. Chen and F. Allgöwer, "A quasi-infinite horizon nonlinear model predictive control scheme with guaranteed stability," *Automatica*, vol. 34, no. 10, pp. 1205–1217, 1998.

[12] P. Mhaskar, "Robust model predictive control design for fault-tolerant control of process systems," *Industrial & engineering chemistry research*, vol. 45, no. 25, pp. 8565–8574, 2006.

[13] D. Wang, Q. Pan, Y. Shi, J. Hu, and C. Zhao, "Efficient nonlinear model predictive control for quadrotor trajectory tracking: Algorithms and experiment," *IEEE Transactions on Cybernetics*, vol. 51, no. 10, pp. 5057–5068, 2021.

[14] D. Mayne, M. Seron, and S. Raković, "Robust model predictive control of constrained linear systems with bounded disturbances," *Automatica*, vol. 41, no. 2, pp. 219–224, 2005.

[15] D. Q. Mayne, S. V. Raković, R. Findeisen, and F. Allgöwer, "Robust output feedback model predictive control of constrained linear systems," *Automatica*, vol. 42, no. 7, pp. 1217–1222, 2006.

[16] L. Chisci, J. Rossiter, and G. Zappa, "Systems with persistent disturbances: predictive control with restricted constraints," *Automatica*, vol. 37, no. 7, pp. 1019–1028, 2001.

[17] I. Kolmanovsky and E. G. Gilbert, "Theory and computation of disturbance invariant sets for discrete-time linear systems," *Mathematical Problems in Engineering*, vol. 4, no. 4, p. 317 – 367, 1998.

[18] S. Yu, C. Maier, H. Chen, and F. Allgöwer, "Tube MPC scheme based on robust control invariant set with application to Lipschitz nonlinear systems," *Systems & Control Letters*, vol. 62, no. 2, pp. 194–200, 2013.

[19] B. T. Lopez, J.-J. E. Slotine, and J. P. How, "Dynamic tube MPC for nonlinear systems," in *Proceedings of American Control Conference (ACC)*, Philadelphia, PA, USA, Jul. 2019, pp. 1655–1662.

[20] P. J. Campo and M. Morari, "Robust model predictive control," in *Proceedings of American Control Conference (ACC)*, Minneapolis, MN, USA, Jun. 1987, pp. 1021–1026.

[21] D. Limon, T. Alamo, F. Salas, and E. Camacho, "Input to state stability of min–max MPC controllers for nonlinear systems with bounded uncertainties," *Automatica*, vol. 42, no. 5, pp. 797–803, 2006.

[22] J. Lofberg, "Approximations of closed-loop minimax MPC," in *Proceedings of IEEE International Conference on Decision and Control (CDC)*, vol. 2, Maui, HI, USA, Dec. 2003, pp. 1438–1442.

[23] A. Li and J. Sun, "Robust event-triggered distributed min–max model predictive control of continuous-time non-linear systems," *IET Control Theory & Applications*, vol. 14, no. 19, pp. 3320–3329, 2020.

[24] H. Wei, K. Zhang, and Y. Shi, "Self-triggered min–max DMPC for asynchronous multiagent systems with communication delays," *IEEE Transactions on Industrial Informatics*, vol. 18, no. 10, pp. 6809–6817, 2022.

[25] Y. Shi and K. Zhang, "Advanced model predictive control framework for autonomous intelligent mechatronic systems: A tutorial overview and perspectives," *Annual Reviews in Control*, vol. 52, pp. 170–196, 2021.

[26] J. Primbs, V. Nevistic, and J. Doyle, "A receding horizon generalization of pointwise min-norm controllers," *IEEE Transactions on Automatic Control*, vol. 45, no. 5, pp. 898–909, 2000.

[27] P. Mhaskar, "Robust model predictive control design for fault-tolerant control of process systems," *Industrial & Engineering Chemistry Research*, vol. 45, no. 25, pp. 8565–8574, 2006.

[28] H. Wei, C. Shen, and Y. Shi, "Distributed Lyapunov-based model predictive formation tracking control for autonomous underwater vehicles subject to disturbances," *IEEE Transactions on Systems, Man, and Cybernetics: Systems*, vol. 51, no. 8, pp. 5198–5208, 2021.

[29] A. Bemporad and C. Rocchi, "Decentralized hybrid model predictive control of a formation of unmanned aerial vehicles," in *Proceedings of IFAC World Congress*, vol. 44, no. 1, Milano, Italy, Aug. 2011, pp. 11 900–11 906.

[30] C. E. Luis and A. P. Schoellig, "Trajectory generation for multiagent point-to-point transitions via distributed model predictive control," *IEEE Robotics and Automation Letters*, vol. 4, no. 2, pp. 375–382, 2019.

[31] B. Li and Y. Wang, "An enhanced model predictive controller for quadrotor attitude quick adjustment with input constraints and disturbances," *International Journal of Control, Automation and Systems*, vol. 20, no. 2, pp. 648–659, 2022.

[32] K. Alexis, G. Nikolakopoulos, and A. Tzes, "Experimental model predictive attitude tracking control of a quadrotor helicopter subject to wind-gusts," in *Proceedings of Mediterranean Conference on Control and Automation*, Marrakech, Morocco, Jun. 2010, pp. 1461–1466.

[33] ——, "On trajectory tracking model predictive control of an unmanned quadrotor helicopter subject to aerodynamic disturbances," *Asian Journal of Control*, vol. 16, no. 1, pp. 209–224, 2014.

[34] M. Elhesasy, T. N. Dief, M. Atallah, M. Okasha, M. M. Kamra, S. Yoshida, and M. A. Rushdi, "Non-linear model predictive control using CasADi package for trajectory tracking of quadrotor," *Energies*, vol. 16, no. 5, p. 2143, 2023.

[35] K. Zhang, Y. Shi, and H. Sheng, "Robust nonlinear model predictive control based visual servoing of quadrotor uavs," *IEEE/ASME Transactions on Mechatronics*, vol. 26, no. 2, pp. 700–708, 2021.

[36] A. Richards and J. P. How, "Robust variable horizon model predictive control for vehicle maneuvering," *International Journal of Robust and Nonlinear Control: IFAC-Affiliated Journal*, vol. 16, no. 7, pp. 333–351, 2006.

[37] S. A. P. Quintero, D. A. Copp, and J. P. Hespanha, "Robust UAV coordination for target tracking using output-feedback model predictive control with mov-

ing horizon estimation," in *Proceedings of American Control Conference (ACC)*, Chicago, IL, USA, Jul. 2015, pp. 3758–3764.

[38] M. A. Santos, A. Ferramosca, and G. V. Raffo, "Tube-based MPC with nonlinear control for load transportation using a UAV," *IFAC-PapersOnLine*, vol. 51, no. 25, pp. 459–465, 2018.

[39] B. Xu, A. Suleman, and Y. Shi, "A multi-rate hierarchical fault-tolerant adaptive model predictive control framework: Theory and design for quadrotors," *Automatica*, vol. 153, p. 111015, 2023.

[40] M. Moarref, C. Ossa-Gomez, and L. Rodrigues, "Multiloop controller design for a fly-by-wireless UAV quadrotor based on a multirate sampled-data model," *IEEE Transactions on Aerospace and Electronic Systems*, vol. 51, no. 3, pp. 2319–2331, 2015.

[41] W. Zhang, M. S. Branicky, and S. M. Phillips, "Stability of networked control systems," *IEEE Control Systems Magazine*, vol. 21, no. 1, pp. 84–99, 2001.

[42] L. Ding, Q.-L. Han, L. Y. Wang, and E. Sindi, "Distributed cooperative optimal control of DC microgrids with communication delays," *IEEE Transactions on Industrial Informatics*, vol. 14, no. 9, pp. 3924–3935, 2018.

[43] J. Wang, B. Ding, and J. Hu, "Security control for LPV system with deception attacks via model predictive control: A dynamic output feedback approach," *IEEE Transactions on Automatic Control*, vol. 66, no. 2, pp. 760–767, 2020.

[44] X.-M. Zhang, Q.-L. Han, X. Ge, D. Ding, L. Ding, D. Yue, and C. Peng, "Networked control systems: A survey of trends and techniques," *IEEE/CAA Journal of Automatica Sinica*, vol. 7, no. 1, pp. 1–17, 2019.

[45] X.-M. Zhang, Q.-L. Han, and X. Yu, "Survey on recent advances in networked control systems," *IEEE Transactions on Industrial Informatics*, vol. 12, no. 5, pp. 1740–1752, 2016.

[46] H. Zhang, Y. Shi, J. Wang, and H. Chen, "A new delay-compensation scheme for networked control systems in controller area networks," *IEEE Transactions on Industrial Electronics*, vol. 65, no. 9, pp. 7239–7247, 2018.

[47] H. Gao, X. Meng, and T. Chen, "Stabilization of networked control systems with a new delay characterization," *IEEE Transactions on Automatic Control*, vol. 53, no. 9, pp. 2142–2148, 2008.

[48] Y. Shi and B. Yu, "Output feedback stabilization of networked control systems with random delays modeled by Markov chains," *IEEE Transactions on Automatic Control*, vol. 54, no. 7, pp. 1668–1674, 2009.

[49] Y. Chen, A. Zulfiqar, D. Ma, Y. Shi, J. Chen, and F. Allgöwer, "Simultaneous stabilization of discrete-time delay systems and bounds on delay margin," *Automatica*, vol. 101, pp. 296–308, 2019.

[50] Y. Yang, Y. Shi, and D. Constantinescu, "Connectivity-preserving synchronization of time-delay Euler–Lagrange networks with bounded actuation," *IEEE Transactions on Cybernetics*, vol. 51, no. 7, pp. 3469–3482, 2021.

[51] H. Wei, K. Zhang, and Y. Shi, "Self-triggered min–max dmpc for asynchronous multiagent systems with communication delays," *IEEE Transactions on Industrial Informatics*, vol. 18, no. 10, pp. 6809–6817, 2022.

[52] W. Zhou, Y. Wang, and Y. Liang, "Sliding mode control for networked control systems: A brief survey," *ISA transactions*, vol. 124, pp. 249–259, 2022.

[53] P. K. Mishra, D. Chatterjee, and D. E. Quevedo, "Stabilizing stochastic predictive control under Bernoulli dropouts," *IEEE Transactions on Automatic Control*, vol. 63, no. 6, pp. 1579–1590, 2017.

[54] ——, "Stochastic predictive control under intermittent observations and unreliable actions," *Automatica*, vol. 118, p. 109012, 2020.

[55] D. E. Quevedo and D. Nešić, "Robust stability of packetized predictive control of nonlinear systems with disturbances and Markovian packet losses," *Automatica*, vol. 48, no. 8, pp. 1803–1811, 2012.

[56] X. Tang, L. Deng, J. Yu, and H. Qu, "Output feedback predictive control of interval type-2 T–S fuzzy systems with Markovian packet loss," *IEEE Transactions on Fuzzy Systems*, vol. 26, no. 4, pp. 2450–2459, 2017.

[57] S. Yan, M. Cannon, and P. J. Goulart, "Stochastic output feedback MPC with intermittent observations," *Automatica*, vol. 141, p. 110282, 2022.

[58] B. Sinopoli, L. Schenato, M. Franceschetti, K. Poolla, M. I. Jordan, and S. S. Sastry, "Kalman filtering with intermittent observations," *IEEE Transactions on Automatic Control*, vol. 49, no. 9, pp. 1453–1464, 2004.

[59] P. K. Mishra, S. S. Diwale, C. N. Jones, and D. Chatterjee, "Reference tracking stochastic model predictive control over unreliable channels and bounded control actions," *Automatica*, vol. 127, p. 109512, 2021.

[60] D. Wang, Z. Wang, B. Shen, F. E. Alsaadi, and T. Hayat, "Recent advances on filtering and control for cyber-physical systems under security and resource constraints," *Journal of the Franklin Institute*, vol. 353, no. 11, pp. 2451–2466, 2016.

[61] Q. Sun, K. Zhang, and Y. Shi, "Resilient model predictive control of cyber–physical systems under DoS attacks," *IEEE Transactions on Industrial Informatics*, vol. 16, no. 7, pp. 4920–4927, 2019.

[62] Z.-H. Pang, L.-Z. Fan, H. Guo, Y. Shi, R. Chai, J. Sun, and G.-P. Liu, "Security of networked control systems subject to deception attacks: a survey," *International Journal of Systems Science*, vol. 53, no. 16, pp. 3577–3598, 2022.

[63] S. Xiong, M. Chen, and Q. Wu, "Predictive control for networked switch flight system with packet dropout," *Applied Mathematics and Computation*, vol. 354, pp. 444–459, 2019.

[64] C. Berbra, D. Simon, S. Gentil, and S. Lesecq, "Hardware in the loop networked control and diagnosis of a quadrotor dron," *IFAC Proceedings Volumes*, vol. 42, no. 8, pp. 971–976, 2009.

[65] L. Xiao, A. Hassibi, and J. How, "Control with random communication delays via a discrete-time jump system approach," in *Proceedings of American Control Conference (ACC)*, vol. 3, Chicago, IL, USA, Jun. 2000, pp. 2199–2204 vol.3.

[66] P. Seiler and R. Sengupta, "Analysis of communication losses in vehicle control problems," in *Proceedings of American Control Conference. (ACC)*, vol. 2, Arlington, VA, USA, Jun. 2001, pp. 1491–1496 vol.2.

[67] J. Xiong and J. Lam, "Stabilization of linear systems over networks with bounded packet loss," *Automatica*, vol. 43, no. 1, pp. 80–87, 2007.

[68] M. Yu, L. Wang, T. Chu, and G. Xie, "Stabilization of networked control systems with data packet dropout and network delays via switching system approach," in *Proceedings of IEEE Conference on Decision and Control (CDC)*, vol. 4. Nassau, Bahamas: IEEE, Dec. 2004, pp. 3539–3544.

[69] C. Tan and H. Zhang, "Necessary and sufficient stabilizing conditions for networked control systems with simultaneous transmission delay and packet dropout," *IEEE Transactions on Automatic Control*, vol. 62, no. 8, pp. 4011–4016, 2017.

[70] J.-P. Georges, D. Theilliol, V. Cocquempot, J.-C. Ponsart, and C. Aubrun, "Fault tolerance in networked control systems under intermittent observations," *International Journal of Applied Mathematics and Computer Science*, vol. 21, no. 4, pp. 639–648, 3911.

[71] C.-C. Huang and R. R. Bitmead, "Escape time formulation of state estimation and stabilization with quantized intermittent communication," *Automatica*, vol. 61, pp. 201–210, 2015.

[72] Z. Li, L. Wang, X. Lai, and S. Xu, "Stability of constrained model predictive control for networked control systems with data packet dropout," in *Proceedings of IEEE International Conference on Automation and Logistics*, Jinan, China, Aug. 2007, pp. 3018–3023.

[73] H. Li and Y. Shi, "Networked min–max model predictive control of constrained nonlinear systems with delays and packet dropouts," *International Journal of Control*, vol. 86, no. 4, pp. 610–624, 2013.

[74] M. Pezzutto, M. Farina, R. Carli, and L. Schenato, "Remote MPC for tracking over lossy networks," *IEEE Control Systems Letters*, vol. 6, pp. 1040–1045, 2021.

[75] H. Li and Y. Shi, "Network-based predictive control for constrained nonlinear systems with two-channel packet dropouts," *IEEE Transactions on Industrial Electronics*, vol. 61, no. 3, pp. 1574–1582, 2014.

[76] Q. Lu, P. Shi, J. Liu, and L. Wu, "Model predictive control under event-triggered communication scheme for nonlinear networked systems," *Journal of the Franklin Institute*, vol. 356, no. 5, pp. 2625–2644, 2019.

[77] X. Tang, M. Wu, M. Li, and B. Ding, "On designing the event-triggered multistep model predictive control for nonlinear system over networks with packet dropouts and cyber attacks," *IEEE Transactions on Cybernetics*, 2021.

[78] Y. Mo and B. Sinopoli, "A characterization of the critical value for Kalman filtering with intermittent observations," in *Proceedings of IEEE Conference on Decision and Control (CDC)*, Cancun, Mexico, Dec. 2008, pp. 2692–2697.

[79] L. Shi, M. Epstein, and R. M. Murray, "Kalman filtering over a packet-dropping network: A probabilistic perspective," *IEEE Transactions on Automatic Control*, vol. 55, no. 3, pp. 594–604, 2010.

[80] H. Li and Y. Shi, "Output feedback predictive control for constrained linear systems with intermittent measurements," *Systems & Control Letters*, vol. 62, no. 4, pp. 345–354, 2013.

[81] H. Xie, J. Wang, and X. Tang, "Constrained model predictive control of interval type-2 T–S fuzzy systems with Markovian packet loss," *Journal of Control, Automation and Electrical Systems*, vol. 28, no. 3, pp. 323–336, 2017.

[82] L. Zhang, B. Wang, Y. Zheng, A. Zemouche, X. Zhao, and C. Shen, "Robust packetized MPC for networked systems subject to packet dropouts and input saturation with quantized feedback," *IEEE Transactions on Cybernetics*, 2022.

[83] X. Tang, L. Deng, N. Liu, S. Yang, and J. Yu, "Observer-based output feedback MPC for T–S fuzzy system with data loss and bounded disturbance," *IEEE Transactions on Cybernetics*, vol. 49, no. 6, pp. 2119–2132, 2018.

[84] A. Cetinkaya, K. Kikuchi, T. Hayakawa, and H. Ishii, "Randomized transmission protocols for protection against jamming attacks in multi-agent consensus," *Automatica*, vol. 117, p. 108960, 2020.

[85] L. Zhang, S. Zhuang, P. Shi, and Y. Zhu, "Uniform tube based stabilization of switched linear systems with mode-dependent persistent dwell-time," *IEEE Transactions on Automatic Control*, vol. 60, no. 11, pp. 2994–2999, 2015.

[86] S. Bouabdallah, "Design and control of quadrotors with application to autonomous flying," p. 155, 2007. [Online]. Available: http://infoscience.epfl.ch/record/95939

[87] D. Shi, Z. Wu, and W. Chou, "Anti-disturbance trajectory tracking of quadrotor vehicles via generalized extended state observer," *Journal of Vibration and Control*, vol. 26, no. 13-14, pp. 1173–1186, 2020.